

Hybrid AC/DC Hubs for Network Connection and Integration of Renewables

Kai Huang

**A thesis presented in fulfilment of the requirements for the
degree of Doctor of Philosophy**

Department of Electronic and Electrical Engineering

University of Strathclyde, Glasgow, UK

June 2021

This thesis is the result of the author's original research. It has been composed by the author and has not been previously submitted for examination which has led to the award of a degree.

The copyright of this thesis belongs to the author under the terms of the United Kingdom Copyright Acts as qualified by University of Strathclyde Regulation 3.50. Due acknowledgement must always be made of the use of any material contained in, or derived from, this thesis.

Signed: *Kai Huang*

Date: 06/26/2021

Acknowledgements

I would like to express a deep sense of gratitude to the following people, without whom I would not have been able to complete this Ph.D. program, and without whom I would not have made it through my life in the UK.

First and foremost, I would like to thank my supervisor Professor Lie Xu for his continuous support, encouragement and guidance. His immense knowledge, motivation, enthusiasm and patience contributes tremendously to the accomplishment of my Ph.D. in time. Moreover, his rigorous research attitudes, innovative ideas and efficient research methods benefit me throughout my lifetime, which also illuminates my career life.

My gratitude extends remarkably to Dr. Wang Xiang and Dr. Shuren Wang for the technical and proofreading support through my publications, with their valuable comments and suggestions. I would also like to thank Dr Agusti Egea Alvarez, Prof. Derrick Holliday, Dr. Rui Li, and other colleagues in the PEDEC (Power Electronics, Drives and Energy Conversion) research group for all the help and suggestions.

Grateful acknowledgement is made to my friends, Lei Shi, Xiyang Liu, Xiaozuo Huang, Yin Chen, Deyang Guo, Ding Zhou and for all concerns and companies in the past time.

Finally, I would like to express my most gratitude to my family for their support and understanding during my life in the UK.

Abstract

High-voltage direct current (HVDC) technology has been identified as a preferred choice for long-distance power transmission, especially offshore. With the rapid development of wind energy, many point-to-point HVDC systems with different voltage levels have been built. For increased operation flexibility and reliability, and better use of the existing assets, there is a need to interconnect different AC and DC networks as part of the future transmission network infrastructure development. To address the demands of connecting wind farm converter stations with other AC/DC systems, different hybrid HVDC converters for network connection and integration of renewables are proposed and evaluated in this thesis with the consideration of converter power rating, cost, efficiency and operation flexibility including response during faults.

A hybrid LCC-MMC AC/DC hub (LCC-MMC Hub) is proposed in this research, where a modular multilevel converter (MMC) and a line-commutated converter (LCC) are paralleled at the AC side to integrate onshore wind power, and connected in series at the DC sides to interconnect two DC networks with different voltages. To investigate the design requirement and performance of the hybrid AC/DC hub, power flow analysis is assessed to evaluate the converter power rating requirement. Compared to the “conventional” DC network interconnection based on a DC/DC converter, the proposed hybrid LCC-MMC Hub requires the lower power rating of a MMC with large part of the power handled by a LCC, potentially leading to higher overall efficiency and lower cost. Coordinated controls of the LCC and MMC are developed to ensure stable system operation and system safety. To ride through DC faults at either side of the interconnected DC networks, a coordinated DC fault protection method for the hybrid AC/DC hub is proposed and studied. This hybrid hub uses large AC side filters, which might be the disadvantage for certain applications.

Considering the future development of offshore production platforms (e.g. oil/gas and hydrogen production plants), a diode rectifier-modular multilevel converter AC/DC hub (DR-MMC Hub) is proposed to integrate offshore wind power to onshore DC network and offshore production platforms with different DC voltage levels. In this design, the DR and MMCs are connected in parallel at the offshore AC collection network to integrate offshore wind power, and in series at the DC terminals of the offshore production platform and the onshore DC network. Compared to the parallel operation of the DR-MMC HVDC system, the required MMC power rating in the proposed DR-MMC Hub can be reduced due to the series connection, potentially leading to lower investment cost and power loss. System control of the DR-MMC AC/DC hub is designed for different operating scenarios. System behaviours and requirements during AC and DC faults are investigated. The hybrid MMCs with half-bridge and full-bridge sub-modules (HBSMs and FBSMs) are used for safe operation and protection during DC faults. Power regulation of series-connected configuration might be problematic in certain applications.

To address the needs for increased DC network interconnection and the high cost of the existing F2F DC/DC converter design, a hybrid F2F DC/DC converter, as a potential option, is proposed for unidirectional applications. In the proposed DC/DC converter, the internal AC grid is established by a small MMC based STATCOM, and the active power is transferred through the DR and LCC. Compared to the conventional F2F DC/DC converters in terms of topological features and operation efficiency, the proposed DC/DC converter could offer higher power capability, higher converter efficiency and lower investment cost than those of the MMC based F2F DC/DC converters. The operation and control of the LCC and MMC-STATCOM is designed, and the system start-up procedure is presented. Detailed analysis of the behaviours and protection methods during DC faults is demonstrated. It needs to acknowledge that the converter requires large amount of passive AC filters which may lead to large footprint. In addition, the proposed DC/DC converter only support unidirectional power flow.

For the three proposed topologies, extensive time-domain simulation results based on PSCAD/EMTDC software have been provided to verify the feasibilities and effectiveness (including steady state and dynamic performance) in normal operation and various fault scenarios.

List of Abbreviations

| | |
|-------------|----------------------------------|
| AAC | Alternative Arm Converter |
| AC | Alternating Current |
| ACCB | AC Circuit breaker |
| CCC | Constant Current Control |
| DAB | Dual Active Bridge |
| DC | Direct Current |
| DC AUTO | DC Autotransformer |
| DCCB | DC Circuit Breaker |
| DR | Diode Rectifier |
| DR-MMC Hub | Hybrid Diode-MMC AC/DC Hub |
| LCC-MMC Hub | Hybrid LCC-MMC AC/DC Hub |
| LCOE | Levelised Cost of Electricity |
| FBSM | Full Bridge Submodule |
| F2F | Front-to-Front |
| GSC | Generator-Side Converter |
| HBSM | Half Bridge Submodule |
| HV Side | Higher-Voltage Side |
| HVAC | High Voltage Alternating Current |
| HVDC | High Voltage Direct Current |

| | |
|-----------|---|
| IGBT | Insulated Gate Bipolar Transistor |
| IPOP | Input Parallel Output Parallel |
| IPOS | Input Parallel Output Series |
| ISOP | Input Series Output Parallel |
| ISOS | Input Series Output Series |
| LCC | Line-Commutated Converter |
| LV Side | Lower-Voltage Side |
| MMC | Modular Multilevel Converter |
| MTDC | Multi-Terminal HVDC |
| OHL | Overhead Line |
| PCC | Point of Common Coupling |
| PLL | Phase-Locked Loop |
| p2p | Pole-to-Pole |
| PROMOTioN | Progress on Meshed HVDC Offshore Transmission Networks |
| Q2L | Quasi Two-Level |
| RSC | Rotor-Side Converter |
| STATCOM | Static synchronous compensator |
| TAC | Transition Arm Converter |
| VDCOL | Voltage-Dependent Current Order Limiter |
| VSC | Voltage Source Converter |

List of Symbols

LCC-MMC Hub

| | |
|--------------|--|
| E_1 | DC network with a lower-voltage E_1 |
| E_2 | DC network with a higher-voltage E_2 |
| AC_{WF} | Local AC grid |
| m | DC voltage stepping ratio |
| k | Power transfer ratio |
| P_{dc1} | DC power of E_1 |
| P_{dc2} | DC power of E_2 |
| P_{WF} | Active power from AC_{WF} |
| L_{s_MMC} | DC smoothing reactance of the MMC |
| L_{s_LCC} | DC smoothing reactance of the LCC |
| I_1 | DC current of the MMC |
| I_2 | DC current of the LCC |
| I_3 | Sum of I_1 and I_2 |
| V_{MMC} | DC voltage of the MMC |
| V_{LCC} | DC voltage of the LCC |
| P_{MMC} | Active power of the MMC |
| P_{LCC} | Active power of LCC |
| P_{direct} | Active power transferred by the direct electrical connection |
| P_{hybrid} | Total power rating of the LCC-MMC Hub |
| P_{F2F} | Total power rating of the F2F scheme |
| P_{AT} | Total power rating of the DC AUTO scheme |
| C_1 | Reactive power compensation capacitance |
| C_2 | Capacitance of high frequency filter |
| C_3, C_4 | Capacitances of low frequency filter |

| | |
|-------------------|--|
| R_1 | Resistance of high frequency filter |
| R_2, R_3 | Resistances of low frequency filter |
| L_1 | Inductance of high frequency filter |
| L_2 | Inductance of low frequency filter |
| P_{dc1}^* | Active power reference of E_1 |
| P_{MMC}^* | Active power reference of the MMC |
| I_{LCC}^* | DC current reference of the LCC |
| α | Firing angle order of the LCC |
| $V_{arm_SM}^R$ | Required capacitor voltages of the MMC in each arm |
| $V_{arm_FBSM}^R$ | Required capacitor voltages of the FBSMs in each arm |
| V_{arm_SM} | DC voltage rating of the MMC in each arm |
| N_{SM} | SM number of each MMC arm without fault considerations |
| N_{FB}^R | Required FBSMs number of each MMC arm to isolate LV side fault |
| N_{HB}^R | Required HBSMs number of each MMC arm to isolate HV side fault |
| η_{LCC} | Power loss of the LCC |
| η_{HB} | Power loss of the HBSMs |
| η_{FB} | Power loss of the FBSMs |
| η_{hybrid} | The estimated power loss of the LCC-MMC Hub with HB-MMC |
| η_{hybrid}^R | The estimated power loss of the LCC-MMC Hub with hybrid MMC |
| η_{F2F} | The estimated power loss of the F2F scheme |
| η_{AT}^R | The estimated power loss of the DC AUTO scheme |
| Q_{MMC} | Reactive power of the MMC |
| Q_{LCC} | Reactive power of the LCC |
| Q_{WF} | Reactive power from AC_{WF} |
| i_{pa} | MMC arm current |
| i_{pa_IGBT} | Currents through IGBTs |
| V_C | MMC capacitor voltage |

DR-MMC Hub

| | |
|-------------------|--|
| S_1 | Onshore DC network |
| S_2 | Offshore production platform DC network |
| E_1 | DC voltage of S_1 |
| E_2 | DC voltage of S_2 |
| m | DC voltage stepping ratio |
| a | Power transfer ratio |
| P_{dc1} | DC power to S_1 |
| P_{dc2} | DC power to S_2 |
| P_{WF} | Active power from the offshore wind farm |
| I_1 | DC current of S_1 |
| I_2 | DC current of the DR |
| I_3 | DC current of S_2 |
| V_{DR} | DC voltage of the DR |
| V_{MMC_P} | DC voltage of the MMC _P |
| V_{MMC_N} | DC voltage of the MMC _N |
| P_{MMC_hybrid} | Total active power of the two MMCs in the DR-MMC Hub |
| P_{DR_hybrid} | Active power of the DR in the DR-MMC Hub |
| P_{MMC_con} | Total power rating of the two MMCs in the “conventional” parallel system |
| P_{DR_con} | Power rating of the DR in the “conventional” parallel system |
| v_d^* | d-axis voltage reference of the MMC |
| v_q^* | q-axis voltage reference of the MMC |
| T_{DR} | Turn ratio of the DR transformer |
| X_{DR} | Reactance of the DR transformer |
| V_{PCC} | PCC voltage |

| | |
|-------------------|--|
| P_{DR} | Active power of the DR |
| P_{DR}^* | Active power reference of the DR |
| P_{dc2}^* | Active power reference of S_2 |
| v_0 | Set-point of the offshore AC voltage |
| $V_{arm_SM}^R$ | Required SM capacitor voltage of the MMCs in each arm |
| V_{arm_SM} | Nominal SM capacitor voltage of the MMCs in each arm |
| $V_{arm_FBSM}^R$ | Required SM capacitor voltage of the FBSMs in each arm |
| N_{SM} | SM number of each MMC arm without fault considerations |
| N_{FB}^R | Required FBSMs number of each MMC arm for isolating F_1 faults |
| N_{HB}^R | Required HBSMs number of each MMC arm for isolating F_2 faults |
| η_{DR} | Power loss of the DR |
| η_{HB} | Power loss of the HBSMs |
| η_{FB} | Power loss of the FBSMs |
| η_{con} | The estimated power loss of the “conventional” parallel system |
| η_{HB} | The estimated power loss of the DR-MMC Hub |
| F_1 | A p2p fault happened at S_1 |
| F_2 | A p2p fault happened at S_2 |
| P_{MMC_p} | Reactive power of the MMC _p |
| Q_{DR} | Reactive power of the LCC |
| Q_{WF} | Reactive power from the offshore wind farm |
| Q_{MMC_p} | Reactive power of the MMC _p |
| V_{rms} | RMS AC voltage |
| $i_{pa_MMC_p}$ | Phase A MMC _p upper arm current |
| $V_{c_MMC_p}$ | Average capacitor voltage of MMC _p phase A |

Unidirectional hybrid F2F DC/DC converter

| | |
|-------|-------------------------------|
| E_1 | DC network with voltage E_1 |
|-------|-------------------------------|

| | |
|-------------|---|
| E_2 | DC network with voltage E_2 |
| P_{dc} | DC power of the unidirectional hybrid F2F DC/DC converter |
| P_{DR} | Active power of the DR |
| P_{LCC} | Active power of the LCC |
| Q_{DR} | Reactive power of the DR |
| Q_{LCC} | Reactive power of the LCC |
| Q_{MMC} | Reactive power of the MMC-STATCOM |
| Q_f | Reactive power of the AC filters |
| V_{DR} | DC voltage of the DR |
| V_{LCC} | DC voltage of the LCC |
| V_{MMC} | DC voltage of the MMC-STATCOM |
| C_{MMC} | Total capacitance of the MMC-STATCOM DC capacitors |
| P_{DR}^* | Active power reference of the DR |
| V_{MMC}^* | DC voltage reference of the MMC-STATCOM |
| abc | variables in the abc frame |
| dq | variables in the dq frame |
| i_{MMC} | AC current of the MMC-STATCOM |
| i_{LCC} | AC current of the LCC |
| i_{DR} | AC current of the DR |
| C_f | Total capacitance at the internal AC bus |
| ω | Grid frequency in rad/s |
| V_{ac} | Internal AC bus voltage |
| T_{DR} | Turn ratio of the DR transformer |
| X_{DR} | Reactance of the DR transformer |
| C_{MMC} | Total capacitance of the MMC-STATCOM |
| F_1 | A p2p fault happened at the DC cable between the DR and E_1 |
| F_2 | A p2p fault happened at the DC cable between the DR and E_2 |
| P_{MCC} | Active power of the MMC-STATCOM |

| | |
|-------------|---|
| Q_{total} | Sum of the reactive power of the DR and LCC |
| V_{rms} | RMS internal AC voltage |
| I_{DR} | DC current of the DR |
| I_{LCC} | DC current of the LCC |
| I_{DCCB} | DC current of the DCCB |
| i_{pa} | MMC-STATCOM arm current |

List of Figures

| | |
|---|----|
| Fig. 1.1 Estimated renewable energy share of global electricity production, 2010-2020 [1]. | 1 |
| Fig. 1.2 Total offshore wind power installations by region [5]. | 3 |
| Fig. 2.1 Point-to-point HVDC link. | 10 |
| Fig. 2.2 Parallel of point-to-point HVDC links. | 11 |
| Fig. 2.3 Multi-terminal DC network. | 11 |
| Fig. 2.4 Scope of future HVDC grids [27, 28]. | 12 |
| Fig. 2.5 Twelve-pulse thyristor bridges of LCC. | 13 |
| Fig. 2.6 Two-level VSC. | 14 |
| Fig. 2.7 MMC with two submodule topologies. | 15 |
| Fig. 2.8 DR-HVDC system. | 17 |
| Fig. 2.9 HVDC system with hybrid terminals. | 18 |
| Fig. 2.10 HVDC system with parallel connected hybrid terminals. | 19 |
| Fig. 2.11 HVDC system with hybrid poles. | 20 |
| Fig. 2.12 HVDC system with hybrid converters in series connection. | 21 |
| Fig. 2.13 Classification for DC/DC converters for HVDC grids [53]. | 22 |
| Fig. 2.14 Dual active bridge. | 23 |
| Fig. 2.15 Different possible configurations of cascaded multi-converter DABs: (a) Input Series Output Series (ISOS), (b) Input Parallel Output Series (IPOS), (c) Input Series Output Parallel (ISOP), (d) Input Parallel Output Parallel (IPOP). | 24 |
| Fig. 2.16 Modular multilevel DABs (F2F-MMCs): (a) Topology, (b) Quasi two-level | |

| | |
|---|----|
| operation [61]. | 25 |
| Fig. 2.17 Hybrid F2F-MMCs: (a) the AAC [63], (b) the TAC [64]. | 26 |
| Fig. 2.18 HVDC autotransformer. | 27 |
| Fig. 2.19 Hybrid topologies of the DC AUTO: (a) Topology 1, (b) Topology 2, (c) Topology 3, (d) Topology 4. | 28 |
| Fig. 3.1 Topology of the envisaged scenario for DC network interconnection. | 31 |
| Fig. 3.2 Simplified mono-polar configuration of the proposed LCC-MMC Hub. | 32 |
| Fig. 3.3 Relationship of total power ratings for different operation scenarios with different power ratio k and DC voltage ratio m . | 35 |
| Fig. 3.4 Current and power directions in two power reversal situations: E_2 transmits power and E_2 receives power (green dotted arrows). | 37 |
| Fig. 3.5 System layout and control of the LCC-MMC Hub: (a) Layout of the LCC-MMC Hub, (b) Control of the MMC, (c) Control of the LCC. | 39 |
| Fig. 3.6 Performance of MMC blocking during different DC faults: (a) LV DC side fault, (b) HV DC side fault. | 42 |
| Fig. 3.7 Power loss comparison of different LCC-MMC Hubs with conventional HB-MMC or hybrid MMC. | 45 |
| Fig. 3.8 Power loss comparison of different connection scenarios with different m ($k = 1$). | 46 |
| Fig. 3.9 Power loss comparison of different connection scenarios with different k ($m = 2$). | 47 |
| Fig. 3.10 Equivalent circuits of the system and MMC during E_I fault. | 48 |
| Fig. 3.11 Flow chart of coordinated current protection. | 50 |

| | |
|--|----|
| Fig. 3.12 Response to power flow change: (a) DC power of E_1 and E_2 , (b) Active power of converters and wind farm, (c) MMC arm current, (d) Zoomed MMC arm current (e) MMC SM capacitor voltages. | 53 |
| Fig. 3.13 Response to AC fault: (a) AC voltage, (b) DC voltages of MMC and LCC, (c) DC currents, (d) MMC arm currents. | 55 |
| Fig. 3.14 Response to DC faults: (a) DC voltages of E_1 and E_2 , (b) Converter DC currents, (c) DC current of I_3 , (d) active power of converters and wind farm. | 58 |
| Fig. 3.15 MMC Response to DC faults: (a) MMC DC voltage, (b) MMC capacitor voltages, (c) MMC arm currents, (d) currents through IGBTs. | 59 |
| Fig. 4.1 Envisaged scenario for DC network interconnection. | 63 |
| Fig. 4.2 Symmetrical monopole configuration of the proposed DR-MMC Hub. | 64 |
| Fig. 4.3 Converter power ratings for different system configurations versus different power ratio α and DC voltage ratio m : (a) MMC power rating, (b) DR power rating. | 67 |
| Fig. 4.4 Aggregated wind farm model. | 68 |
| Fig. 4.5 System control diagram of the MMC. | 68 |
| Fig. 4.6 Fault current path of blocked MMCs during different DC faults: (a) current flow during F_2 fault, (b) current flow during F_1 fault (FBSMs are required). | 73 |
| Fig. 4.7 Required number of HBSMs and FBSMs in the hybrid MMCs to isolate DC faults. | 75 |
| Fig. 4.8 System operation in V_{dc} - V_{ac} control mode: (a) DC voltage, (b) DC power, (c) Active power, (d) Reactive power, (e) RMS AC voltage. | 81 |
| Fig. 4.9 System operation in P - V_{ac} control mode: (a) DC power, (b) Active power, (c) Reactive power, (d) Power reference, (e) RMS AC voltage. | 83 |

| | |
|--|-----|
| Fig. 4.10 System performance to AC fault in V_{dc} - V_{ac} control mode: (a) AC voltage, (b) DC voltage, (c) DC current, (d) Phase A MMC _p upper arm current..... | 85 |
| Fig. 4.11 System performance to AC fault in P - V_{ac} control mode: (a) AC voltage, (b) DC current, (c) Phase A MMC _p upper arm current, (d) DC voltage..... | 86 |
| Fig. 4.12 System performance to DC faults: (a) System DC voltage, (b) Converter DC voltage, (c) System DC current, (d) Upper arm current of MMC _p phase A, (e) Average upper / lower arms FBSM and HBSM capacitor voltage of MMC _p phase A. | 89 |
| Fig. 5.1 Conventional F2F DC/DC converters. | 93 |
| Fig. 5.2 Proposed unidirectional hybrid F2F DC/DC converter. | 93 |
| Fig. 5.3 Schematic control diagrams of the unidirectional hybrid F2F DC/DC converter: (a) Control of the MMC-STATCOM, (b) Control of the LCC inverter. | 95 |
| Fig. 5.4 Flow chart of system start-up..... | 99 |
| Fig. 5.5 System during DC faults..... | 100 |
| Fig. 5.6 Potential locations of the DCCB..... | 102 |
| Fig. 5.7 System start-up operation: (a) DC voltage, (b) DC power, (c) Active power, (d) Reactive power, (e) RMS AC voltage. | 107 |
| Fig. 5.8 System performance during active power step changes: (a) DC voltage, (b) DC power, (c) Active power, (d) Reactive power, (e) RMS AC voltage. | 109 |
| Fig. 5.9 System response during F_1 fault: (a) DC voltage, (b) Converter DC current, (c) DCCB DC current, (d) Active power, (e) Reactive power, (f) AC voltage, (g) Phase A upper arm current of MMC-STATCOM..... | 112 |
| Fig. 5.10 System response during F_2 fault: (a) DC voltage, (b) Converter DC current, (c) Active power, (d) Reactive power, (e) AC voltage, (f) Phase A upper arm current of MMC-STATCOM..... | 114 |

List of Tables

| | |
|---|-----|
| Table 1.1 HVDC offshore projects in Europe. | 5 |
| Table 2.1 Characteristics of MMCs. | 16 |
| Table 3.1 System parameters of LCC-MMC Hub. | 51 |
| Table 4.1 Comparison on power ratings and losses with different configurations. ... | 78 |
| Table 4.2 Simulated system parameters | 79 |
| Table 5.1 Parameters of the unidirectional hybrid F2F DC/DC converter | 104 |

Table of Contents

| | |
|---|--------------|
| Acknowledgements..... | I |
| Abstract..... | II |
| List of Abbreviations..... | V |
| List of Symbols | VII |
| List of Figures..... | XIII |
| List of Tables..... | XVII |
| Contents | XVIII |
| Chapter 1 Introduction..... | 1 |
| 1.1 Overview of wind energy development | 1 |
| 1.2 Comparison of HVAC and HVDC for wind farm integration | 3 |
| 1.3 Motivation and contribution | 5 |
| 1.3.1 Research motivations | 5 |
| 1.3.2 Thesis contributions | 7 |
| 1.4 Thesis outline..... | 8 |
| Chapter 2 Literature Review..... | 10 |
| 2.1 Overview of HVDC transmission system configurations..... | 10 |
| 2.1.1 Point-to-point HVDC link..... | 10 |
| 2.1.2 Multi-terminal DC networks | 11 |
| 2.2 Review of AC/DC converters for HVDC application..... | 12 |
| 2.2.1 Line-commutated converter..... | 12 |
| 2.2.2 Voltage source converter | 13 |
| 2.2.3 Diode rectifier | 16 |
| 2.3 Hybrid HVDC systems | 17 |
| 2.3.1 Hybrid terminal HVDC system | 17 |
| 2.3.2 Hybrid pole HVDC system | 19 |
| 2.3.3 Hybrid converter HVDC system | 20 |
| 2.4 Review on HVDC DC/DC converters | 21 |
| 2.4.1 Isolated topologies of DC/DC converters..... | 22 |
| 2.4.2 Non-isolated topologies of DC/DC converters..... | 27 |

| | | |
|------------------|---|-----------|
| 2.5 | Summary | 29 |
| Chapter 3 | Hybrid LCC-MMC AC/DC Hub | 30 |
| 3.1 | Introduction..... | 30 |
| 3.2 | System topology and power flow analysis..... | 31 |
| 3.2.1 | Envisaged application scenario | 31 |
| 3.2.1 | Topology of the LCC-MMC Hub..... | 32 |
| 3.2.2 | Power flow analysis..... | 33 |
| 3.2.3 | Power reversal to the offshore HVDC system..... | 36 |
| 3.3 | Control principles | 37 |
| 3.3.1 | Control of MMC..... | 39 |
| 3.3.2 | Control of LCC..... | 40 |
| 3.4 | DC fault protection | 41 |
| 3.4.1 | System behaviour during DC fault | 41 |
| 3.4.2 | DC fault protection analysis and power loss estimation..... | 42 |
| 3.4.3 | Principle of coordinated current protection | 49 |
| 3.5 | Simulation studies..... | 51 |
| 3.5.1 | Normal operation and power reversal | 52 |
| 3.5.2 | AC fault ride-through..... | 54 |
| 3.5.3 | Response to DC fault..... | 55 |
| 3.6 | Summary | 60 |
| Chapter 4 | Hybrid DR-MMC AC/DC Hub..... | 61 |
| 4.1 | Introduction..... | 61 |
| 4.2 | Proposed topology and efficiency analysis | 63 |
| 4.2.1 | Envisaged operation scenario | 63 |
| 4.2.2 | DR-MMC Hub configuration..... | 64 |
| 4.3 | Control principles | 67 |
| 4.4 | Fault ride-through of the DR-MMC Hub..... | 70 |
| 4.4.1 | AC fault ride-through..... | 70 |
| 4.4.2 | DC fault ride-through..... | 71 |
| 4.5 | Power loss estimation | 76 |
| 4.6 | Simulation studies..... | 78 |
| 4.6.1 | Operation in V_{dc} - V_{ac} control mode..... | 80 |

| | | |
|------------------------------|---|------------|
| 4.6.2 | Operation in $P-V_{ac}$ control mode | 82 |
| 4.6.3 | AC fault ride-through | 84 |
| 4.6.4 | DC fault ride-through | 87 |
| 4.7 | Summary | 90 |
| Chapter 5 | Unidirectional Hybrid F2F DC/DC Converter | 91 |
| 5.1 | Introduction | 91 |
| 5.2 | Converter topology and efficiency comparison | 92 |
| 5.2.1 | Topologies of conventional F2F DC/DC converters | 92 |
| 5.2.2 | Topology of unidirectional hybrid F2F DC/DC converter | 93 |
| 5.3 | Control principles | 95 |
| 5.3.1 | Control of MMC-STATCOM | 95 |
| 5.3.2 | Control of LCC | 97 |
| 5.4 | System start-up procedure | 98 |
| 5.5 | DC fault protection | 100 |
| 5.5.1 | DC protection under F_1 fault | 101 |
| 5.5.2 | DC protection under F_2 fault | 103 |
| 5.6 | Simulation results | 103 |
| 5.6.1 | System start-up and normal active power variation | 105 |
| 5.6.2 | System response during F_1 fault | 109 |
| 5.6.3 | System response during F_2 fault | 112 |
| 5.7 | Summary | 114 |
| Chapter 6 | Conclusion and Future Work | 116 |
| 6.1 | General conclusion | 116 |
| 6.2 | Future work | 119 |
| References | | 120 |
| Author's Publications | | 133 |

Chapter 1 Introduction

1.1 Overview of wind energy development

Due to significant environmental issues and the growing depletion of traditional fossil energy, renewable and sustainable energy utilisation have seen rapid growth globally. According to the Renewables 2021 Global Status Report [1], renewable energy capacity has significantly increased from 2581 GW to 2838 GW in a year. Fig. 1.1 shows the renewable electricity ratio of global electricity production from 2010-2020, which took approximately 29% of global electricity generation. As one of the most advanced and mature technologies, wind power makes up the most renewable electricity generation apart from traditional hydropower [1].

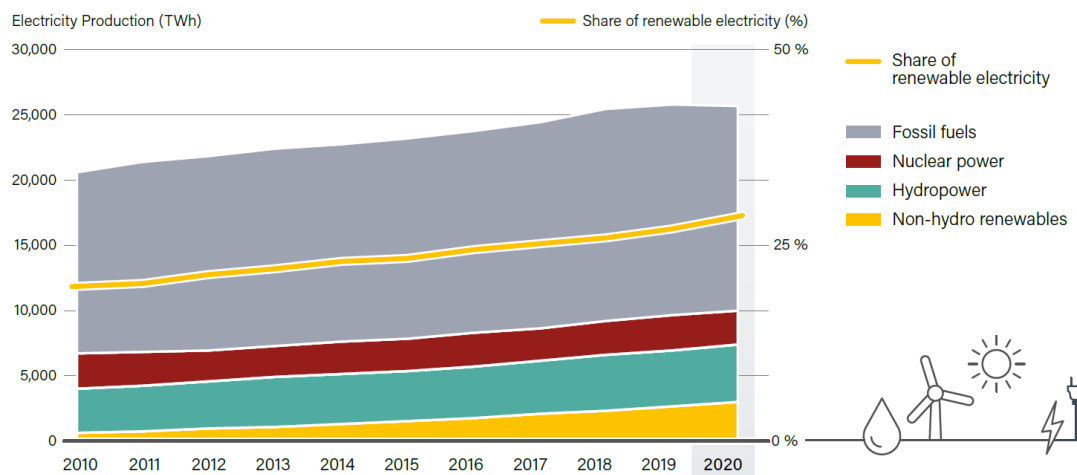


Fig. 1.1 Estimated renewable energy share of global electricity production, 2010-2020 [1].

With continuous cost reduction, wind power can be cheaper to build and maintain than fossil fuel power generation in some projects. The UK government has indicated that the levelised cost of electricity (LCOE) of the gas-fired electricity is expected to cost twice as much as wind energy in 2025 [2]. The Global Wind Energy Council report indicated that by the end of 2020, 93 GW of newly onshore and offshore wind power installations (increased by 59% compared to 2019), contributing to the

worldwide total wind power capacity of 743 GW [3]. In addition, more than 469 GW of new wind capacity is expected to be added by 2025.

“Onshore” and “Offshore” are two primary ways for wind farm construction. For onshore wind power exploitation, countries like China, the US and India with vast lands are playing a leading role. Many large-scale onshore wind farms (more than 10 GW of each) have been developed in stages [4]. For example, Jiuquan Wind Power Base in western China is the world's biggest onshore wind farm, with an expected capacity of 20 GW when fully developed.

Building large-scale onshore wind farms is restricted by land occupation, environmental impacts, limited wind speed, etc. Offshore wind farms are hence preferred, especially for European countries, leading to more sustainable growth. The main advantages of offshore wind farms when compared to onshore ones are [3, 5, 6]:

- Eliminating visual and noisy influences.
- Higher wind speed and thus power generation than onshore by up to 30%.
- More available spaces with consistent and robust wind resources compared to onshore.
- Suitable for coastal city areas to meet the power and environmental demands.

Europe is leading the world in the offshore wind market with advanced commercial off-the-shelf technologies. The installed offshore wind power installations in Europe have reached 25 GW in 2020, where Europe remains the biggest offshore market, taking 75% of the cumulative global offshore wind power capacity as shown in Fig. 1.2 [5, 6]. Although technology improvements have significantly reduced the cost of offshore wind farm in the last 10 years, some key issues still require further research and development, such as energy transition, grid connection, further cost reduction, and safety optimisation.

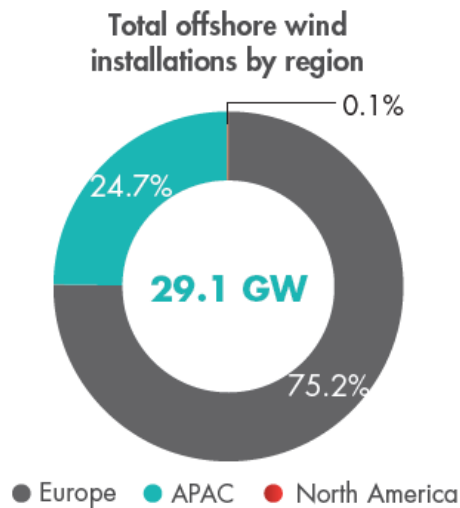


Fig. 1.2 Total offshore wind power installations by region [5].

In addition to transmitting generated electrical power from offshore wind farms to onshore power network, there has also been increased interest in offshore production platforms, for example, the benefit of utilising offshore wind power and onshore HVDC grid to supply offshore oil/gas platform has been considered to replace power generated by offshore gas turbines for carbon reduction [7]. As an efficient and clean form of storing energy, offshore hydrogen can be produced from offshore wind power through power-to-gas technology to accommodate a large amount of intermittent renewable energy into power network [8, 9], which could be deployed using unused oil/gas platforms as a financially attractive solution [10]. A concept for integrating offshore wind farm and offshore hydrogen production (delivering power up to 400MW) is proposed in [8], where the offshore wind power is transmitted to both onshore power grid and offshore hydrogen platform by the offshore converter stations at different DC voltage levels.

1.2 Comparison of HVAC and HVDC for wind farm integration

Reference [11] indicates that HVAC transmission system is the simplest method for wind farm integration, though it is only recommended under the distance of 300 km for overhead lines (OHLs) or 80 km for cable-based links to provide an economical

and stable connection [12-14]. In dealing with rapid load changes and fault conditions, dynamic reactive power compensation is required at a cable connection distance over 50 km [11]. In addition, AC cable with relatively high capacitance can also lead to high reactive power and potential resonance phenomenon.

HVDC transmission system is the most attractive solution for large-scale wind farm integration over a long distance. It can overcome the above challenges and offer many merits for wind farm connections, as summarised below [11-15]:

- Higher capacity and lower loss (per km) of the DC cable than AC.
- Interconnectable asynchronous AC grids with no AC fault propagations on the two sides.
- No transmission distance limit on the DC cable due to no charging current.
- Better power flow control and AC grid support by VSC technology.
- Lower cost than HVAC transmission systems over a long distance.

The increase of capacity and transmission distance of offshore wind farms, especially in Europe, has promoted the use of HVDC transmission technology in offshore wind power connection. For example, most of the offshore wind farm projects in Germany have adopted HVDC transmission technology, and the latest Dogger Bank offshore wind farm in the UK which is currently under development has also chosen HVDC technology [16-19]. Table 1.1 shows some of the existing offshore HVDC projects and projects under construction in Europe, which consists of different DC voltage levels.

Table 1.1 HVDC offshore projects in Europe.

| Project | Capacity | Voltage | Length | Year |
|----------------|-----------------|----------------|---------------|-------------|
| Borwin1 | 400 MW | ± 150 kV | 200 km | 2010 |
| Borwin2 | 800 MW | ± 300 kV | 200 km | 2015 |
| Dolwin1 | 800 MW | ± 320 kV | 165 km | 2015 |
| Helwin1 | 576 MW | ± 250 kV | 130 km | 2015 |
| Helwin2 | 690 MW | ± 320 kV | 130 km | 2015 |
| Sylwin1 | 864 MW | ± 320 kV | 205 km | 2015 |
| Dolwin2 | 916 MW | ± 320 kV | 135 km | 2016 |
| Dolwin3 | 900 MW | ± 320 kV | 160 km | 2018 |
| Borwin3 | 900 MW | ± 320 kV | 160 km | 2019 |
| Nemo Link | 1000 MW | ± 400 kV | 140 km | 2019 |
| NordLink | 1400 MW | ± 525 kV | 623 km | 2021 |
| Dolwin6 | 900 MW | ± 320 kV | 90 km | 2023 |
| Dolwin5 | 900 MW | ± 320 kV | 130 km | 2024 |
| NorthConnect | 1400 MW | ± 500 kV | 655 km | 2024 |

1.3 Motivation and contribution

1.3.1 Research motivations

The core motivation of this research is to investigate and analyse hybrid AC/DC hub concept to potentially provide economical and efficient solutions for interconnecting DC networks and wind farms.

The need for DC network interconnection will arise as the size of DC grids grows in the future, which necessitates the installation of DC/DC converters. Although many DC/DC converters have been proposed and analysed, none of them provides an ideal solution while none has been commercially installed. The front-to-front modular multilevel converter (F2F-MMC) and DC autotransformer (DC AUTO) concepts are the two most viable solutions due to the maturity of MMC, but the required power semiconductor devices for high-power applications lead to high investment costs. The unidirectional converters, e.g., line-commutated converter (LCC) and diode rectifier (DR) can reduce the converter cost and power loss, but they cannot provide the internal AC grid without voltage source converter (VSC).

For connecting multiples AC and DC networks, parallel connection of multiple point-to-point HVDC links may be used which can improve the system availability. However, proper power sharing in the HVDC stations should be managed with extra controls in the MMCs [20], and the total power rating of the HVDC converters (e.g. MMCs) in this scheme can be quite high, considering the different operation requirements and conditions. A cost-effective HVDC system for integrating wind farms and interconnecting various DC networks at specific hub locations may become the flexible transmission solution for overcoming the above challenges. At the same time, the system during different fault scenarios should be fully considered.

For different converter designs for HVDC systems, DR potentially offers lower investment, smaller footprint and higher efficiency than other converters. However, for DC network interconnection, a hybrid configuration combining uncontrolled DR and fully-controlled MMC is likely to be required as DRs alone cannot separately control power transmissions to multiple terminals. On the other hand, LCC may be considered as the substitute for DR as it can provide additional control through the firing angle. Several hybrid HVDC solutions have been proposed to combine the advantages of different converter topologies, but few are able to connect various AC

and DC systems to achieve flexible interconnection. MMC based DC AUTO systems have been considered for connecting the inner AC bus of the DC AUTO to an external AC system, to achieve power exchange between the two DC networks and the AC system [67]. However, the operation control and fault ride-through of the DC AUTO connecting an offshore wind farm and DC networks have not been investigated. In summary, systems that connect external AC grid and various DC networks could potentially provide cost-effective solutions and thus are worth exploring.

1.3.2 Thesis contributions

The main contributions of this thesis are summarized as follows:

- A hybrid AC/DC hub configuration consisted of LCC and MMC technologies (LCC-MMC Hub) is proposed to interconnect onshore and offshore DC networks with different voltage levels, and to integrate onshore wind farms through the AC terminal. In the LCC-MMC Hub, the onshore wind farm is directly connected to the LCC, and a MMC is connected in series between the LCC (higher DC voltage side) and DC terminals of the offshore DC network (lower DC voltage side). Compared to the “conventional” interconnection approach using DC/DC converters, in the proposed hybrid system, part of the power from the offshore DC network can be transmitted to the onshore DC network directly, therefore, potentially reducing the costs and power losses of converters.
- A hybrid DR-MMC AC/DC hub (DR-MMC Hub) is proposed to transmit offshore wind power to an onshore DC network and an offshore production platform with different DC voltage levels. In the DR-MMC Hub, the DR and MMCs are connected in parallel at the AC side and in series at the DC side. Compared to the “conventional” approach using parallel DR and MMC in

which the DR is used to transmit power to the offshore production platform while the MMCs transmit power to the onshore grid, the proposed DR-MMC Hub enables part of the power from the DR to be transferred to the onshore DC network directly, potentially resulting in lower rated MMC and lower power loss of the overall converter system.

- A unidirectional hybrid F2F DC/DC converter composed of DR, LCC and MMC (acting as a static synchronous compensator (MMC-STATCOM)) is studied for unidirectional power transmission applications, such as wind power collections through DC grids. In the proposed DC/DC converter, the conventional F2F-MMCs are replaced by the DR and LCC, while the internal AC grid is established by the MMC-STATCOM, which also provides reactive power compensation for the DR and LCC. Since the DR and LCC offer higher efficiency and potentially lower cost than the same sized MMC, the cost and power loss can be potentially reduced compared to conventional F2F DC/DC converters using MMCs.

1.4 Thesis outline

The thesis is organised as follows:

Chapter 2: Literature Review

Chapter 2 depicts the research review on HVDC technologies, including transmission system configurations, AC/DC converters, hybrid systems and DC/DC converters.

Chapter 3: Hybrid LCC-MMC AC/DC Hub

Chapter 3 proposes a hybrid AC/DC hub composed of LCC and MMC technologies to integrate onshore wind power and interconnect onshore and offshore DC networks. The system layout, power flow analysis and control principle are

presented. In addition, a comprehensive DC fault protection scheme for the proposed system is designed. Simulation validations on power flow change, DC fault and AC fault responses (including the study of AC fault ride-through capability) are provided.

Chapter 4: Hybrid DR-MMC AC/DC Hub

Chapter 4 proposes a hybrid DR-MMC AC/DC Hub for connecting offshore wind farm and offshore production platform. The topology and efficiency between the DR-MMC Hub and the envisaged parallel configuration are compared, while the system control principle of the DR-MMC Hub is described. A comprehensive AC/DC fault ride-through and converter power loss estimation of the DR-MMC Hub are investigated. Simulation results of the DR-MMC Hub during normal operation, AC and DC faults verify the system effectiveness.

Chapter 5: Unidirectional Hybrid F2F DC/DC Converter

A unidirectional hybrid F2F DC/DC converter including DR, LCC and MMC-STATCOM is studied in Chapter 5. The converter topology and efficiency comparison between the proposed DC/DC converter and the conventional F2F DC/DC converter using MMCs are introduced. The system control strategies of the proposed DC/DC converter are designed. The DC fault phenomenon and protection methods are also considered. Simulation studies are provided to validate the system performance during system start-up, normal power variation, and DC fault conditions.

Chapter 6: Conclusions and Future Works

Chapter 6 draws the conclusions of the research and outlines future works.

Chapter 2 Literature Review

2.1 Overview of HVDC transmission system configurations

2.1.1 Point-to-point HVDC link

As the simplest and most commonly deployed structure, the point-to-point HVDC link shown in Fig. 2.1 utilises a rectifier station to convert the AC power into DC, the DC power is transferred via the DC cables or OHLs and then converted back to AC. A number of HVDC converter designs can be deployed based on different HVDC applications, such as LCC, VSC, DR and other hybrid topologies [14].

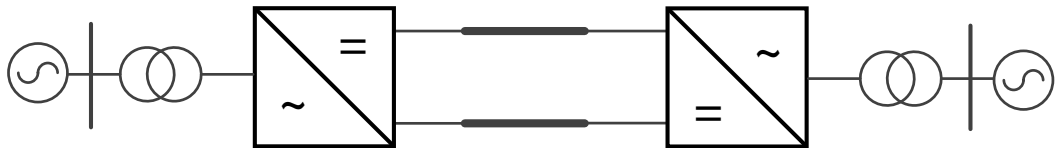


Fig. 2.1 Point-to-point HVDC link.

One AC grid can be connected to more than one point-to-point HVDC links with different DC voltage levels, as shown in Fig. 2.2. The majority of the generated power can be exported through the other HVDC links when one link is out of service during fault scenarios, which improves the transmission availability and system reliability. Nevertheless, extra controls need to be allocated to the HVDC converters to allow proper power sharing [20]. In addition, the economic assessment, regulatory and geographical limitations of the paralleled HVDC links should be further considered.

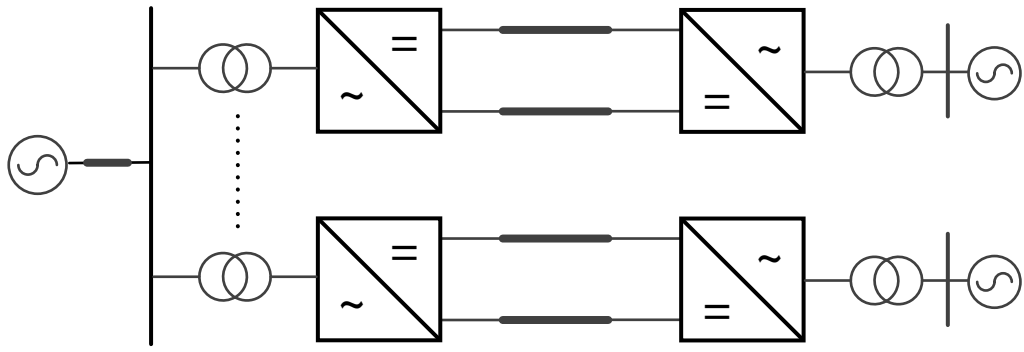


Fig. 2.2 Parallel of point-to-point HVDC links.

2.1.2 Multi-terminal DC networks

A conventional point-to-point HVDC link can only interconnect two AC systems. Large numbers of converters can be connected on the DC side through different DC lines to form a multi-terminal DC (MTDC) system which allows integration of many remote renewable generation sites, and transmission of bulk energy to different load centres [21, 22]. Compared with point-to-point HVDC, the meshed MTDC shown in Fig. 2.3 brings enhanced power exchange flexibility between different AC systems, as well as reduced investment and better system redundancy [23]. Coordinated controls for MTDCs have been well studied to ensure stable operation and proper power-sharing, such as optimal droop controls [24-26].

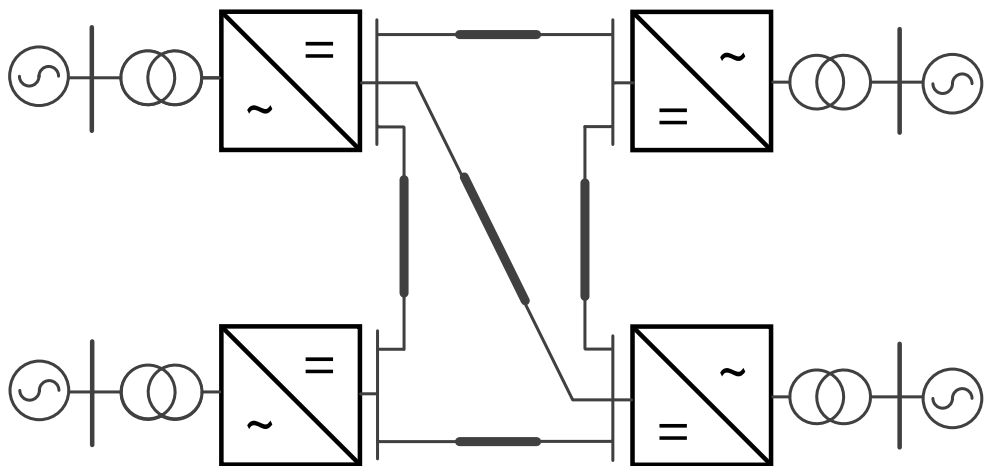


Fig. 2.3 Multi-terminal DC network.

In the near future, different MTDC systems could be further interconnected to form large HVDC grids [27]. This concept has received significant attention from policymakers and utility planners to reinforce and provide more flexibility to the existing grid. Fig. 2.4 demonstrates two examples of future HVDC grids. A global DC supergrid that connects six continents are illustrated in Fig. 2.4 (a) [22], which offers the potential to integrate a wide-ranging mix of energy resources and exploit financial benefits from load capacity diversity driven by time zone differences [27]. Fig. 2.4 (b) shows a localised European HVDC grid layout proposed in the PROMOTioN project [28], for connecting offshore wind farms to onshore grids.

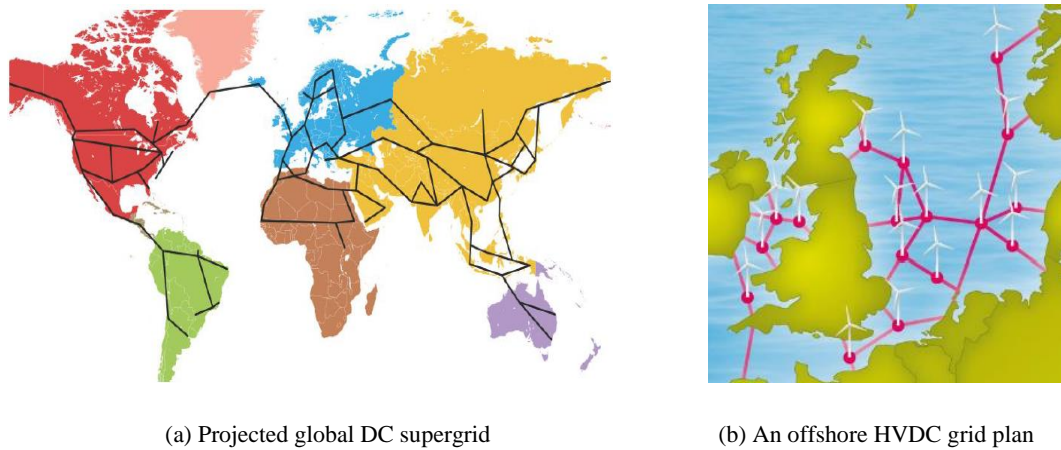


Fig. 2.4 Scope of future HVDC grids [27, 28].

2.2 Review of AC/DC converters for HVDC application

2.2.1 Line-commutated converter

Since the first commercial HVDC project (Gotland HVDC link) was built in 1954, LCC-HVDC technology has been well developed and is regarded as a proven solution for decades. Over the last 70 years, LCC-HVDC systems have been widely used for bulk power transmission over long distance connecting remote generation sources to load areas, due to the low economic cost and power loss, high reliability and overloaded capacity [15].

As shown in Fig. 2.5, LCC is usually composed of two six-pulse thyristor bridges connected in series on the DC side and in parallel on the AC side through two Y/Y and Y/ Δ connected transformers to form a 12-pulse converter configuration, effectively eliminating the 5th and 7th harmonic currents at the AC side. AC filters are inserted to absorb AC side harmonics and to supply reactive power to the converter.

However, LCC is likely not suitable for offshore applications. LCC needs a strong AC network to provide commutation voltages, which means that a weak AC network may cause the LCC commutation failure. Large numbers of AC filters and reactive power compensation devices result in large footprint and heavyweight of LCC converter station.

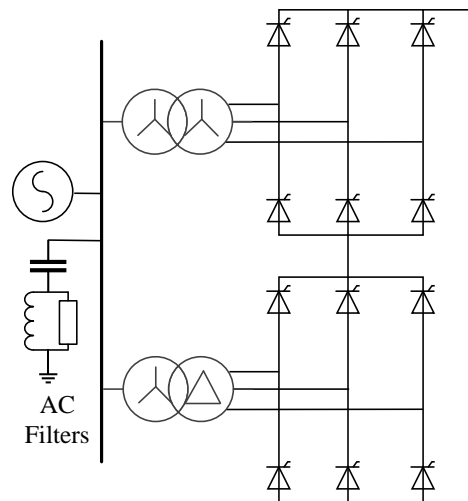


Fig. 2.5 Twelve-pulse thyristor bridges of LCC.

2.2.2 Voltage source converter

As an alternative, VSC based HVDC system is more attractive for offshore application due to its compact design and flexible control and operation. Fig. 2.6 illustrates a conventional two-level VSC using series connected insulated gate bipolar transistors (IGBTs). Compared with LCC-HVDC, VSC-HVDC offers the following advantages [15, 29, 30]:

- Independent active and reactive power control, and power reversal can be easily achieved by reversing DC current (while for LCC, power reversal is achieved by reversing the DC voltage).
- Lower converter station volume.
- Flexible control and operation for connecting offshore wind farms, e.g., it can generate offshore AC grid voltages and start-up offshore wind turbines.

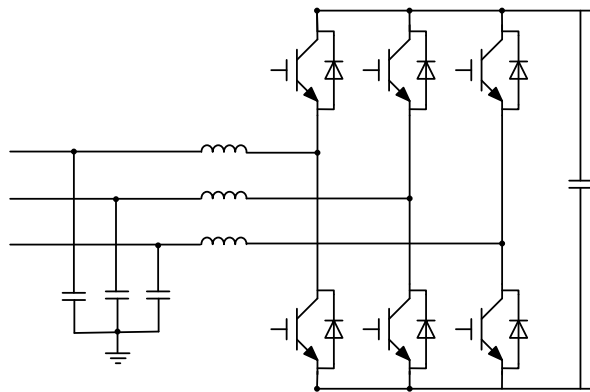


Fig. 2.6 Two-level VSC.

Despite its earlier application, e.g., the 400 MW BorWin 1 project commissioned in 2009 [17], there are various challenges of using two-level VSC for integrating offshore wind farms, e.g., limited difficulty to scale up for high-power applications, still requiring substantial filters for harmonic suppression, high power losses due to high switching frequency, dynamic voltage sharing issue of series connected IGBTs, and overcurrent discharged by DC link capacitors during DC faults [14, 15].

To overcome the issues related to 2-level VSC, modular multilevel converter (MMC), first proposed in 2003, has been extensively researched in academia and industry, becoming one of the most attractive technologies for HVDC applications [31-33]. Fig. 2.7 shows a configuration of a MMC-HVDC system. For each MMC station, there are 6 arms and each arm constitutes an arm inductor and N number of

the so-called submodules (SMs). The popularities of SM topologies can be half-bridge submodules (HBSMs), full-bridge submodules (FBSMs) or combination of them (hybrid scheme), depending on different applications [34, 35]. The output voltage of each SM can be regulated and thus the overall voltage generated by each arm in a MMC can be controlled to resemble a desirable voltage shape, e.g., a staircase waveform resembling a sinusoidal waveform.

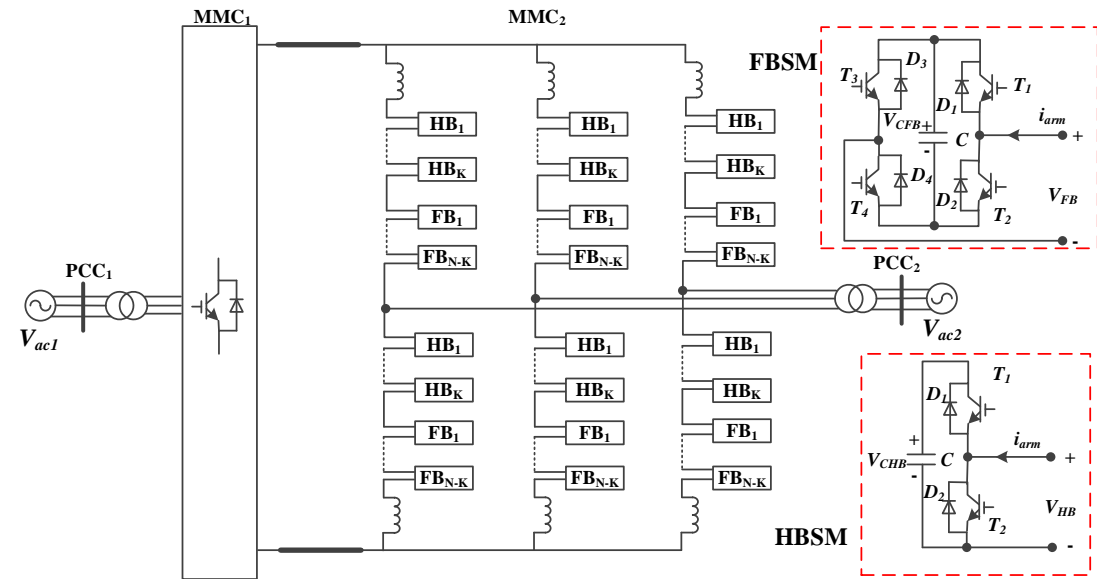


Fig. 2.7 MMC with two submodule topologies.

Table 2.1 summarises the advantages of MMC when compared with two-level VSC [31-34].

Table 2.1 Characteristics of MMCs.

| Features | Reasons |
|-----------------------------------|--|
| High modularity | <ol style="list-style-type: none"> 1. Good scalability to configure the desired voltage level. 2. Strong fungibility; convenient for maintenance. 3. Easy for redundant work. |
| Small or no AC filters required | High quality of AC output. |
| Lower switching loss | <ol style="list-style-type: none"> 1. Small harmonic content due to the modularity of MMCs (so no need to have high switching frequency). 2. Less high-frequency noise and smaller switching frequency contribute to lower switching loss. |
| Ability to ride through DC faults | <ol style="list-style-type: none"> 1. Reduced fault current due to distributed and controlled SM capacitors. 2. DC fault isolating capability provided by specific SM topologies (such as FBSM). |

2.2.3 Diode rectifier

DR based HVDC system has received considerable interests for offshore wind power transmission [36-39]. As shown in Fig. 2.8, a DR-HVDC system is composed of several 12-pulse DRs which are connected in series on the DC side and in parallel to the offshore AC grid. Filter banks are inserted in each DRs for harmonic filtering and reactive power compensation. Due to the simple structure, DR-HVDC could reduce the converter volume, capital cost and transmission losses by 80%, 30% and 20%, respectively, compared with MMC-HVDC for offshore wind farm integration [39].

However, the transmitted power through DRs depends on the offshore AC voltage amplitude. Thus, the offshore AC grid voltage and frequency control need to be provided by wind turbine converters.

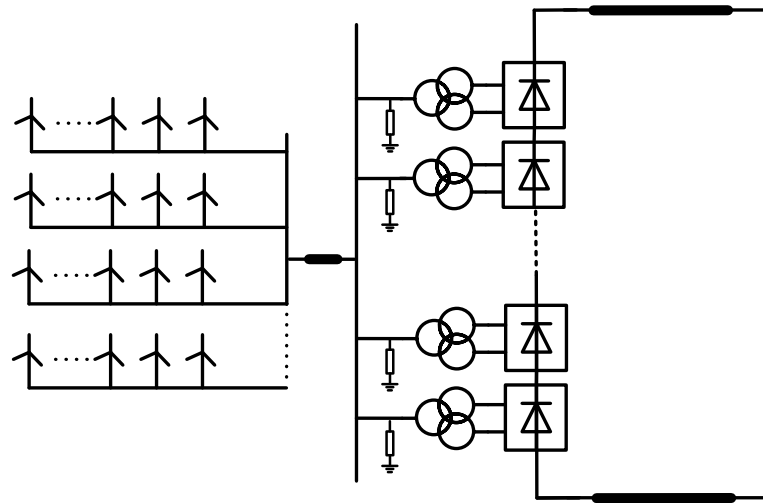


Fig. 2.8 DR-HVDC system.

2.3 Hybrid HVDC systems

To take the advantages of different converter systems, converters with different structures can be incorporated into hybrid designs. Considering from the system level [40], hybrid HVDC systems may be divided into three categories: (1) hybrid terminal system; (2) hybrid pole system; and (3) hybrid converter system.

2.3.1 Hybrid terminal HVDC system

In a hybrid terminal HVDC system, each terminal deploys one type of AC/DC converters. Two hybrid terminal HVDC systems with different configurations are shown in Fig. 2.9 and Fig. 2.10 [41-46].

Fig. 2.9 illustrates an example of a HVDC system with hybrid terminals. As seen, the rectifier terminal adopts LCC while the inverter terminal uses VSC. The LCC rectifier offers lower power losses and investment costs, while no commutation failure will occur in the system when the VSC operates in the inverter mode. For a two-terminal system, the LCC and VSC in this topology have the same DC voltage and current, while their ratings can be different in a multi-terminal HVDC system. A three-

terminal HVDC system with hybrid converter terminals called Wudongde HVDC project has been developed in China [44], which transmits the hydropower from Yunnan Province by an 8000 MW LCC station to the load centers through a 3000 MW MMC station at Guangxi and a 5000 MW MMC station at Guangdong. The total transmission distance is about 1500 km. This project takes the high power/low cost advantages of LCC converter while eliminating commutation failure issue on the receiving ends by using MMCs.



Fig. 2.9 HVDC system with hybrid terminals.

Fig. 2.10 shows an example of a HVDC system with parallel connected hybrid terminals. As can be seen, the LCC and VSC are connected in parallel to the same DC line. Therefore, the DC voltages of LCC and VSC are the same but their DC currents can be different. Since only one HVDC transmission line is needed for two different AC/DC converters in this parallel topology, the investment of transmission corridors can be reduced. Nevertheless, there are limited studies proposing this parallel system in the literature [45, 46] and no related project has been built or under planning.

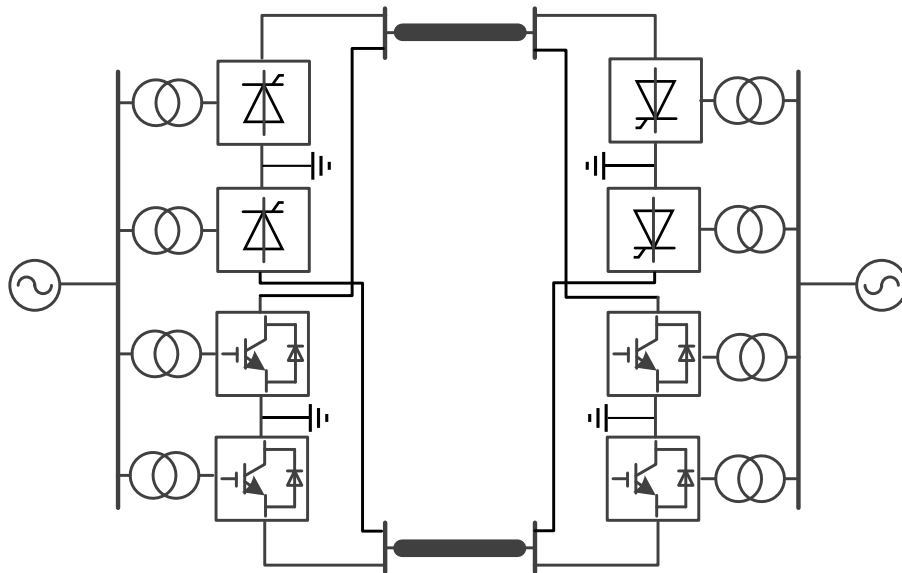


Fig. 2.10 HVDC system with parallel connected hybrid terminals.

2.3.2 Hybrid pole HVDC system

For a bipolar HVDC system, the two poles in the converter terminals can deploy different converter technologies. Fig. 2.11 shows an example of a HVDC system with hybrid poles of LCC and VSC. The DC voltages of the LCC and VSC can be different while the DC currents are the same. The hybrid pole topology has been used to upgrade the existing monopolar LCC-HVDC to improve system control flexibility, e.g. the Skagerrak HVDC project [47]. In this project, a LCC-HVDC link and a VSC-HVDC link are tied together to form a bipolar hybrid pole HVDC system. The combination of the system improves power transmission capacity and efficiency. The inherent characteristics of VSC reduce the need for reactive power compensation, improve AC grid stability and simplify overall system operation.

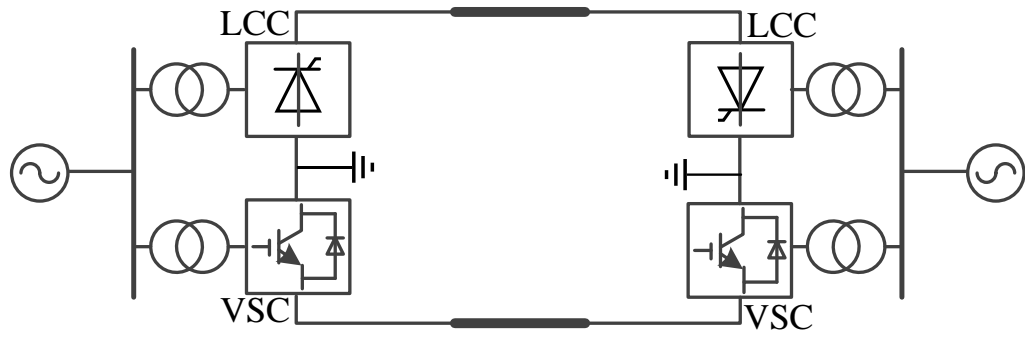


Fig. 2.11 HVDC system with hybrid poles.

2.3.3 Hybrid converter HVDC system

HVDC systems using hybrid converter deploy converters that are composed of different types of converter configurations, which can be connected in the series [40, 48, 49].

Fig. 2.12 shows an example of a symmetrical bipole HVDC system with hybrid converters in series connection. The converters in each pole consist of a LCC and a VSC in series. The voltages of the LCC and VSC can be different but their currents are the same. This topology can supply power for the weak AC grid due to the use of VSC. The Baihetan-Jiangsu ± 800 kV HVDC project with series-connected hybrid converters is under planning [40]. This project aims to deliver the hydropower at Beihetan to Jiangsu. The receiving end in Jiangsu adopts the LCC and VSC in series, so that the grid stability of Jiangsu can be improved due to the AC voltage support capability of VSC. Moreover, the VSC can also supply part of the reactive power consumed by the LCC.

Several HVDC systems with hybrid converter configurations composed of series-connected LCC-VSC or DR-VSC have been proposed to integrate wind farms [48, 49]. The VSC is capable of establishing the AC voltage for the commutation of LCC or DR, while the LCC and DR can increase the transmission capacity with potentially

reduced power loss and cost. DR is likely to be more desirable for offshore wind farms due to the reduced footprint, power loss, capital expenditure and maintenance, compared to LCC.

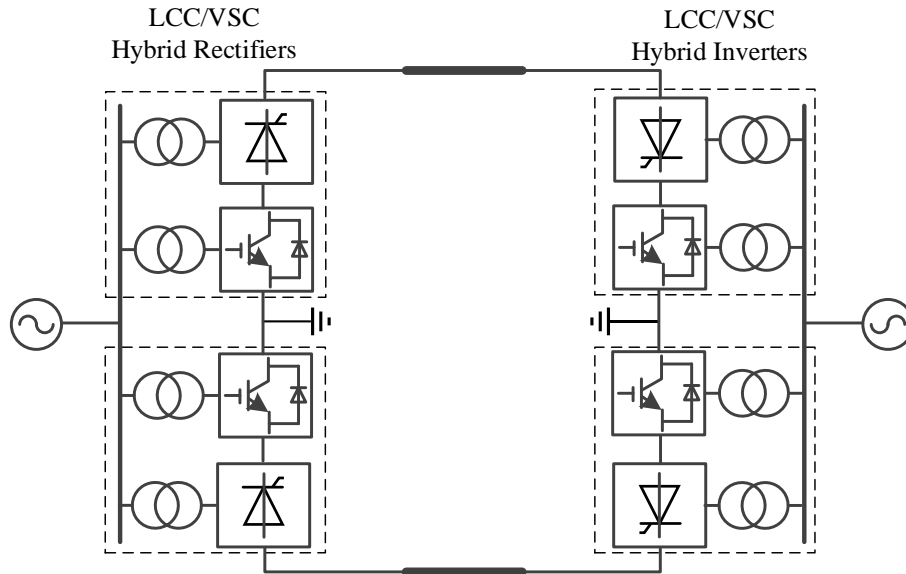


Fig. 2.12 HVDC system with hybrid converters in series connection.

2.4 Review on HVDC DC/DC converters

Forming a large HVDC grid by connecting existing HVDC links likely requires DC voltage matching as the existing links may operate at different voltage levels. For instance, several HVDC links (mostly LCC) ranged from ± 500 kV to ± 1000 kV have been commissioned in China to transmit onshore wind power over 1000 km [50]. In the meantime, many offshore wind farms in Europe have been installed or are currently under construction, MMC-HVDC technologies have been largely used for their grid connection [51-52]. Over the 30 HVDC links in the North Sea, they have a diversity of voltage levels from ± 150 kV to ± 500 kV [23]. High voltage, high power DC/DC converters will be required for interconnecting the DC links. In addition to HVDC network interconnection, DC/DC converters can also be employed in various HVDC applications, such as HVDC tapping, power flow control and fault interruption [27, 53]

High voltage, high power DC/DC converters can be classified into different categories based on different considerations [53, 54]. As shown in Fig. 2.13, the primary classification of galvanic isolation is considered. Several DC/DC converter designs will be described in more details as follows.

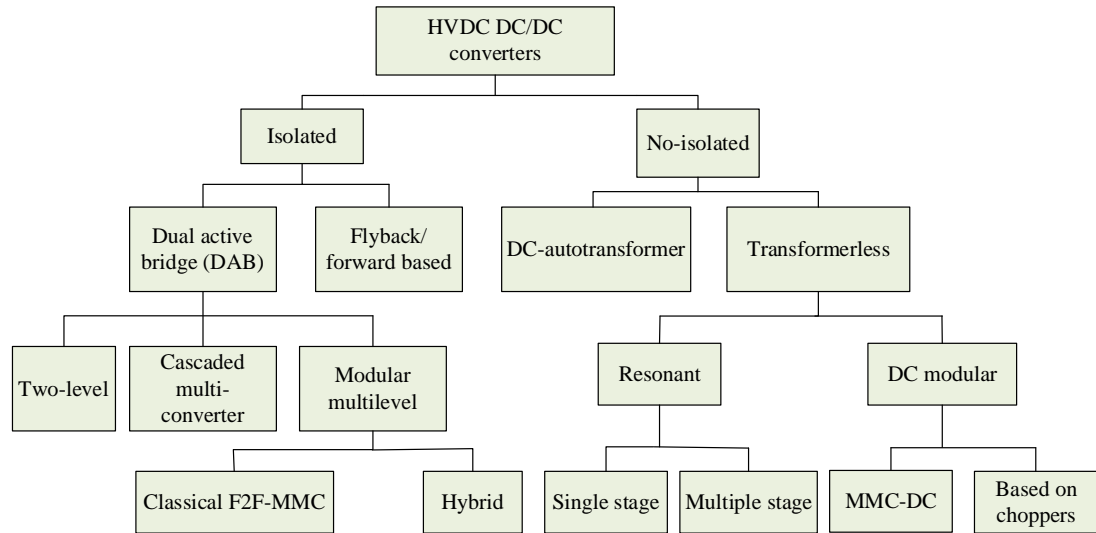


Fig. 2.13 Classification for DC/DC converters for HVDC grids [53].

2.4.1 Isolated topologies of DC/DC converters

The isolated DC/DC converters usually include three stages (DC-AC-DC), and the galvanic isolation is provided at the AC stage through magnetic coupling using coupled inductors or AC transformers. The main benefits of isolated DC/DC converters include:

- Achieve high voltage stepping ratio with cost-effective design.
- No ground current between the two DC systems.
- Different grounding schemes offering easy interconnection between two DC grids.
- Inherent fault blocking capability.

Dual active bridge (DAB) which consists of two 2-level VSCs interconnected with a transformer, as shown in Fig. 2.14 (a), is the most popular isolated topology [55]. However, the main drawbacks of DAB converters are the reduced efficiency by circulating power and additional core losses of the high-frequency transformers.

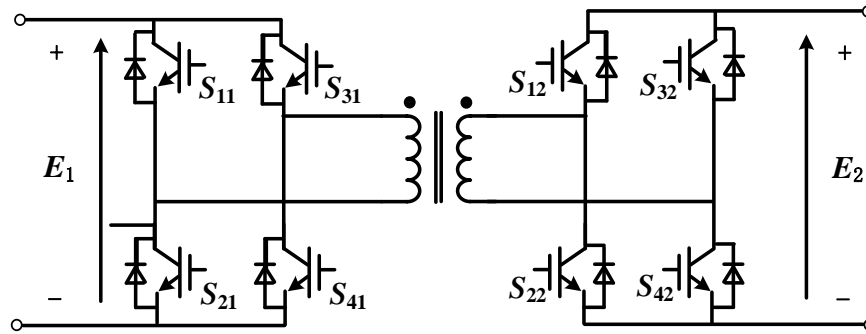


Fig. 2.14 Dual active bridge.

A variety of DAB topologies based on modular structures have been introduced for DC network interconnection. Cascaded multi-converter DAB uses low-power, low-voltage DAB converters as elementary cells to produce high DC voltage or current. Furthermore, since every converter cell only handles a small portion of the total power, the current rating of the semiconductors can be decreased [56]. Fig. 2.15 displays the family of cascaded multi-converter DABs in different configurations [57]. The series-connected cell terminals are used to produce high voltage, while the parallel-connected cell terminals are preferred to deal with high DC current. The combination of both schemes can cater to different application demands [57, 58]. However, the fundamental issue of cascaded multi-converter DAB is the high insulation requirement of the transformers, which restricts their utilisation for high voltage applications.

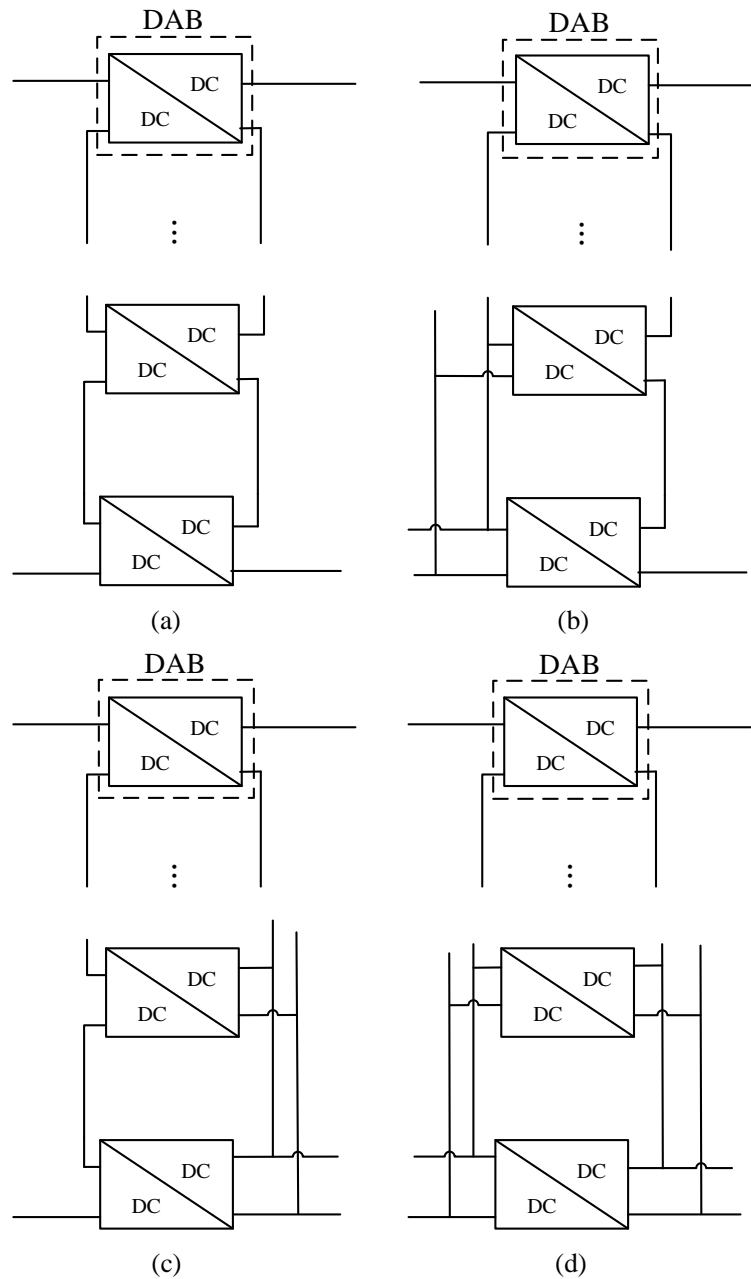


Fig. 2.15 Different possible configurations of cascaded multi-converter DABs: (a) Input Series Output Series (ISOS), (b) Input Parallel Output Series (IPOS), (c) Input Series Output Parallel (ISOP), (d) Input Parallel Output Parallel (IPOP).

Instead of using modular converters connected in series and parallel, the F2F converters using MMCs (or F2F-MMCs) are another isolated approach with modular structures for high power applications [59]. It consists of two MMCs and an AC

transformer, as shown in Fig. 2.16 (a). These topologies acquire the advantages of the MMC, thereby high-voltage and high-power rating requirements can be promptly fulfilled. In addition, since the AC link is internal to the F2F system, medium frequency operation is applicable to reduce the size of the transformer, passive elements and SM capacitors [60, 61]. Fig. 2.16 (b) shows a generated waveform of F2F-MMCs based on the quasi two-level (Q2L) operation [61]. Q2L operation of multilevel converters controls the MMC as a two-level converter, while the SM capacitors of the MMCs are used as a clamping circuit. With the short duration of intermediate voltage level (5 to 25 μ s), the energy storage requirement of the SM capacitors and MMC footprint could be reduced. This potentially makes the F2F-MMC with Q2L mode more suitable for DC/DC converters for multi-terminal HVDC networks [54]. The main drawback of the Q2L operation is the narrowed modulation index range (between 0.81 and 1.27 due to the Q2L feature) [61]. Although this range can be extended by auxiliary techniques [62], the switching losses will increase if the modulation index is too low.

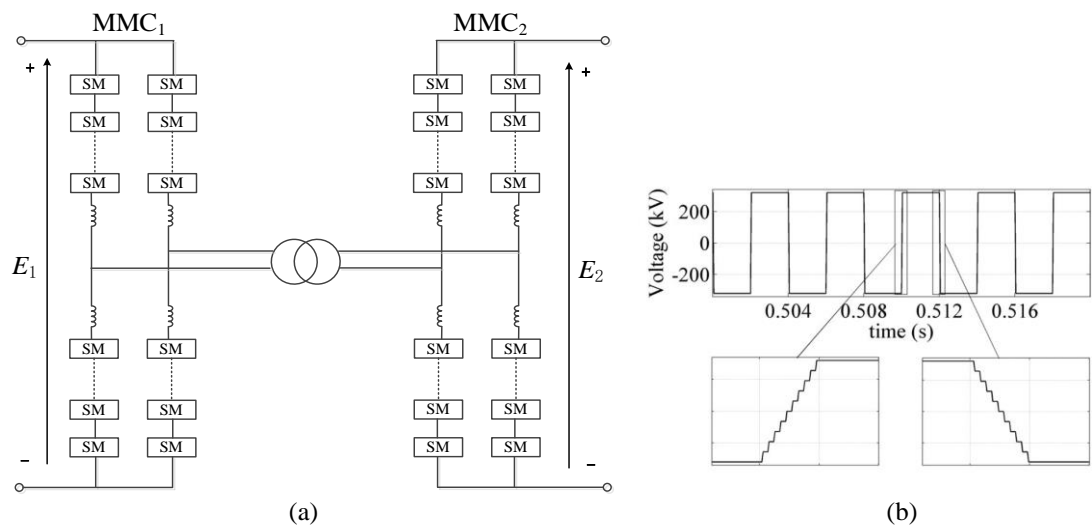


Fig. 2.16 Modular multilevel DABs (F2F-MMCs):

(a) Topology, (b) Quasi two-level operation [61].

To reduce the size and cost of F2F-MMCs, some hybrid versions have also been introduced by replacing some SMs with transistor valves [63, 64]. Fig. 2.17 shows two

F2F-MMCs with different hybrid topologies. Fig. 2.17 (a) shows the alternative arm converter (AAC) based F2F-MMC, which uses series-connected transistor valves to reduce the required number of FBSMs [63]. The transition arm converter (TAC) based F2F-MMC is shown in Fig. 2.17 (b) [64]. As can be seen, compared to the conventional F2F-MMC, the HBSMs of the upper arms (also applicable for lower arms) are replaced by transistor valves.

In these hybrid topologies shown in Fig. 2.17, the SMs improves waveforms and achieves valve soft-switching. Also, dv/dt on the transformer is reduced. The transistor valves regulate the arm current path and decreases conduction losses. Due to the operational difference from conventional MMCs, these hybrid topologies require specific controls and balancing approaches [63, 64].

Nevertheless, even in the hybrid versions of F2F-MMCs, the size and cost are still considerable since two fully rated MMCs are required [53].

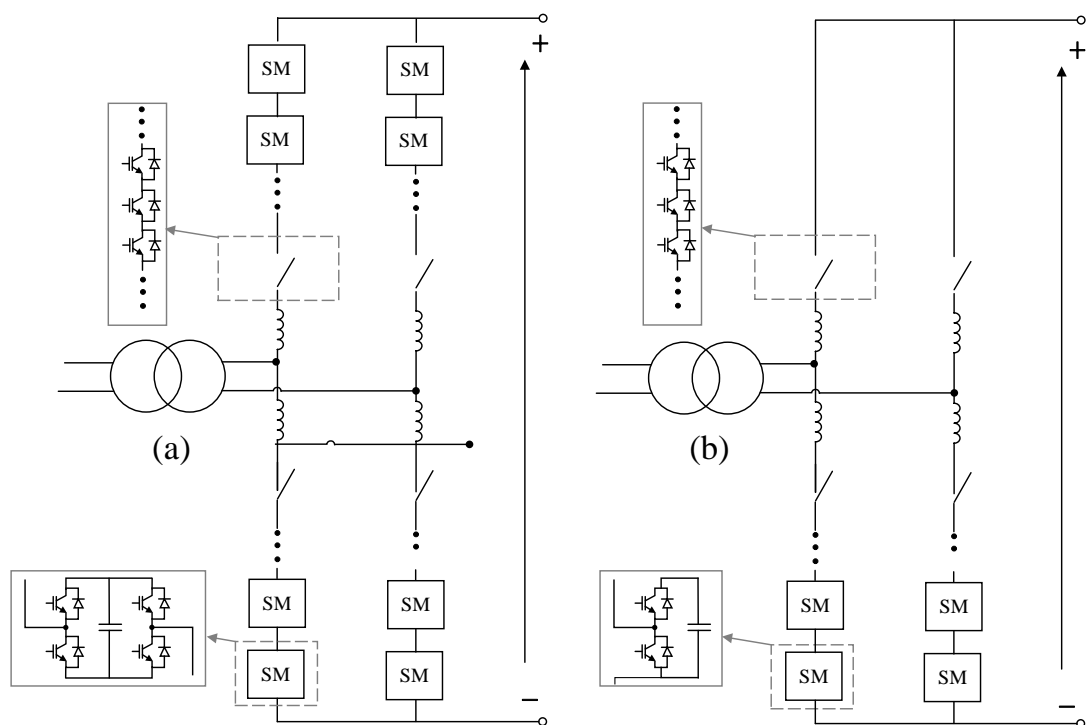


Fig. 2.17 Hybrid F2F-MMCs: (a) the AAC [63], (b) the TAC [64].

2.4.2 Non-isolated topologies of DC/DC converters

The isolated DC/DC converters require two AC/DC conversion stages, resulting in higher overall converter power rating and operating power loss. The non-isolated DC/DC converters without complete DC-AC-DC conversion have been presented as an efficient alternative.

Among the wide range of non-isolated topologies, the HVDC autotransformer (DC AUTO) is one of the most attractive and feasible non-isolated DC-DC converters [65-69]. As shown in Fig. 2.18, in a DC AUTO, two MMC converters are connected in series at the DC side and interconnected through an AC transformer at the AC side. Therefore, part of the DC power is transferred through the direct electrical connection between the interconnected converters, leading to reduced overall converter capacity, transformer rating and power losses. Moreover, with the use of FBSMs, DC AUTO can provide DC fault blocking capability [66, 67]. However, these advantages gradually weaken with the increase of the DC voltage stepping ratio, as the HBSMs need be replaced by full-bridge or self-blocking counterparts to achieve bidirectional fault blocking capability, which increase costs and losses [65, 69].

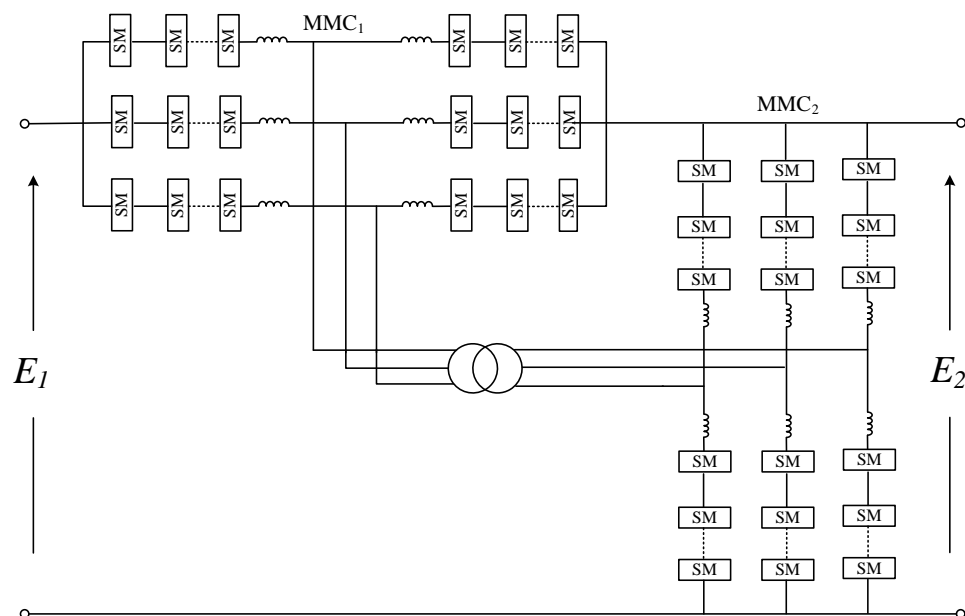


Fig. 2.18 HVDC autotransformer.

From the DC AUTO concept, several alternative unidirectional topologies for specific applications have been proposed to further minimise the costs and losses, such as the VSC-LCC and VSC-DR [67, 70]. Fig. 2.19 shows four possible hybrid topologies of the DC AUTO composed of MMC-LCC or MMC-LCC. Topologies shown in Figs. 2.19 (a) and (b) can achieve unidirectional power transfer from E_1 to E_2 , where LCC or DR is adopted in the middle and side of a rectifier direction, respectively. Unidirectional power transfer from E_2 to E_1 can be realised by the other topologies shown in Figs. 2.19 (c) and (d), where LCC is adopted in the middle and side of a inverter direction, respectively.

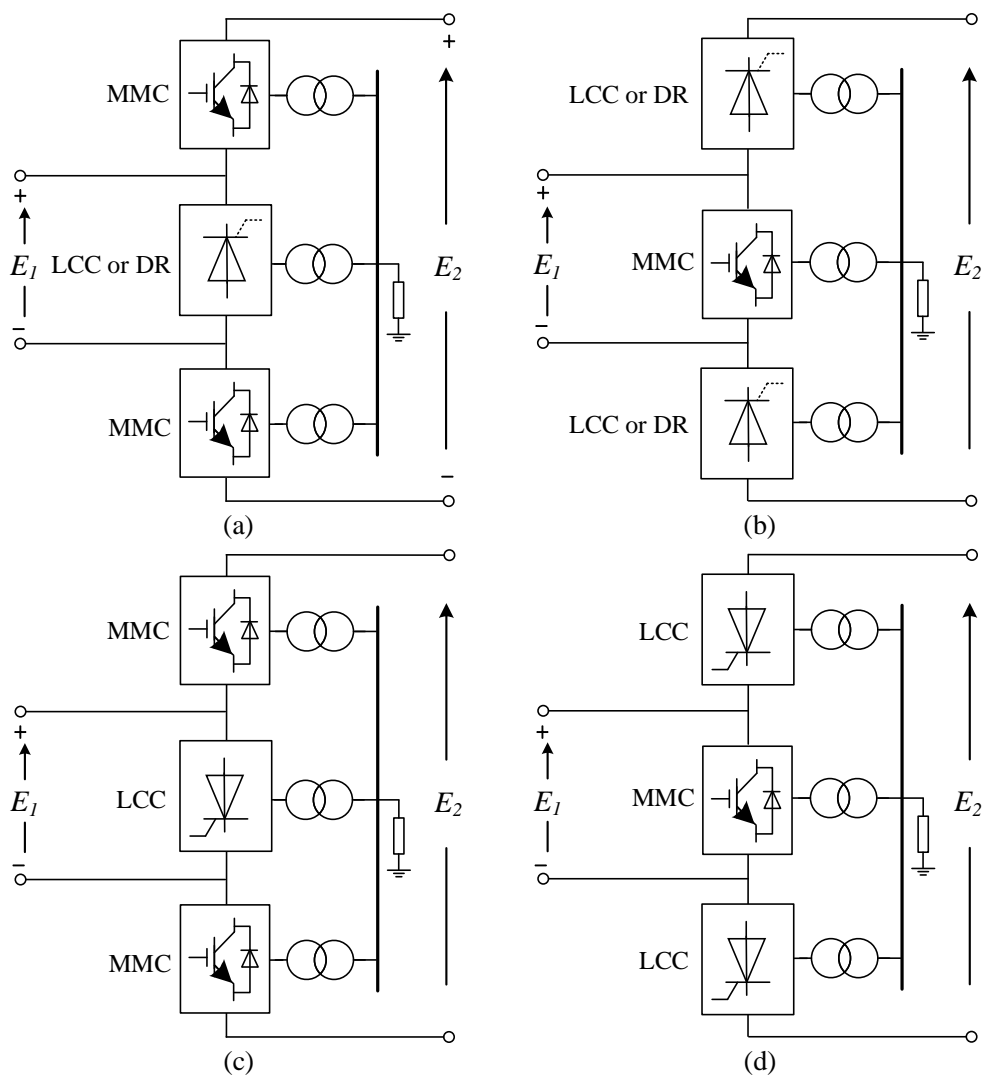


Fig. 2.19 Hybrid topologies of the DC AUTO:

(a) Topology 1, (b) Topology 2, (c) Topology 3, (d) Topology 4.

Since LCC and DR typically have higher power and voltage rating than MMC, the voltage and power ratings of the DC AUTO can be scaled up more easily by using DR or LCC. Compared to LCC, the use of DR in the DC AUTO can further simplify the topology and improve the efficiency, but sacrifices controllability. Nevertheless, these hybrid DC AUTOs are not suitable for interconnecting DC networks requiring power reversal operation. In addition, different to the classical DC AUTO, the corresponding control principle and fault ride-through of each hybrid topology need to be further investigated.

2.5 Summary

This chapter reviews HVDC technologies, including transmission system configurations, AC/DC converters, hybrid systems and DC/DC converters. The rapid development of renewable energy and decarbonization increasingly requires large scale network interconnection including interconnecting DC networks at different voltage levels. Different types of HVDC converters are introduced, and their superiorities and limitation are presented. Hybrid HVDC systems and DC/DC converters with different converter technologies can potentially improve system capacity, controllability, reliability and efficiency. However, the possibilities of combining MMC, DR, and/or LCC have not been investigated in depth.

Based on the identified challenges and gaps, this thesis focuses on the following three areas in an effort to explore the merits of hybrid converter configuration for efficient integration of renewable energy and DC network interconnection.

Chapter 3 Hybrid LCC-MMC AC/DC Hub

3.1 Introduction

To improve the transmission efficiency, onshore and offshore HVDC systems could be connected to existing DC networks that directly supply load centres. Due to the different voltage ratings between different DC networks, e.g., onshore OHL based LCC-HVDC systems and offshore MMC-HVDC systems, DC-DC converters are required to interconnect the two systems.

As discussed in Chapter 2, high power DC-DC converters can be galvanic isolated or non-isolated. Typical isolated DC-DC converters require two AC/DC conversion stages, resulting in higher converter power rating and operating power loss. Among the non-isolated DC-DC converters, the DC AUTO is an attractive and feasible solutions without full DC-AC-DC conversion, due to its reduced converter capacity and power loss [67]. However, to achieve bidirectional DC fault blocking capability, the half-bridge submodules should be replaced by full-bridge or self-blocking counterparts, resulting in increased cost and power loss [71]. From the DC AUTO concept, several unidirectional topologies for specified applications have been proposed as cost-effective alternatives [70], though they are not suitable for interconnecting DC networks requiring bi-directional power flow operation.

In this chapter, a hybrid LCC-MMC AC/DC hub (LCC-MMC Hub) configuration consisted of LCC and MMC technologies is proposed, for applications such as integrating onshore wind power and interconnecting onshore and offshore DC networks. The system layout and control principle of the proposed LCC-MMC Hub are depicted, and power flow analysis is presented. A comprehensive DC fault protection scheme is investigated and additional bidirectional thyristors associated with coordinated current based DC fault detection algorithm are proposed to protect

the converters during DC faults. Simulation validations of the proposed system on power flow change, DC fault and AC fault responses (including the study of AC fault ride-through capability) are confirmed by numerical simulations in PSCAD/EMTDC.

3.2 System topology and power flow analysis

3.2.1 Envisaged application scenario

Fig. 3.1 illustrates an envisaged application scenario to interconnect onshore and offshore DC networks. An onshore wind farm is integrated with the local AC grid, where an LCC is used to transmit the power to the DC network with a higher-voltage (HV) E_2 . The DC power at the HV side is transmitted to the load centre through long-distance OHLs. The existing offshore DC network with a lower-voltage (LV) E_1 can be interconnected to the onshore DC system to increase system availability. Due to the different DC voltages (E_1 and E_2), a DC-DC converter (shown as the F2F type as an example [72]) is required for this interconnection. A DCCB is also installed between the LCC and MMC_2 for DC fault isolation. Alternative DC-DC converter configurations, e.g. a DC AUTO, might be used instead of the F2F one to reduce converter power rating and power loss. However, additional submodules should be employed in the DC AUTO converters to achieve bidirectional DC fault isolating capability [67].

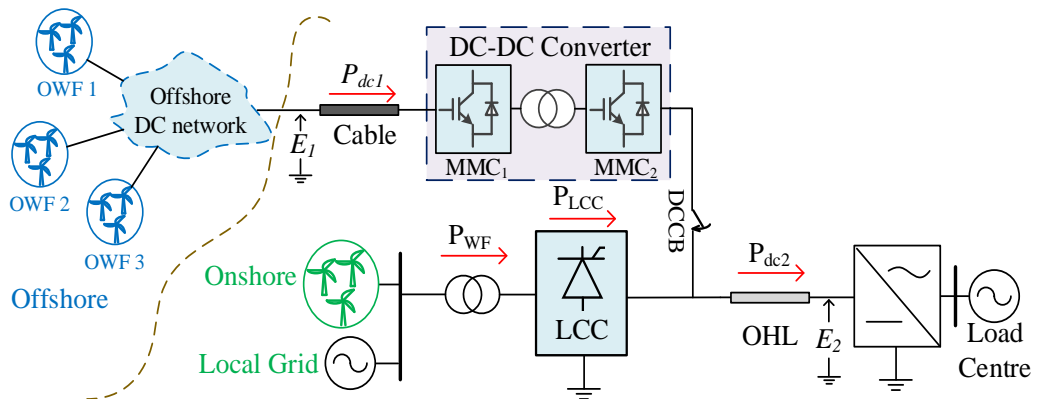


Fig. 3.1 Topology of the envisaged scenario for DC network interconnection.

3.2.1 Topology of the LCC-MMC Hub

Fig. 3.2 shows the simplified diagram of the proposed LCC-MMC Hub for the envisaged application scenario. For the convenience of power flow analysis, the onshore wind farm and the local AC grid is simplified as an AC system (AC_{WF}). The AC terminals of the MMC and LCC are interconnected to the onshore AC system through AC transformers. The offshore and onshore HVDC systems marked as DC systems E_1 and E_2 , respectively, are connected through the DC side of the MMC. The output of the LCC is connected to the DC terminal of E_2 through OHLs. Neglecting the voltage drops on the transmission lines, the DC voltage of the MMC is equal to the voltage difference between E_2 and E_1 under steady state.

Compared with the approach shown in Fig. 3.1, the direct electrical connection between converters is achieved in this hybrid system. The power exchange between E_1 and E_2 can be achieved through the MMC and LCC on the AC side. A DCCB is located between the MMC and LCC terminals for DC fault protection, as will be detailed in Section 3.3.

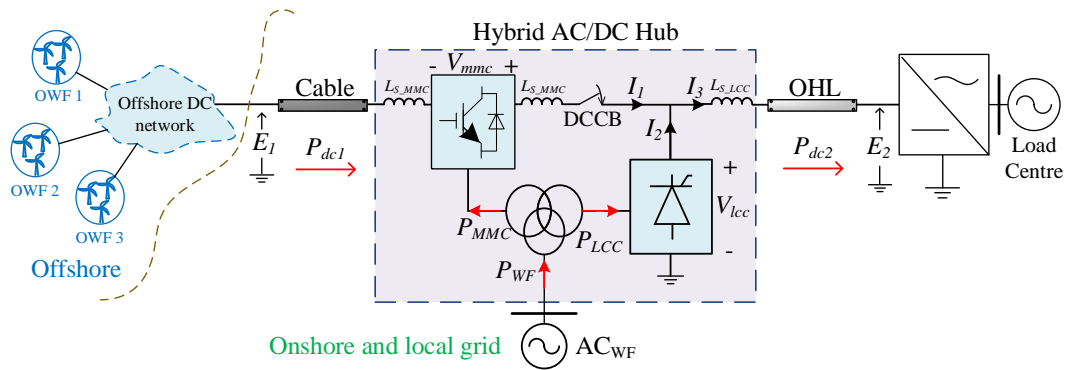


Fig. 3.2 Simplified mono-polar configuration of the proposed LCC-MMC Hub.

3.2.2 Power flow analysis

Taking power transferring from E_1 (LV) to E_2 (HV) as the positive direction, as shown in Fig. 3.2, the DC voltage stepping ratio and power transfer ratio between E_1 and AC_{WF} are defined as:

$$\begin{cases} m = E_2 / E_1, & m > 1 \\ k = P_{dc1} / P_{WF}, & k > 0 \end{cases} \quad (3.1)$$

where P_{dc1} is the active power from LV HVDC system E_1 and P_{WF} is the active power from AC_{WF} . In this study, the range of m is between 1 and 5, and the range of k is between 0 and 3.

Neglecting the power losses of the transmission lines and converters, the total power transferred to the HV side of the HVDC system is:

$$P_{dc2} = P_{dc1} + P_{WF} = (k + 1)P_{WF} \quad (3.2)$$

The DC currents at the LV side and HV side are given respectively as:

$$I_1 = P_{dc1} / E_1, \quad I_3 = P_{dc2} / E_2 \quad (3.3)$$

The DC current of the LCC is:

$$I_2 = I_3 - I_1 = (P_{dc2} / E_2 - P_{dc1} / E_1) \quad (3.4)$$

Neglecting the voltage drop on the DC transmission lines, the DC voltages of the LCC and MMC are:

$$\begin{cases} V_{LCC} = E_2 \\ V_{MMC} = E_2 - E_1 \end{cases} \quad (3.5)$$

Therefore, the active power transferred by the MMC is:

$$\begin{aligned} P_{MMC} &= V_{MMC} I_1 = (E_2 - E_1) \frac{P_{dc1}}{E_1} \\ &= k P_{WF} (m - 1) \end{aligned} \quad (3.6)$$

Similarly, the active power of LCC is:

$$\begin{aligned} P_{LCC} &= V_{LCC} I_2 = V_{LCC} (I_3 - I_1) \\ &= E_2 (P_{dc2} / E_2 - P_{dc1} / E_1) = (k + 1 - km) P_{WF} \end{aligned} \quad (3.7)$$

The power transferred by the direct electrical connection (without being converted by either the MMC or the LCC) is given as:

$$P_{direct} = E_2 I_1 = mk P_{WF} \quad (3.8)$$

The total converter power rating of the LCC-MMC Hub can be obtained by adding (3.6) and (3.7) as:

$$P_{hybrid} = P_{LCC} + P_{MMC} = P_{WF}. \quad (3.9)$$

The total power transferred by the MMC and LCC can also be obtained from a point of view of active power balance. The active power of AC_{WF} which is equal to P_{WF} , flowing into the MMC and LCC separately, as shown in Fig. 3.2.

For comparison, the total converter power rating of the “conventional” F2F DC network interconnection as shown in Fig. 3.1 is given as:

$$P_{F2F} = 2P_{dc1} + P_{WF} = (2k + 1)P_{WF} > P_{hybrid} \quad (3.10)$$

Alternatively, if the F2F DC-DC converter in Fig. 3.1 is replaced by the DC AUTO based on [67], the total converter power rating is given as:

$$P_{AT} = 2kP_{WF}(1-1/m) + P_{WF} = (2k+1-2k/m)P_{WF} > P_{hybrid} \quad (3.11)$$

It is shown from (3.10) and (3.11) that the total converter power rating of the LCC-MMC Hub is lower than those using DC-DC converters based on either F2F or DC AUTO configurations. Fig. 3.3 compares the total power ratings of the three different designs under different voltage and power ratios m and k . From Fig. 3.3 compares, the efficiency advantage of the proposed LCC-MMC Hub is clearly demonstrated, especially for higher k and m . For example, with $m = 4$ ($E_2 / E_1 = 4$) and $k = 3$ ($P_{dc1} / P_{WF} = 3$), the total converter ratings of the F2F and AUTO schemes are 7 and 5.25 times of that of the proposed LCC-MMC Hub. Alternatively, for $m = 1.5$ and $k = 1$, the total converter ratings of the F2F and AUTO schemes are 5 and 2.33 times of that of the proposed LCC-MMC Hub.

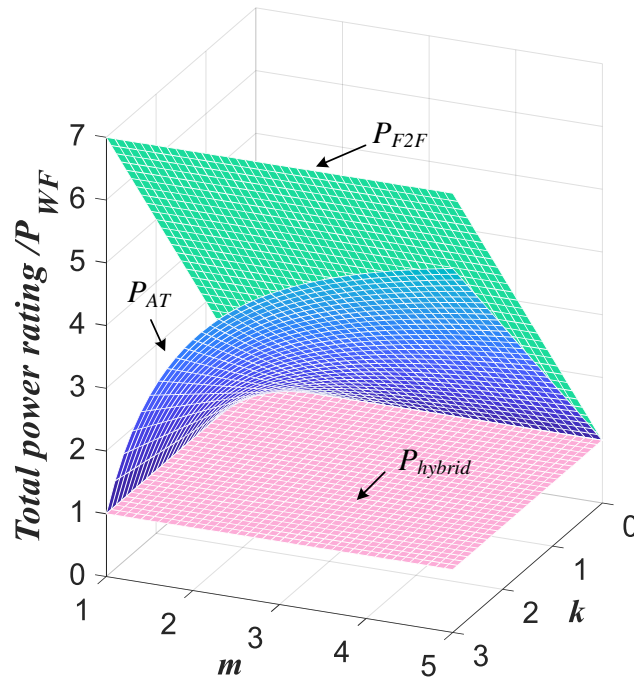


Fig. 3.3 Relationship of total power ratings for different operation scenarios with different power ratio k and DC voltage ratio m .

In addition, converter cost and power loss of LCC for high power schemes are lower than those of MMC [73]. According to (3.6) and (3.7), when k is fixed, lower m

leads to smaller MMC and larger LCC, which would lead to higher overall efficiency and lower cost of the LCC-MMC Hub. The power loss calculations considering the MMC topology (e.g. the number of HBSMs and FBSMs) will be presented in Section 3.4.

3.2.3 Power reversal to the offshore HVDC system.

Power reversal to the offshore HVDC system may be required for the start-up of the offshore DC network, as well as providing power supply to other loads in the offshore system during wind farm shutdown or low wind condition.

Depending on the power flow direction of the HV side, Fig. 3.4 shows power transmitted to the offshore LV side of the LCC-MMC Hub in two scenarios. As the active power of the LCC can only keep the same direction, it has to continuously receive power from the AC network connecting to the MMC and the onshore AC system. The reversed power to the LV side can be expressed by rewriting (3.6), as:

$$P_{dc1} = E_1 I_1 = E_1 \left(\frac{P_{MMC}}{E_2 - E_1} \right) \quad (3.12)$$

Equation (3.12) indicates that the reversed power will be limited by the MMC's power ratings. As shown in Fig. 3.4, the red arrows show that both the WF/LCC and onshore HVDC (E_2) networks feed power to the LV side (i.e. $P_{dc1} = P_{LCC} + P_{dc2}$), whereas the green dotted arrows show the case when the LCC supplies power to both the LV and HV sides (i.e. $P_{dc1} = P_{LCC} - P_{dc2}$).

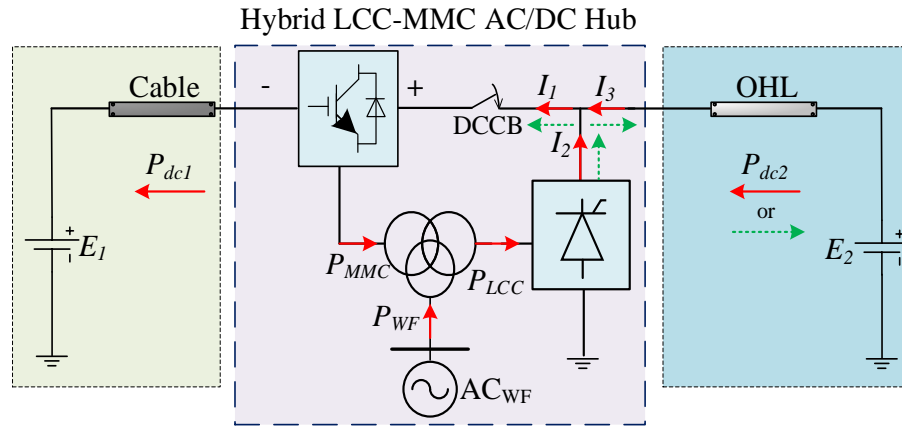
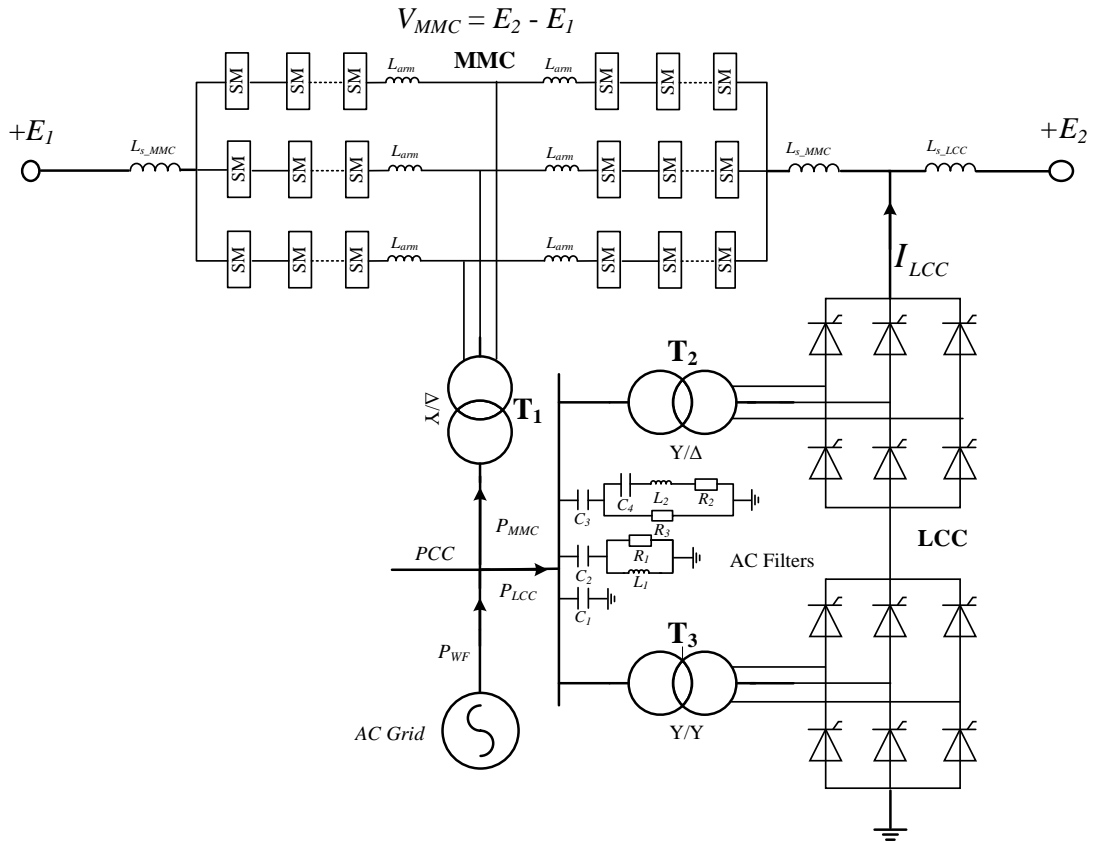


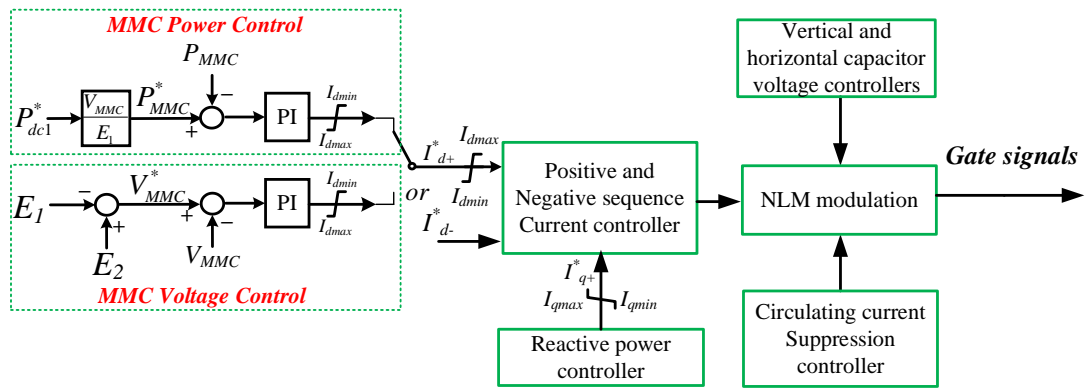
Fig. 3.4 Current and power directions in two power reversal situations:
 E_2 transmits power and E_2 receives power (green dotted arrows).

3.3 Control principles

The layout and control principles of the proposed LCC-MMC Hub are shown in Fig. 3.5. As shown in Fig. 3.5 (a), each arm of the MMC constitutes an arm inductor and a number of submodules (SMs) which can be half-bridge sub-modules (HBSMs), full-bridge sub-modules (FBSMs) or combination of them (hybrid scheme). The LCC rectifier is composed of two six-pulse thyristor bridges in series with two corresponding transformers to form a 12-pulse converter configuration. AC filters are used to absorb AC side harmonics and to supply reactive power to the converter. DC smoothing reactors of the LCC and MMC are used to suppress the rise rate of current during DC faults. In order to simplify the control system design, the impact of MMC and LCC interaction within the proposed system is minor. This research adopts control system based on the above assumption, which can lead to acceptable control system to meet most operation cases.



(a)



(b)

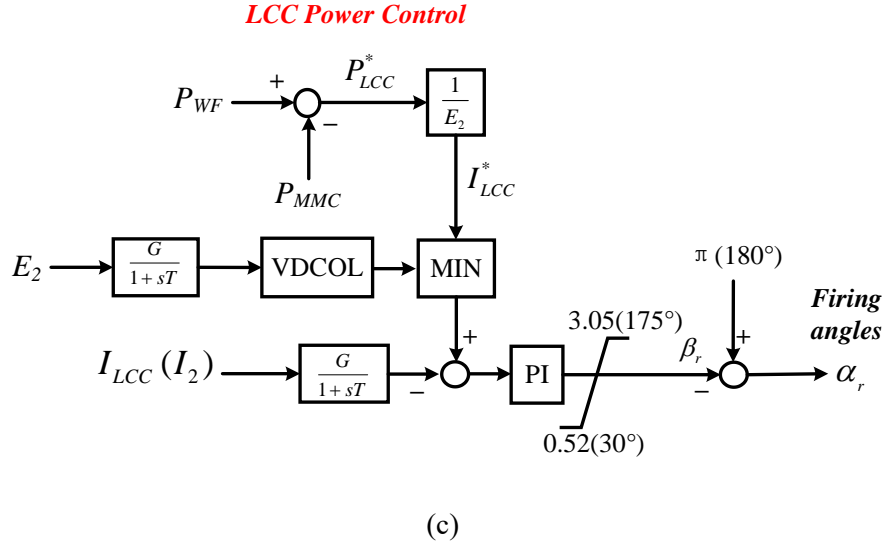


Fig. 3.5 System layout and control of the LCC-MMC Hub:
(a) Layout of the LCC-MMC Hub, (b) Control of the MMC, (c) Control of the LCC.

3.3.1 Control of MMC

Fig. 3.5 (b) shows the block diagrams of the MMC controllers. The inner current controllers usually implemented in the synchronous $d-q$ reference frame generate the required AC components of the arm voltage and limit current contribution in the event of AC faults [74]. To ensure the energy in the individual arms are controlled and balanced, the so-called horizontal and vertical capacitor voltage balancing controllers are implemented [74]. Due to the voltage ripples in the SM capacitors and modulation strategy used, potentially there exist 2nd order current circulating among the arms in the three phases which can cause additional power loss and further impact on SM capacitor voltage ripple. Therefore, a circulation current suppression controller is implemented to suppress the 2nd order harmonic current. Nearest level modulation (NLM) is used to select the SMs to be switched in and out so as to closely resemble the output voltage reference and ensure SM capacitor voltage balance, with reduced switching frequency [75]. The PI compensator parameters for the outer loop controller, inner current controller and circulation current suppression controller were calculated based on [76].

For the different control arrangements of the offshore DC network, the MMC can operate in two different control modes. If the DC voltage of the LV side E_1 is controlled by the offshore DC network, the MMC power control is used to regulate the transmitted DC power from the LV side. Alternatively, if the transmitted DC power from the LV side P_{dcl} is regulated by the offshore system, the MMC voltage control is activated to control the DC voltage of the LV side. As seen in Fig. 3.5 (b), the output active power / DC voltage loops generate the positive sequence d -axis current order for the inner current loop of the MMC. Similarly, MMC's reactive power exchange with the connected AC network can also be regulated to provide reactive power compensation for the LCC. Thus, the outer reactive power controller produces the positive sequence q -axis current order based on the reactive power requirement. The negative sequence current orders can be simply set at zero or other value based on the condition of the connected AC network [77]. Since it is not the focus of the thesis, no further description is provided here. As described above, both positive and negative sequence currents are regulated in the inner current controllers.

3.3.2 Control of LCC

Considering the HV DC voltage E_2 is regulated by the other part of the DC network, the LCC rectifier station controls the DC current to regulate the active power transmission from the AC to the DC network. Using the power direction definition shown in Fig. 3.2, the active power order of the LCC is the power difference between the required power transmission from the onshore AC system P_{WF} and active power absorbed by the AC side of the MMC which can be measured real-time. As shown in Fig. 3.5 (c), the desired LCC power is then regulated by its DC current I_{LCC}^* using Constant Current Control (CCC) with Voltage-Dependent Current Order Limiter (VDCOL). In normal operation, the CCC compares the measured DC current I_{LCC} and I_{LCC}^* to produce the error signal, which is fed to the PI controller to produce the desired firing angle order α for the LCC. The VDCOL is added as an auxiliary control during

fault conditions as will be discussed in Section 3.4. When the DC voltage of LCC drops to a certain threshold, the DC current is lowered to improve DC voltage recovery and reduced the absorbed reactive power [78].

3.4 DC fault protection

3.4.1 System behaviour during DC fault

In the event of a DC fault on either side of the LCC-MMC Hub, similar to the DC AUTO, the fault current could feed from the healthy DC side into the faulty DC side [66]. If the MMC in the LCC-MMC Hub is designed to block DC faults using HBSMs and FBSMs, it has to provide the full HV side DC voltage in the event of a LV side fault to interrupt the fault current from the HV side, as shown in Fig. 3.6 (a). The power from the onshore wind farm can be transferred through the LCC to E_2 . Similarly, Fig. 3.6 (b) shows that the MMC has to support the full LV side DC voltage to interrupt the fault current from the LV side, in the event of a DC fault on the HV side. The power flow of the onshore wind farm is blocked. The LCC has no influence during DC fault on either side, as it can eliminate its DC current by simply increasing the firing angle. Therefore, additional FBSMs should be inserted into the MMC depending on the voltage ratio m .

If DCCBs are used to isolate DC faults, the MMC will still need to be blocked to protect IGBTs from overcurrent, and to diverge the fault current to the freewheeling diodes. Thus, a comprehensive DC fault protection is required to protect the whole system.

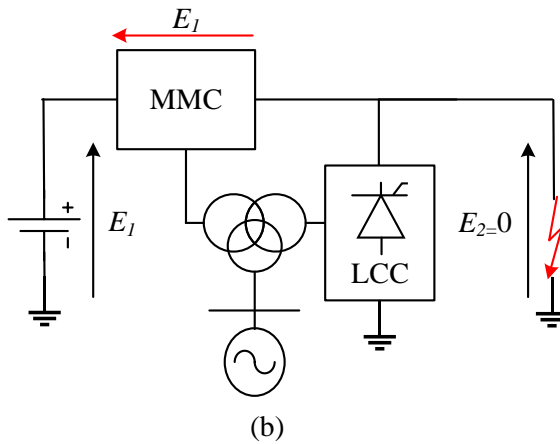
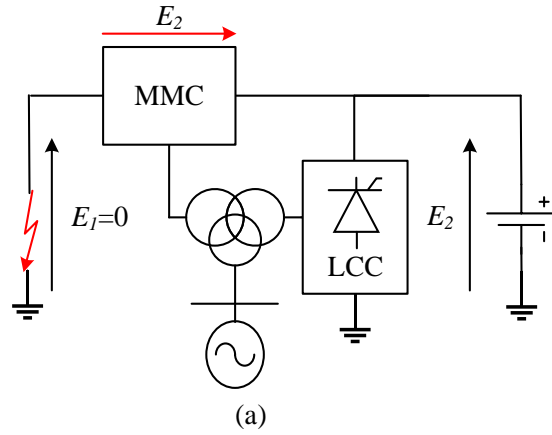


Fig. 3.6 Performance of MMC blocking during different DC faults:

(a) LV DC side fault, (b) HV DC side fault.

3.4.2 DC fault protection analysis and power loss estimation

A hybrid MMC that is composed of HBSMs and FBSMs, can be used to interrupt DC faults on either LV or HV side. Neglecting the voltage drops across the DC lines, the required capacitor voltages of the SMs and FBSMs in each arm ($V_{arm_SM}^R$ and $V_{arm_FBSM}^R$) to isolate DC faults, and the DC voltage rating of the MMC in each arm (V_{arm_SM}) without DC fault considerations are expressed as:

$$\begin{cases} V_{arm_SM}^R = \frac{E_2}{2} = \frac{mE_1}{2} \\ V_{arm_FBSM}^R = \frac{E_1}{2} \\ V_{arm_SM} = (m-1)E_1 \end{cases} \quad (3.13)$$

Based on (3.6) and (3.13), to isolate LV side faults, the required number of FBSMs (N_{FB}^R) in each arm of the hybrid MMC are calculated as:

$$N_{FB}^R = \frac{V_{arm_FBSM}^R}{V_{arm_SM}} N_{SM} = \frac{1}{2(m-1)} N_{SM} \quad (3.14)$$

Where N_{SM} is the SM number of each MMC arm MMC without DC fault considerations.

For LV side faults, if $V_{arm_SM}^R > V_{arm_SM}$ (i.e. $m < 2$), additional HBSMs should be inserted into each arm of the MMC to increase its voltage rating to $E_1/2$ in order to avoid MMC submodule overvoltage. The required number of HBSMs (N_{HB}^R) in each arm of the hybrid MMC with different m is given as:

$$N_{HB}^R = \begin{cases} \left(\frac{V_{arm_SM}^R}{V_{arm_SM}} - \frac{V_{arm_FBSM}^R}{V_{arm_SM}} \right) N_{SM} = \frac{1}{2} N_{SM}, m < 2 \\ \left(1 - \frac{V_{arm_FBSM}^R}{V_{arm_SM}} \right) N_{SM} = \frac{2m-3}{2(m-1)} N_{SM}, m \geq 2 \end{cases} \quad (3.15)$$

If the power losses of the LCC, HBSMs and FBSMs denoted as η_{LCC} , η_{HB} and η_{FB} . the estimated power loss of the LCC-MMC Hub with hybrid MMC to isolate DC faults (η_{hybrid}^R) can be obtained as:

$$\eta_{hybrid}^R = \frac{\left(\eta_{FB} \frac{N_{FB}^R}{N_{SM}} + \eta_{HB} \frac{N_{HB}^R}{N_{SM}} \right) P_{MMC} + \eta_{LCC} P_{LCC}}{P_{dc1} + P_{WF}} \quad (3.16)$$

The estimated power loss of the LCC-MMC Hub with standard HB-MMC (η_{hybrid}) is given as:

$$\eta_{hybrid} = \frac{\eta_{HB} P_{MMC} + \eta_{LCC} P_{LCC}}{P_{dc1} + P_{WF}} \quad (3.17)$$

References [35] and [79] indicate that the valve power losses of the LCC, HBSMs and FBSMs are approximately 0.26%, 0.6% and 1.1%, respectively. Therefore, if k is fixed to 1, (3.16) and (3.17) can be rewritten as, respectively:

$$\eta_{hybrid(k=1)} = (0.17m - 0.04)\%, \quad \eta_{hybrid(k=1)}^R = \begin{cases} (0.02m + 0.385)\%, & m < 2 \\ (0.17m + 0.085)\%, & m \geq 2 \end{cases} \quad (3.18)$$

According to (3.18), the power loss comparison of different LCC-MMC Hubs when $k = 1$ is shown in Fig. 3.7, where the red line is η_{hybrid} and the blue line is η_{hybrid}^R . As can be seen from Fig. 3.7, the difference between η_{hybrid} and η_{hybrid}^R is always the same when k is fixed and $m > 2$. However, η_{hybrid}^R becomes much higher than η_{hybrid} when $m < 2$. For example, if $m = 1.5$, the power loss of the LCC-MMC Hub with hybrid MMC for isolating DC faults is 0.425%, being 93% higher than that with conventional HB-MMC, which is 0.215%. Based on these, the LCC-MMC Hub with hybrid MMC is not a good option if m is small, which could lead to high loss and cost due to additional SMs required to isolate DC faults.

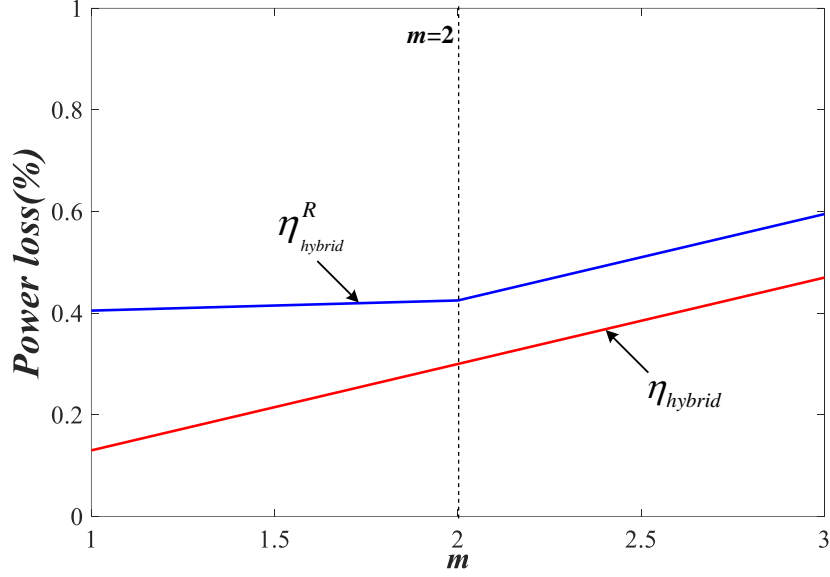


Fig. 3.7 Power loss comparison of different LCC-MMC Hubs with conventional HB-MMC or hybrid MMC.

In terms of other DC network interconnection methods using DC-DC converters, the power loss of the F2F scheme for different voltage ratio m remains the same due to its isolated configuration when considering DC faults. However, the total converter rating of the non-isolated DC AUTO scheme will increase similarly to the LCC-MMC Hub for isolating DC faults. Therefore, the estimated power losses of the F2F scheme (η_{F2F}) and DC AUTO scheme (η_{AT}^R) when $k=1$ can be calculated as, respectively:

$$\eta_{F2F(k=1)} = \frac{2\eta_{HB} + \eta_{LCC}}{2} = 0.73\%, \quad \eta_{AT(k=1)}^R = \begin{cases} \left(\frac{0.43m + 0.25}{m} \right) \%, & m < 2 \\ \left(\frac{0.73m - 0.35}{m} \right) \%, & m \geq 2 \end{cases} \quad (3.19)$$

The power losses of the different connection scenarios with different m when $k = 1$ are demonstrated in Fig. 3.8. As can be seen, the estimated power loss of the F2F scheme (η_{F2F}) is constant with different m values, while DC AUTO scheme (η_{AT}^R) is generally lower than that of the F2F scheme. In general, the power loss of the LCC-MMC Hub with hybrid MMC for isolating DC faults (η_{hybrid}^R) is lower than that of the

DC AUTO scheme when m is less than 3.1, while the power loss of LCC-MMC Hub with standard HB-MMC (η_{hybrid}) is the lowest among all the schemes when m is between 1 and 4.

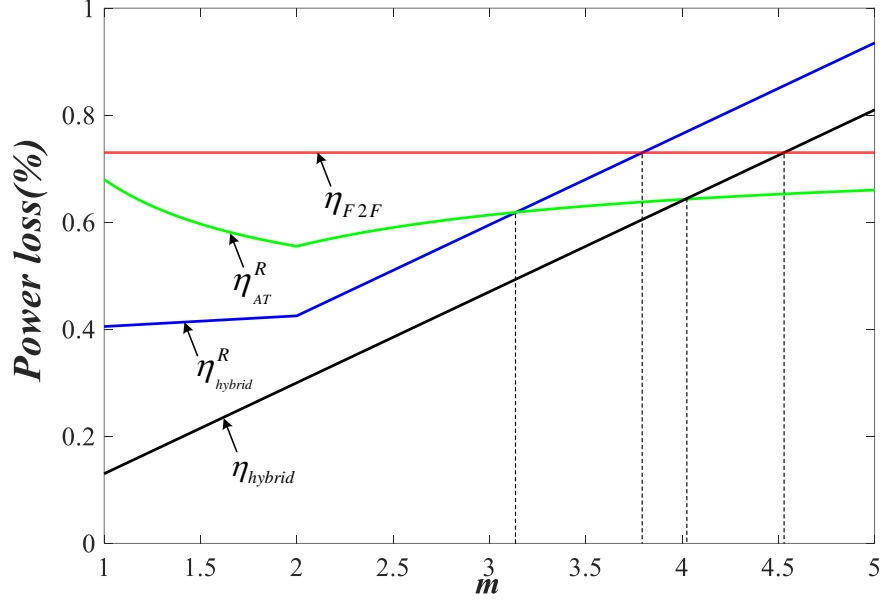


Fig. 3.8 Power loss comparison of different connection scenarios with different m ($k = 1$).

With different power transfer ratio k and fixed DC voltage ratio m ($m = 2$), the estimated power losses of the different connection scenarios can be obtained as, respectively:

$$\left\{ \begin{array}{l} \eta_{hybrid(m=2)} = \frac{(0.59k - 0.26)}{k + 1} \% \\ \eta_{hybrid(m=2)}^R = \frac{(0.34k - 0.26)}{k + 1} \% \end{array} \right\}, \left\{ \begin{array}{l} \eta_{F2F(m=2)} = 1.2k + 0.26\% \\ \eta_{AT(k-1)}^R = 0.85k + 0.26\% \end{array} \right. \quad (3.20)$$

According to (3.20), the power losses of the different connection scenarios with different k when $m = 2$ are displayed in Fig. 3.9. The power losses of the proposed hybrid hub schemes are significantly lower than those of the F2F and DC AUTO schemes in most k ranges. The LCC-MMC Hub with hybrid MMC shows higher power losses than that with standard HB-MMC. Also, an increased k leads to more efficient

operation for the proposed converter schemes, due to the higher power ratio of the LCC within the system. Thus, compared to the “conventional” interconnection approach using DC/DC converters, in the proposed hybrid system, part of the power from the offshore DC network can be transmitted to the onshore DC network directly, therefore, significantly reducing the costs and power losses of converters.

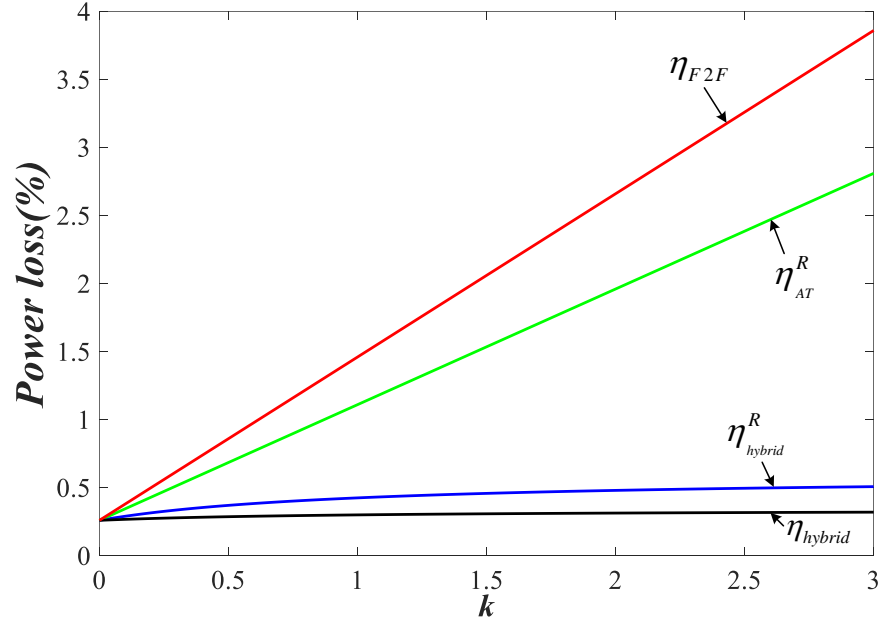
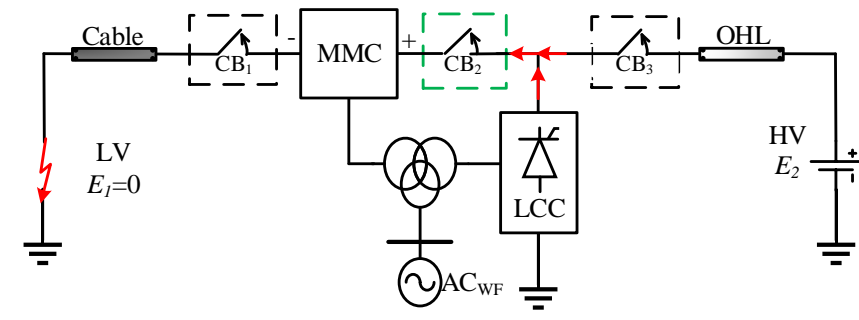


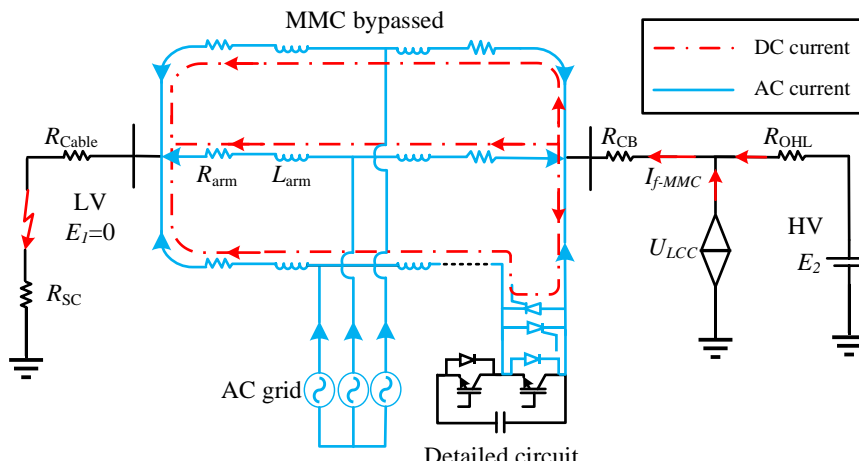
Fig. 3.9 Power loss comparison of different connection scenarios with different k ($m = 2$).

Based on the above analysis, the proposed system with hybrid MMC will result in higher losses. Instead, DCCBs can be used and the MMC can be bypassed during DC faults. Thus, the standard MMC with only HBSMs will be employed in this chapter.

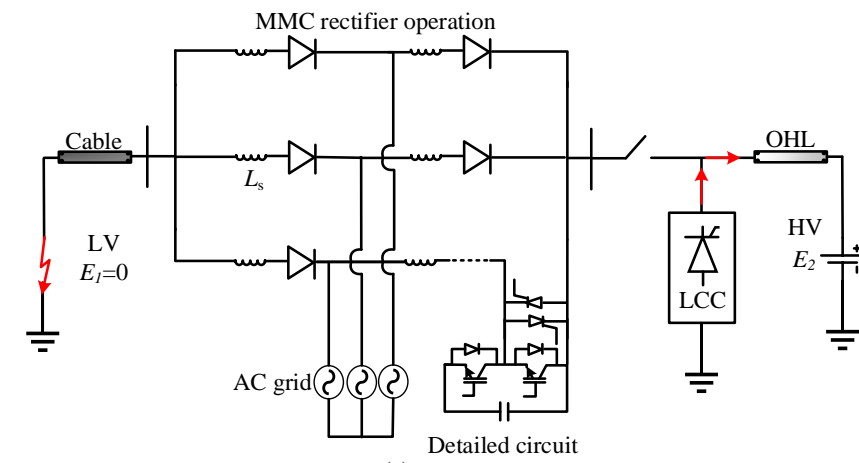
In order to quickly interrupt the DC fault current, hybrid DCCB is considered here [80]. Fig. 3.10 (a) shows three possible locations for installing the DCCB (CB_1 , CB_2 and CB_3). CB_3 is not recommended as the LCC will be prevented from transmitting power to E_2 during E_1 fault after fault isolation by the DCCB. CB_1 and CB_2 have the same effect on the DC fault isolation due to the series connection. Therefore, the CB_2 is chosen as an example in this chapter.



(a)



(b)



(c)

Fig. 3.10 Equivalent circuits of the system and MMC during E_1 fault

In the event of LV side DC faults, the bidirectional thyristors paralleled with each SM are turned on to bypass the MMC and commutate the fault currents to flow through them, as shown in Fig. 3.10 (b), where a representative circuit of one SM is given. In

addition, the MMC capacitor voltages remain the same. As shown, the transient fault current following through the MMC (thyristors) is superimposed by DC and AC sides. The fault current contributed by the DC side is large due to the DC voltage difference between the healthy side and the faulty side, which has to be interrupted by the DCCB. The fault current contributed by the AC side of the MMC has been analysed in [81], which only flows through the MMC arms without any influence on the DC side.

After the opening of the DCCB, the DC fault current is interrupted. Then, the firing pulses to the SM bypass thyristors can be blocked and thyristors will be turned off by the AC grid connected to the MMC [81]. The MMC operates as an uncontrolled rectifier, where the DC voltage of the MMC will be rebuilt for potential power recovery as illustrated in Fig. 3.10 (c). The LCC can continue transmitting power to E_2 as shown. Once the DC fault at the LV side is cleared, the DCCB can be re-closed and the MMC can be restarted.

In the event of HV side DC faults, once the fault is detected, all the thyristors in the MMC are turned on. The fault clearance procedure of the MMC and DCCB is the same as the one on the LV side. However, different from the LV side DC fault, the firing angle of the LCC is increased to limit the current in a similar way to DC fault in a conventional LCC HVDC system [82].

3.4.3 Principle of coordinated current protection

A method of coordinated current protection is proposed to accurately detect the fault side and to determine the system operation state. The protection procedure is shown in Fig. 3.11. As indicated in Fig. 3.2, I_1 is the DC current of the MMC and the DCCB, the DC current of the LCC is I_2 , and I_3 is the sum of I_1 and I_2 .

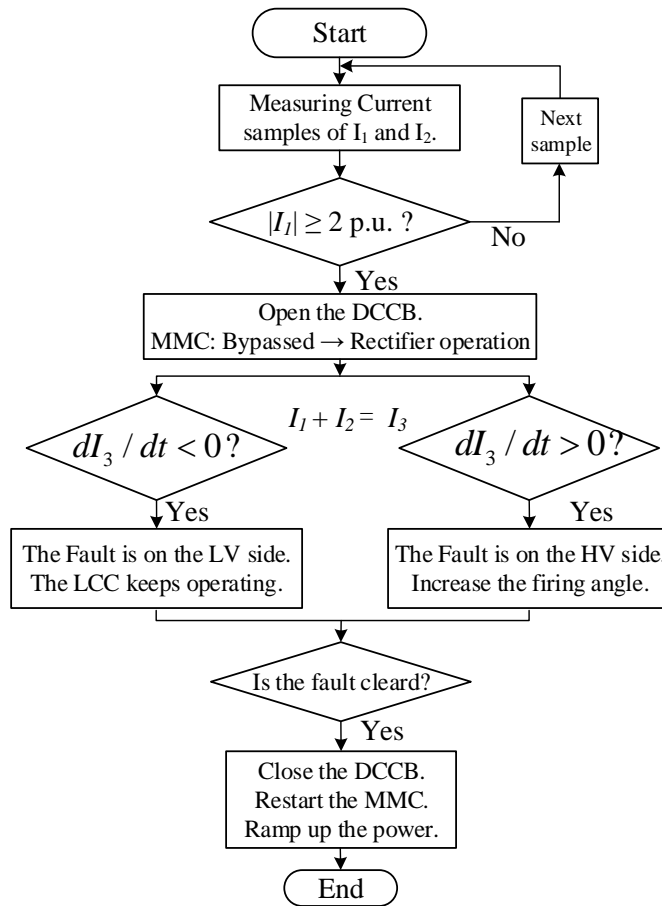


Fig. 3.11 Flow chart of coordinated current protection.

During a DC fault, an opening command is sent to the DCCB once the absolute value of I_1 exceeds twice the rated value. At the same time, the MMC is blocked and the parallel thyristors are turned on. When the DCCB fully opens and the fault current from the LV side I_1 is extinguished, the parallel thyristors are then turned off and MMC behaves as an uncontrolled rectifier. A coordinated current protection is used to identify the fault side by comparing the current derivative value, and will be conducted only after the DCCB receives the opening signal. If $dI_3/dt < 0$, the fault is on the LV side, the LCC can remain in normal operation to transfer the power from the AC side to the HV side. If $dI_3/dt > 0$, the fault is on the HV side, and the LCC should increase the firing angle to extinguish the DC fault current. After the fault is cleared and system recover is required, the DCCB can be reclosed to restart the MMC, the system is recovered by ramping up the power of the LCC and MMC.

3.5 Simulation studies

A simulation model of the circuit shown in Fig. 3.2 is developed in PSCAD/EMTDC to show the operation of the proposed system. The LCC-MMC Hub is rated at 320 kV/500 kV (i.e., $m = 1.56$), the power transferred from AC_{WF} and E_I are rated at 1250 MW and 500 MW (i.e., $k = 0.4$), respectively.

The system parameters are listed in Table 3.1.

Table 3.1 System parameters of LCC-MMC Hub.

| | Parameters | Nominal Value |
|--------------|---|---|
| MMC | Power rating | 300 MW |
| | Rated DC voltage | 180 kV |
| | SM capacitor voltage | 1.83 kV |
| | SM capacitance | 11.5 mF |
| | Arm inductance | 0.0123 H |
| | SM number per arm | 100 |
| | Transformer voltage ratio T_1 | 250 kV/90 kV |
| | DC smoothing reactance L_{s_MMC} | 0.05 H |
| 12-pulse LCC | Power rating | 1000 MW |
| | Rated DC voltage | 500 kV |
| | Transformer voltage ratio $T_2; T_3$ | 250 kV/250 kV; 250 kV/250 kV |
| | DC smoothing reactance L_{s_LCC} | 0.15 H |
| LCC filters | $C_1; C_2$ | 3.342 μ F; 6.685 μ F |
| | $C_3; C_4$ | 6.685 μ F; 74.28 μ F |
| | $L_1; L_2$ | 0.0136 H; 0.1364 H |
| | $R_1; R_2; R_3$ | 83.32 Ω ; 261.87 Ω ; 29.76 Ω |

The 500 kV LCC rectifier is modified from the CIGRE benchmark model [83]. The layout of LCC filters is shown in Fig. 3.5 (a), and their parameters are listed in Table 3.1. The equivalent averaged model is used to model the HB-MMC for faster simulation [84]. The MMC power control is used as the DC voltage of the LV side is given in this simulation test. The 100 km cable and 300 km OHL are modelled using the frequency-dependent model provided by PSCAD/EMTDC. Based on [80], the hybrid DCCB is modelled to quickly interrupt the DC fault.

3.5.1 Normal operation and power reversal

Based on Table 3.1 and Section 3.2.3, the power transfer of the LCC-MMC Hub during normal operation can be up to 500 MW from E_1 (P_{dc1}) and 1250 MW from AC_{WF} (P_{WF}) resulting in a total of 1750 MW to E_2 (P_{dc2}). If the reversal power to E_1 is fully rated at 500 MW, the transferred power from AC_{WF} is 687.5 MW and hence 187.5 MW will be transmitted to E_1 .

Fig. 3.12 shows the system responses under normal operation and power reversal. As shown in Fig. 3.12 (a), the DC power P_{dc1} and P_{wf} ramp up and reach steady state at 1.5 s. At 2.5 s, power reversal is initiated, reaches to the rated reversal values at 3.0 s, and then the power are ramped up again from 3.5 s to the rated normal operation values at 4.5 s.

Fig. 3.12 (b) shows the active power of the converters and wind farms (AC), the total transmitted active power through the LCC and MMC converters is 1250 MW. For comparison, the total active powers are 2250 MW and 1610 MW under the same condition using the F2F DC-DC converter and DC AUTO, respectively.

Figs. 3.12 (c), (d) and (e) show the MMC arm currents, zoomed MMC arm currents and SM capacitor voltages, respectively. It can be seen that they are well

controlled and balanced within their rated values during normal operation and power step changes.

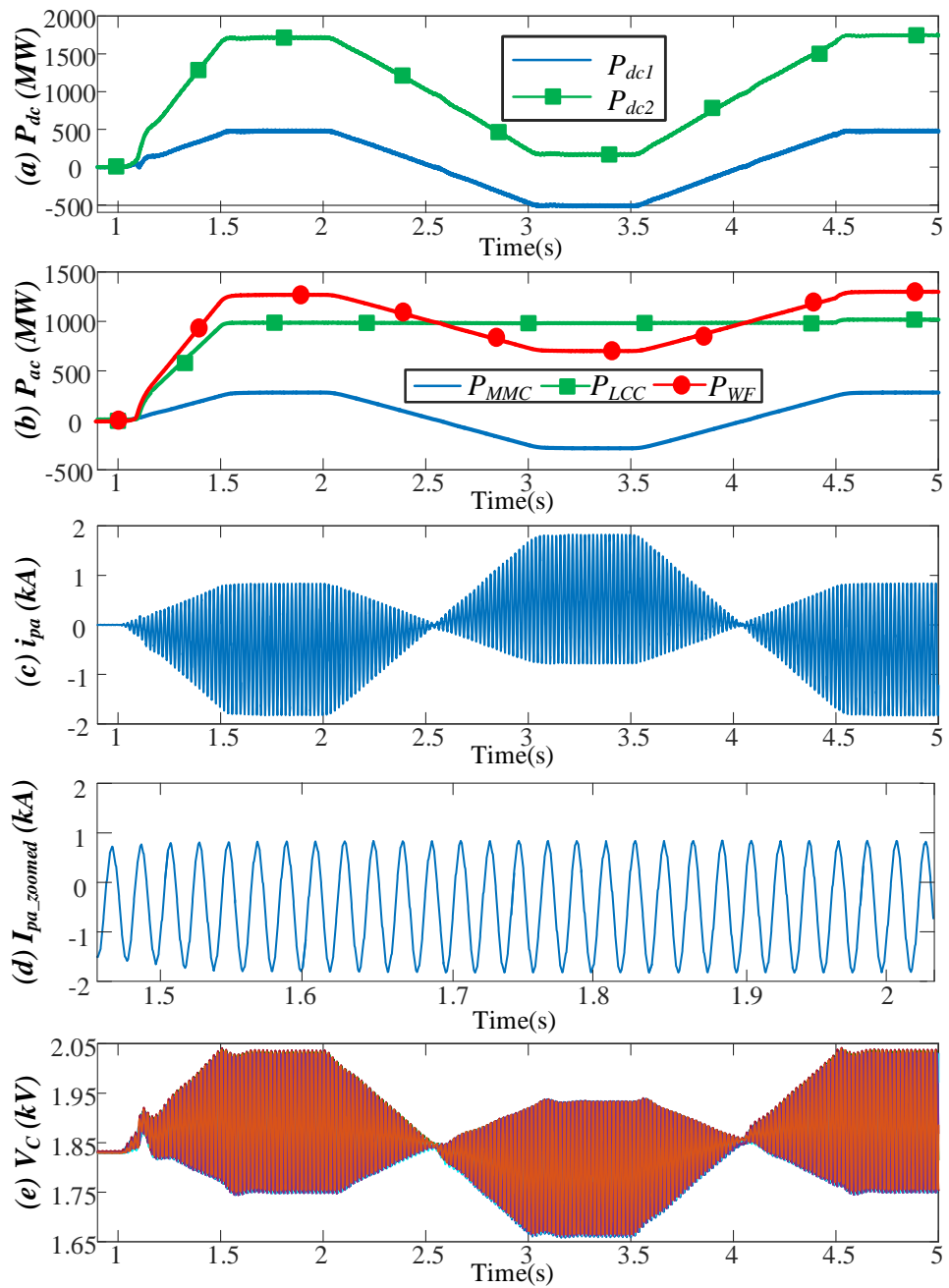


Fig. 3.12 Response to power flow change: (a) DC power of E_1 and E_2 , (b) Active power of converters and wind farm, (c) MMC arm current, (d) Zoomed MMC arm current (e) MMC SM capacitor voltages.

3.5.2 AC fault ride-through

As the MMC and LCC are interconnected to the AC side, system response during AC fault needs to be considered. For the LCC rectifier, AC fault will not lead to overvoltage and/or overcurrent. However, the transmitted active power through the LCC becomes zero during the AC fault which leads to substantial AC voltage drop, but can be restored quickly after the recovery of AC system voltage. On the MMC side, due to the closed-loop current control within the MMC control system, the fault current can be fully controlled, which has been extensively researched [84, 85].

To verify the AC fault ride-through capability of the LCC-MMC Hub, system responses to an AC fault are shown in Fig. 3.13. A temporary three-phase to ground fault is applied at 4.0 s for 200 ms, leading to a significant AC voltage drop as shown in Fig. 3.13 (a). Fig. 3.13 (b) shows the DC voltages of the MMC and LCC, which are remained around the rated values during the AC fault. Fig. 3.13 (c) shows the DC currents of the converters. Due to the voltage drop during AC fault, transferred power is reduced sharply. This causes high di/dt and current oscillation for the transmission line and inductor. The interaction between circuit and converter control leads to the large oscillation of MMC DC current (I_1), which is suppressed by the closed-loop current control. The DC current of the LCC (I_2) is reduced to zero quickly during AC fault. After the fault is cleared, I_1 and I_2 are restored to the pre-fault values at 5.0 s. The arm currents of MMC are also limited by the current control at the occurrence of the AC fault, as shown in Fig. 3.13 (d).

In conclusion, the LCC-MMC Hub can operate securely during AC faults without any specific protection schemes.

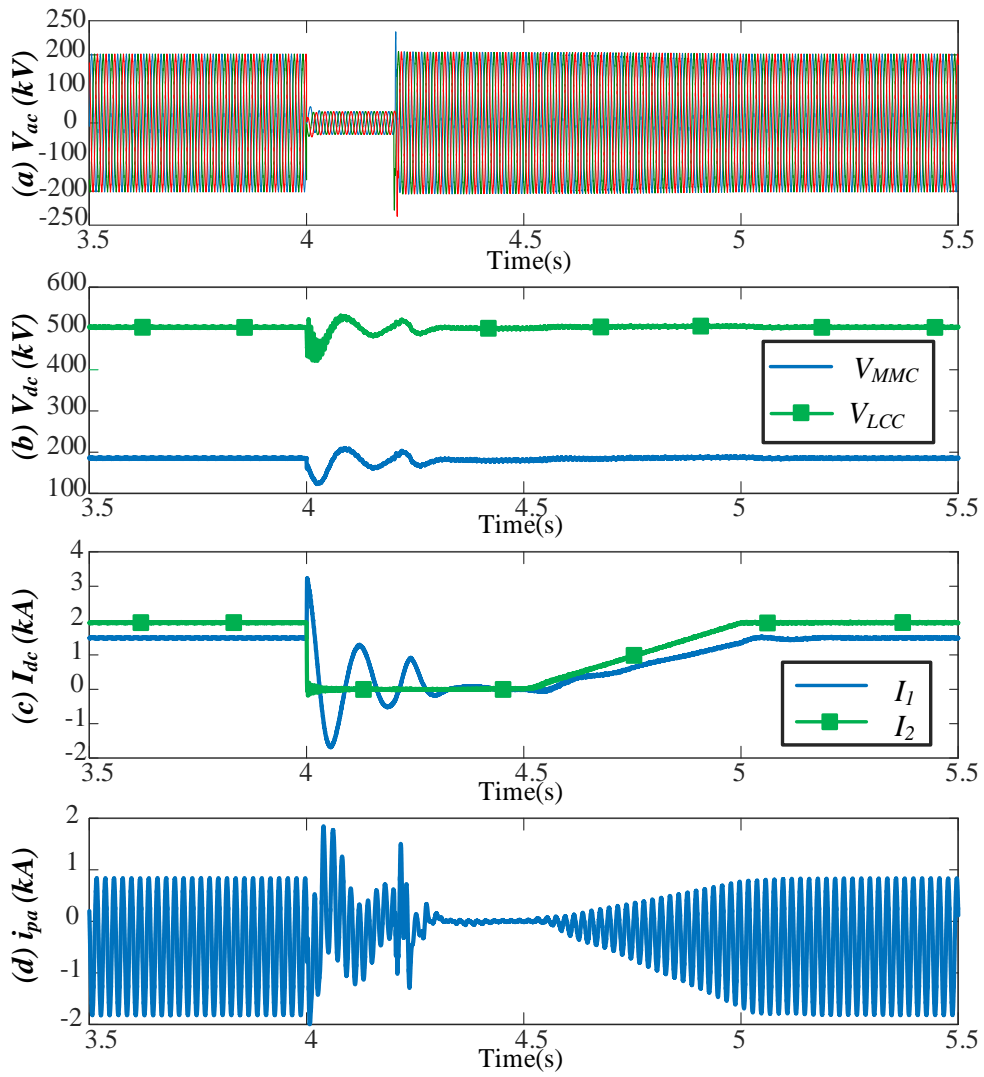


Fig. 3.13 Response to AC fault: (a) AC voltage, (b) DC voltages of MMC and LCC, (c) DC currents, (d) MMC arm currents.

3.5.3 Response to DC fault

System responses during a DC fault are shown in Figs. 3.14 and 3.15. Temporary DC faults are applied on the LV side at 2.0 s, and the HV side at 3.5 s, respectively. The proposed DC fault protection will identify the fault locations and determines the operating status of the LCC. The MMC is bypassed to protect itself during the DC faults, while the hybrid DCCB isolates the DC faults to protect the Hybrid Hub. When the DC fault is cleared, the DCCB is reclosed and the MMC and LCC are recovered to the pre-fault operation. E_1 and E_2 faults are respectively analysed as follows.

a) Performance during E_I fault at 2.0 s

Fig. 3.14 (a) shows the two DC network voltages. When DC voltage of E_I collapses to zero at 2.0 s, Fig. 3.14 (b) shows that the currents of MMC (I_1) and LCC (I_2) increase. Fig. 3.14 (c) shows the current I_3 , and it can be seen that, the derivative of I_3 with time is negative during E_I fault. This identifies E_I fault so that the DCCB receives the opening signal and the LCC continues operating. Due to the fast tripping of the hybrid DCCB, I_1 drops to zero within 10 ms, while I_2 recovers to its nominal value. Fig. 3.14 (d) shows the active power of the converters and wind farms. During E_I fault, the active power of P_{WF} is reduced to transfer through the LCC only while the active power of the MMC is reduced to zero. When E_I fault is cleared (e.g., for remote fault in other branch), the DCCB is reclosed and the MMC is enabled to continue transferring power, as shown in Figs. 3.14 (b) and (d).

Fig. 3.15 (a) shows that the DC voltage of the MMC (V_{MMC}) drops to zero during E_I fault. The MMC receives the blocking signals and operates as an uncontrolled rectifier, such that V_{MMC} increases to a value just below the rated one. When E_I fault is cleared, the MMC can be re-enabled so V_{MMC} restores and stabilises at the rated value. Fig. 3.15 (b) shows the capacitor voltages of the MMC. As can be seen, no capacitor overcharging is observed during E_I fault as the capacitor voltages remain within the rated value. Figs. 3.15 (c) and (d) show the arm currents of the MMC and the currents flowing through the IGBTs, respectively. The arm overcurrents during E_I fault are interrupted rapidly by the DCCB, as shown in Fig. 3.15 (c). The MMC is blocked and bypassed quickly on detecting the DC fault on either side. Therefore, no overcurrents are observed at the IGBTs as they are bypassed by the parallel thyristors, as shown in Fig. 3.15 (d). After clearing E_I fault, Fig. 3.15 shows that the MMC is recovered to the pre-fault operation.

b) Performance during E_2 fault at 3.5 s

For E_2 fault at 3.5 s, as shown in Figs. 3.14 (a) and (b), E_2 drops immediately to zero at 3.5 s while I_1 and I_2 rise. The derivative of I_3 with time shown in Fig. 3.14 (c) is negative. Therefore, the proposed coordinated current protection identifies the fault at HV side, so the DCCB is tripped, and the LCC and MMC are blocked. The fast tripping of the hybrid DCCB makes I_1 and I_2 decrease to zero within 10 ms. The active power of the MMC, LCC and AC_{WF} are all reduced to zero, as shown Fig. 3.14 (d). Figs. 3.14 (b) and (d) also show that the MMC and LCC are recovered to the pre-fault operation after fault clearance and reclosing the DCCB.

MMC responses to E_2 fault in a similar way as during E_1 fault. Fig. 3.15 (a) shows the collapse of V_{MMC} during E_2 fault, and then recovers to a value below the rated one since the MMC behaves as an uncontrolled rectifier. After fault clearance, V_{MMC} also recovers and operates at the rated value. There is no capacitor overcharging at the MMC as shown in Fig. 3.15 (b). Also, Figs. 3.15 (c) and (d) illustrate that the currents flowing through the IGBTs during E_2 fault is bypassed by the parallel thyristors, and the arm overcurrents are also eliminated quickly by opening the DCCB. After the E_2 fault is cleared, the MMC is also deblocked and restored to the pre-fault operation.

In conclusion, with the proposed coordinated current protection and the DCCB, the LCC-MMC Hub can operate securely during DC faults.

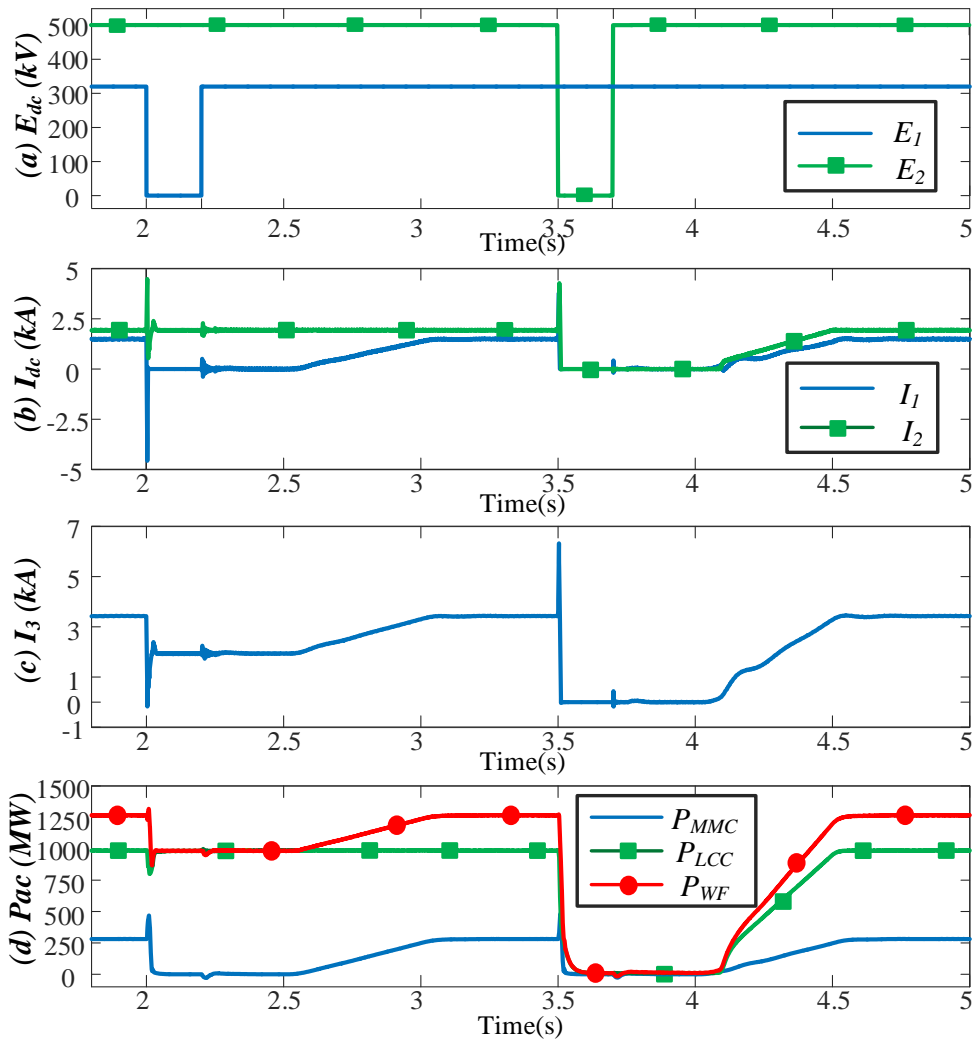


Fig. 3.14 Response to DC faults: (a) DC voltages of E_1 and E_2 , (b) Converter DC currents, (c) DC current of I_3 , (d) active power of converters and wind farm.

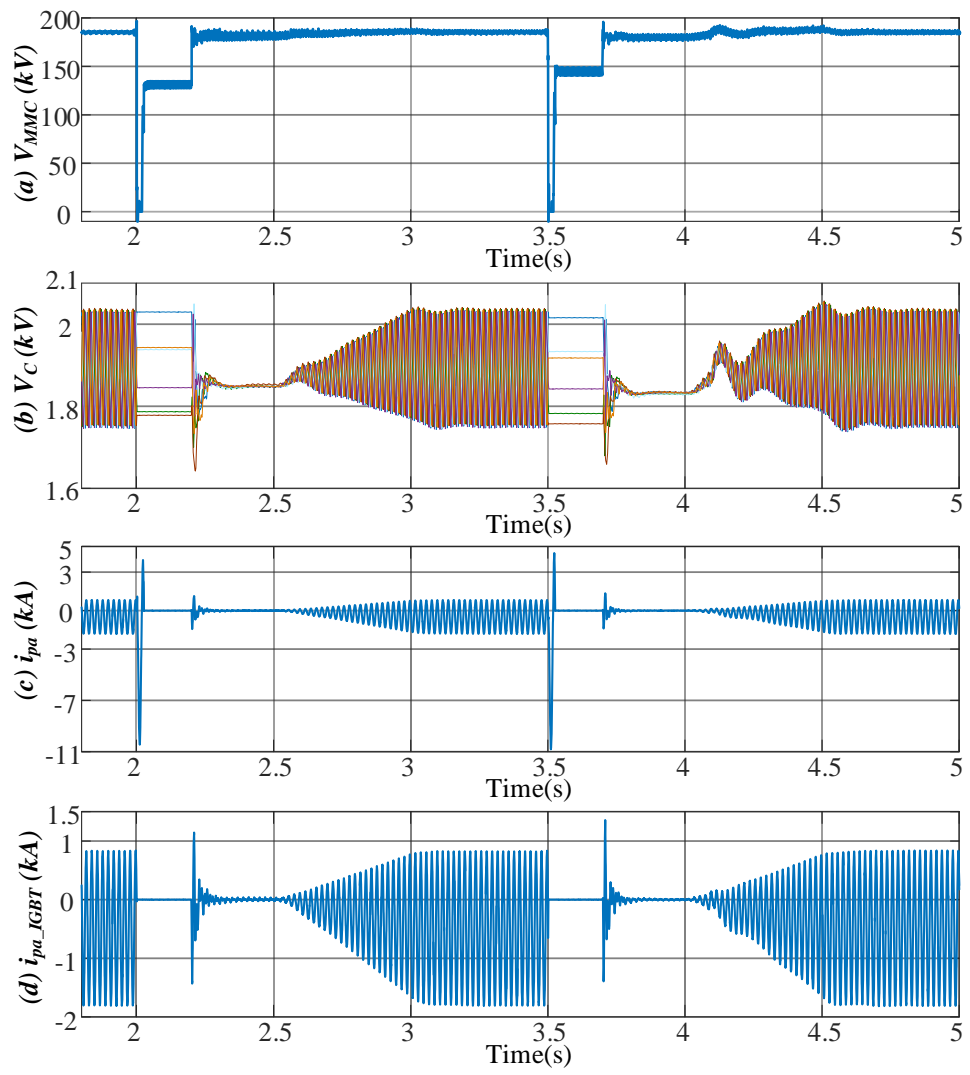


Fig. 3.15 MMC Response to DC faults: (a) MMC DC voltage, (b) MMC capacitor voltages, (c) MMC arm currents, (d) currents through IGBTs.

3.6 Summary

A hybrid LCC-MMC AC/DC hub for integrating onshore wind power and interconnecting onshore and offshore DC networks has been proposed in this chapter. The topology, operation, control and AC/DC fault-ride through of the LCC-MMC Hub has been studied. Compared to the “conventional” DC network interconnection method using DC/DC converters, power flow analysis has shown that the series-connected LCC-MMC Hub results in a lower power rating of MMC and a larger that of LCC, potentially offering higher efficiency and reduced cost. The power loss calculations have indicated that the LCC-MMC Hub has higher efficiency than DC/DC converter schemes when the DC voltage stepping ratio is lower than 4. Unlike the LCC-HVDC system, power reversal can be achieved flexibly in the proposed hybrid topology. By utilising the existing AC grid of onshore system and coordinated control of the LCC and MMC, the LCC-MMC Hub operates stably. By considering the sign of the derivative of the DC current I_3 with time, the proposed DCCB based DC fault protection scheme for the LCC-MMC Hub rapidly identifies and isolates the DC fault on either LV or HV side. Due to the unidirectional conduction character of the LCC rectifier and the closed-loop current control of MMC, the LCC-MMC Hub can also ride through AC faults. PSCAD/EMTDC simulations have validated the technical feasibility of the proposed hybrid AC/DC hub for HVDC applications.

Chapter 4 Hybrid DR-MMC AC/DC Hub

4.1 Introduction

The interest in offshore production platforms (e.g. oil/gas and hydrogen production plants) powered by offshore wind energy has been increasing as described in Chapter 1. It can lead to the need of offshore converter stations with the capability of transmitting wind power to both onshore electrical grid and offshore production platform using different DC voltages.

Several configurations and converters of HVDC transmission systems have been reviewed in Chapter 2. The parallel point-to-point MMC-HVDC links are natural extension of single point-to-point system for large offshore projects, offering many functions such as bidirectional power flow, flexible system control, increased redundancy, system black start capability, etc. However, the investment cost of high power MMC is quite high. Due to the lower investment and footprint, and higher efficiency than other converters, the DR based HVDC systems have received considerable attention for offshore wind power transmission [36-39]. However, for connecting multiple networks including offshore wind/production plant and onshore grid system, using only DR is not suitable as it cannot separately control the power transmissions to different terminals. Thus, a hybrid configuration combining uncontrolled DR and fully-controlled MMC is likely to be required such that some advantages of DR can still be obtained. Parallel operation of MMC-HVDC and DR-HVDC systems to transmit power from offshore wind farms has been analysed in [16], where the MMC regulates the offshore AC voltage to control the active power transmitted through the DR while using distributed wind turbine converters with specific grid-forming control scheme as in [39] is not required. However, the converter power rating of the MMC in this scheme can be quite high considering the different operation requirements and conditions, leading to an increased cost.

Some hybrid HVDC solutions have also been proposed to combine the advantages of different converter topologies as discussed in Chapter 2. A hybrid converter with series-connected MMC and LCC or DR, is proposed for wind farm integration, where the MMC is used to maintain the AC voltage and frequency [48, 49]. However, they are only dedicated to a single DC network. The MMC-based DC AUTO has been considered for connecting the inner AC bus of the DC AUTO to an external AC system, to achieve power exchange between the two DC networks and the AC system [67]. However, the investment cost of the DC AUTO could be still high as it needs two MMCs. In addition, the operation control and fault ride-through of the DC AUTO when connecting with an offshore wind farm have not been investigated. The hybrid LCC-MMC Hub in series connection has been proposed in Chapter 3 for onshore wind power integration and interconnection of two DC networks with different DC voltages, but this hub is not suitable for offshore applications due to the large footprint and heavyweight of the LCC, which also needs a strong AC grid for commutation.

To cater for such application scenarios, a hybrid DR-MMC AC/DC hub (DR-MMC hub) is proposed in this chapter to provide an efficient and economically viable option. The proposed DR-MMC Hub enables part of the power from the DR to be transmitted to the onshore DC network directly. In this chapter, the topology of the DR-MMC Hub is depicted, and its system control principle is described in details based on the operation requirement of the offshore production platform, considering different control modes (power control or DC voltage control). A comprehensive AC/DC fault ride-through and converter power loss estimation of the DR-MMC Hub are also provided. Simulation of the DR-MMC Hub during normal operation, AC and DC faults are carried out to demonstrate its operation.

4.2 Proposed topology and efficiency analysis

4.2.1 Envisaged operation scenario

Considering the benefits of DR and MMC as previously mentioned, the envisaged operation scenario is illustrated in Fig. 4.1, where the offshore converter with parallel-connected MMC and DR transmits wind power to the onshore DC network (S_1) and the offshore production platform DC network (S_2), at different DC voltages of E_1 and E_2 ($E_1 > E_2$) respectively. The MMC transmits the generated wind power P_{dc1} to S_1 and can reverse power to feed S_2 under low/no wind conditions. The wind power P_{dc2} is transmitted to S_2 by the DR. The produced oil/gas or hydrogen can be transported through pipelines or shipped to land (not considered in this study).

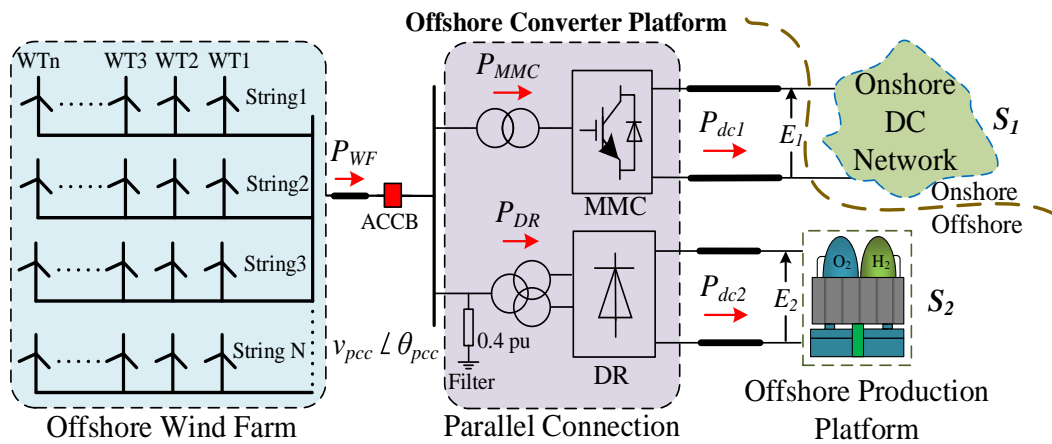


Fig. 4.1 Envisaged scenario for DC network interconnection.

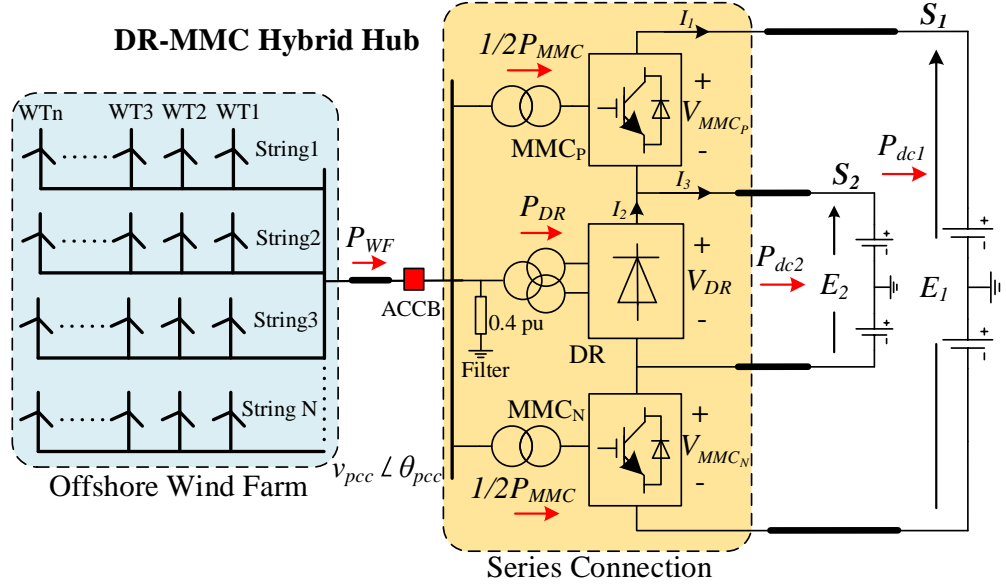


Fig. 4.2 Symmetrical monopole configuration of the proposed DR-MMC Hub.

4.2.2 DR-MMC Hub configuration

Fig. 4.2 depicts the topology of the proposed DR-MMC Hub in a symmetrical monopole setup. The proposed topology is mainly composed of a DR and two MMCs (MMC_P and MMC_N) in series connection as shown.

In order to obtain simple expressions, defining power transmitting from the offshore wind farm to S_1 and S_2 as positive, the ratios of the DC voltages E_2 and E_1 and the power transfer P_{dc1} and P_{dc2} can be expressed as:

$$\begin{cases} m = E_2 / E_1, & 0 < m < 1 \\ \alpha = P_{dc1} / P_{dc2}, & \alpha > 0 \end{cases} \quad (4.1)$$

where P_{dc1} and P_{dc2} are the active power transmitted to S_1 and S_2 , respectively.

Neglecting the power losses on converters and transmission lines, the total transmitted power from the offshore wind farm is:

$$P_{WF} = P_{dc1} + P_{dc2} = (1 + \alpha)P_{dc2} \quad (4.2)$$

The DC current at the DR (I_2) is the sum of the DC currents of the DC networks S_1 (I_1) and S_2 (I_3), as:

$$I_2 = I_1 + I_3 = (P_{dc1} / E_1 + P_{dc2} / E_2) \quad (4.3)$$

Considering the voltage drops on the DC lines are low and thus can be neglected, the DC voltage of the DR and the sum of the two MMCs' DC voltages are:

$$V_{DR} = E_2, \quad V_{MMC} = V_{MMC_P} + V_{MMC_N} = E_1 - E_2 \quad (4.4)$$

Consequently, the total active power of the two MMCs in the DR-MMC Hub is:

$$\begin{aligned} P_{MMC_hybrid} &= V_{MMC} I_1 = (E_1 - E_2) \frac{P_{dc1}}{E_1} \\ &= (1-m)P_{dc1} = (\alpha - \alpha m)P_{dc2} \\ &= \frac{\alpha - \alpha m}{1 + \alpha} P_{WF} \end{aligned} \quad (4.5)$$

Similarly, the active power of the DR is:

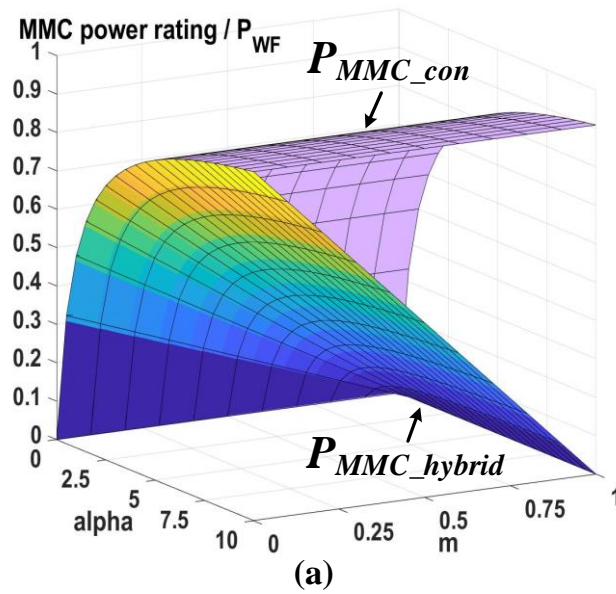
$$\begin{aligned} P_{DR_hybrid} &= V_{DR} I_2 = E_2 (P_{dc1} / E_1 + P_{dc2} / E_2) \\ &= mP_{dc1} + P_{dc2} = (m\alpha + 1)P_{dc2} \\ &= \frac{m\alpha + 1}{1 + \alpha} P_{WF} \end{aligned} \quad (4.6)$$

If the “conventional” parallel system shown in Fig. 4.1 is used, the converter power ratings of the MMC and the DR are:

$$\begin{cases} P_{MMC_con} = P_{dc1} = \alpha P_{dc2} > P_{MMC_hybrid} \\ P_{DR_con} = P_{dc2} < P_{DR_hybrid} \end{cases} \quad (4.7)$$

The converter power ratings of the MMC and DR in the two different system configurations are compared in Fig. 4.3 for different power and voltage ratios. Fig. 4.3

(a) indicates that the MMCs power rating in the DR-MMC Hub is smaller than that in the parallel-connected configuration shown in Fig. 4.1, especially when the voltage ratio m is high (close to 1). In contrast, as shown in Fig. 4.3 (b), the DR power rating of the proposed system is higher than that of the “conventional” parallel system. For example, in a ± 100 kV / ± 320 kV DR-MMC Hub transferring 400 MW P_{dc1} and 400 MW P_{dc2} (i.e. $m = 0.3125$ and $\alpha = 1$), the required power ratings of the MMC and DR are 275 MW and 525 MW, respectively, compared to 400 MW and 400 MW in parallel connection design. The overall efficiency and cost of the DR-MMC Hub is potentially superior to the “conventional” parallel system as the power loss and cost of the DR for high power schemes are much lower than that of the MMC [37, 39]. A detailed assessment on power losses will be provided in Section 4.4.3.



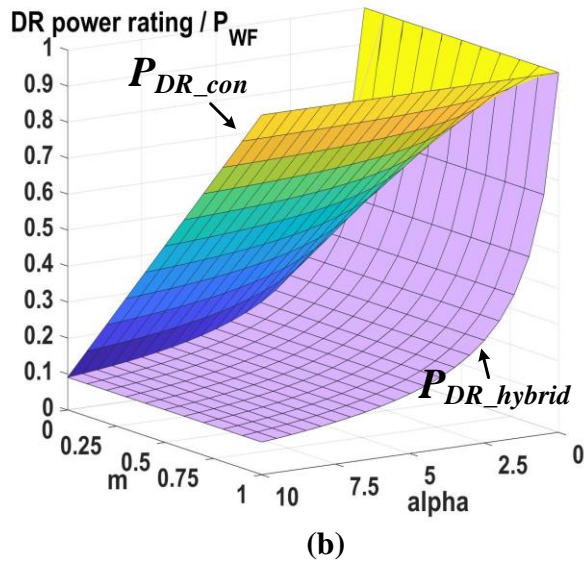


Fig. 4.3 Converter power ratings for different system configurations versus different power ratio α and DC voltage ratio m : (a) MMC power rating, (b) DR power rating.

4.3 Control principles

For the offshore hub shown in Fig. 4.2, a 12-pulse DR and AC filters are used, while hybrid MMCs with HBSMs and FBSMs are adopted for both MMC_P and MMC_N . The details on the need for FBSMs will be discussed later in the chapter. To carry out the study, an aggregated wind turbine model shown in Fig. 4.4 is considered in this thesis, where the rotor-side converter (RSC) controls the DC-link voltage while the grid-side converter (GSC) regulates the active and reactive power [87]. The reactive power of the wind farm is set to be zero in the study, and reactive power compensation is provided by the AC filters and MMCs of the offshore hub.

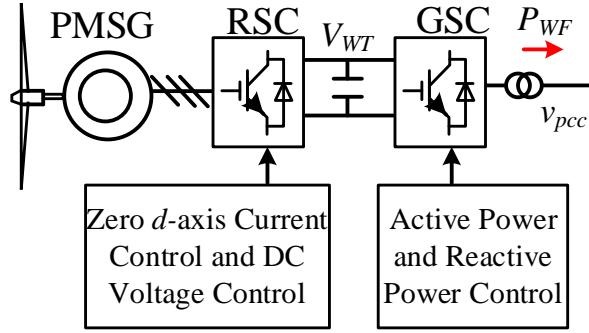


Fig. 4.4 Aggregated wind farm model.

Fig. 4.5 shows the control structure of the DR-MMC Hub. The MMCs in the offshore hub operate in grid-forming mode to control the offshore AC network with desirable voltage amplitude and frequency [77]. As shown in Fig. 4.5, the reference of the q -axis voltage v_q^* is set to be zero, and the local frequency at the point of common coupling (PCC) is set to be a constant value (e.g. 50 Hz), while v_d^* is regulated as described late in the chapter.

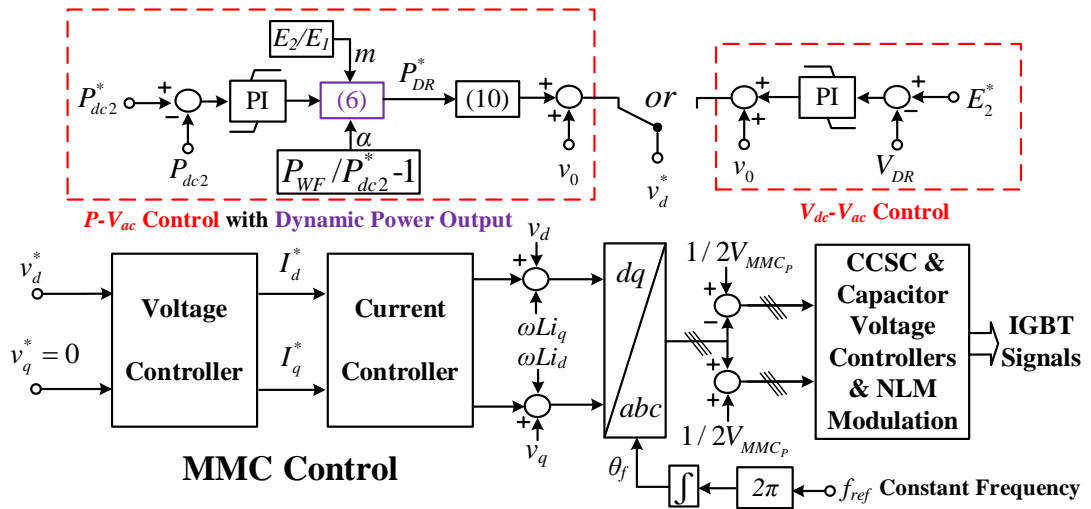


Fig. 4.5 System control diagram of the MMC.

The control target of the DR-MMC Hub is to distribute the offshore wind farm power (P_{WF}) to the two DC systems (i.e. P_{dc1} and P_{dc2}). If P_{dc2} is determined/controlled

by the offshore production platform, the DC voltage of the DR should be maintained at a constant value, which is given as [20]:

$$V_{DR} = \frac{6}{\pi} (\sqrt{3} T_{DR} V_{PCC} - \frac{P_{DR} X_{DR}}{V_{DR}}) \quad (4.8)$$

where the turn ratio and reactance of the DR transformer are denoted as T_{DR} and X_{DR} . V_{DR} and V_{PCC} are the DC voltage of the DR and the AC voltage at the PCC, respectively.

If the offshore production platform controls the DC voltage of the network S_2 , P_{dc2} should be controlled by the DR. Based on (4.2) and (4.6), the relationships between active power, m and α are:

$$\begin{cases} P_{dc1} = P_{WF} - P_{dc2} \\ P_{dc2} = P_{DR} / (1 + ma) \\ \alpha = (P_{WF} / P_{dc2}) - 1 \end{cases} \quad (4.9)$$

In (4.9), the DC voltage ratio m is fixed and the power transfer ratio α varies with the changes of P_{WF} and P_{dc2} . Under low wind conditions, when the wind farm output P_{WF} is insufficient for the offshore production platform P_{dc2} , the power from the onshore HVDC network is reversed through the MMCs.

The active power transmitted by the DR is expressed as [88]:

$$P_{DR} = \frac{\sqrt{2} T_{DR} E_2}{X_{DR}} V_{PCC} - \frac{\pi E_2^2}{6 X_{DR}} \quad (4.10)$$

As can be seen from (4.8) and (4.10), the DR's DC voltage and active power are largely determined by the AC voltage V_{PCC} .

Based on the alternative control targets of the offshore production platform as previously described, i.e., DC voltage (V_{DR}) control or active power (P_{dc2}) control, the

offshore voltage amplitude v_d^* is generated with different outer loops. As shown in Fig. 4.5, when the offshore production platform controls active power and behaves like a passive load, the DC voltage of S_2 is determined by the Hub through the control of the MMCs. In this case, the V_{dc} - V_{ac} loop is used which controls the DC voltage of the DR to the reference value E_2 , where the DC voltage error at S_2 sets the offshore AC voltage reference considering (4.8). When the DC voltage of the offshore production platform is controlled by S_2 , e.g., by other energy storage devices in S_2 , the power transmitted to S_2 needs to be controlled. In this event, the P - V_{ac} control loop is implemented as shown in Fig. 4.5 to regulate P_{dc2} , where the power output P_{DR}^* is dynamically regulated by the desired power reference P_{dc2}^* and the variation of P_{WF} to produce the offshore AC voltage reference. A set-point v_0 is added to keep the offshore AC voltage in the range of 0.9 to 1 p.u. for both cases, as shown in Fig. 4.5. The tuning method for PI compensator parameters can be found in [76].

4.4 Fault ride-through of the DR-MMC Hub

4.4.1 AC fault ride-through

The responses of the DR-MMC Hub during AC faults in the offshore wind farm network are considered in this subsection.

An offshore AC fault leads to a significant reduction of the offshore AC voltage and current-limiting operation of the wind turbine converters [89]. There is no active power transmitted from the DR station as its conduction is blocked when the AC voltage becomes lower than the minimum DR conduction voltage (i.e. $\pi E_2/6\sqrt{2}T_{DR}$).

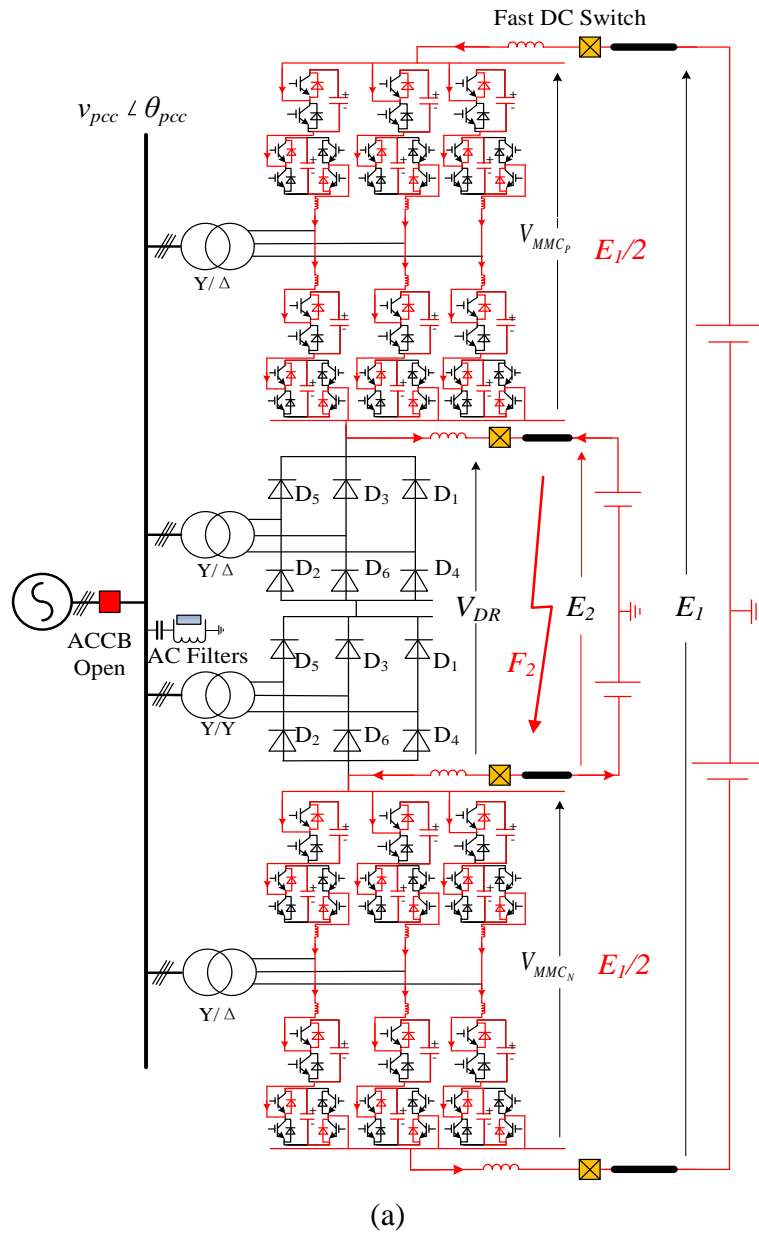
If the offshore production platform behaves as a passive load and E_2 is controlled by the DR-MMC Hub, the DC voltage will collapse with the decrease of the offshore AC voltage, similar to a pole-to-pole (p2p) DC fault at S_2 network. Therefore, the MMCs need to be blocked immediately to support the DC voltage E_1 , as will be

detailed in Section 4.4.2. After fault clearance, the system can quickly recover to the normal operation once the MMCs are re-enabled.

If E_2 is controlled by the offshore production platform while the DR-MMC hub controls the DC power of S_2 , E_2 will be maintained at the rated value even though the offshore AC voltage decreases quickly during the AC fault. No active power is being transmitted through the MMCs or the DR. For the MMCs in the DR-MMC hub, the fault current during the AC faults can be limited without disturbing DC side performance due to the inner current control loop, which has been well researched in [85]. Therefore, E_1 is not affected though no active power can be transmitted to S_1 in such scenarios. After the AC faults, the system will be restored rapidly with the recovery of the AC system voltage.

4.4.2 DC fault ride-through

Pole-to-Pole (p2p) DC faults in DC networks of S_1 and S_2 are considered. If a DC fault occurs on either DC network, the healthy DC side could potentially feed the fault current to the faulty DC side through the MMC due to its direct electrical connection [67, 90]. Considering the large cost and volume relative to ACCBs at comparable voltages, DCCBs are not considered in the proposed offshore hub while ACCB and DC disconnectors (DC switches) are used for DC fault protection [91, 92].



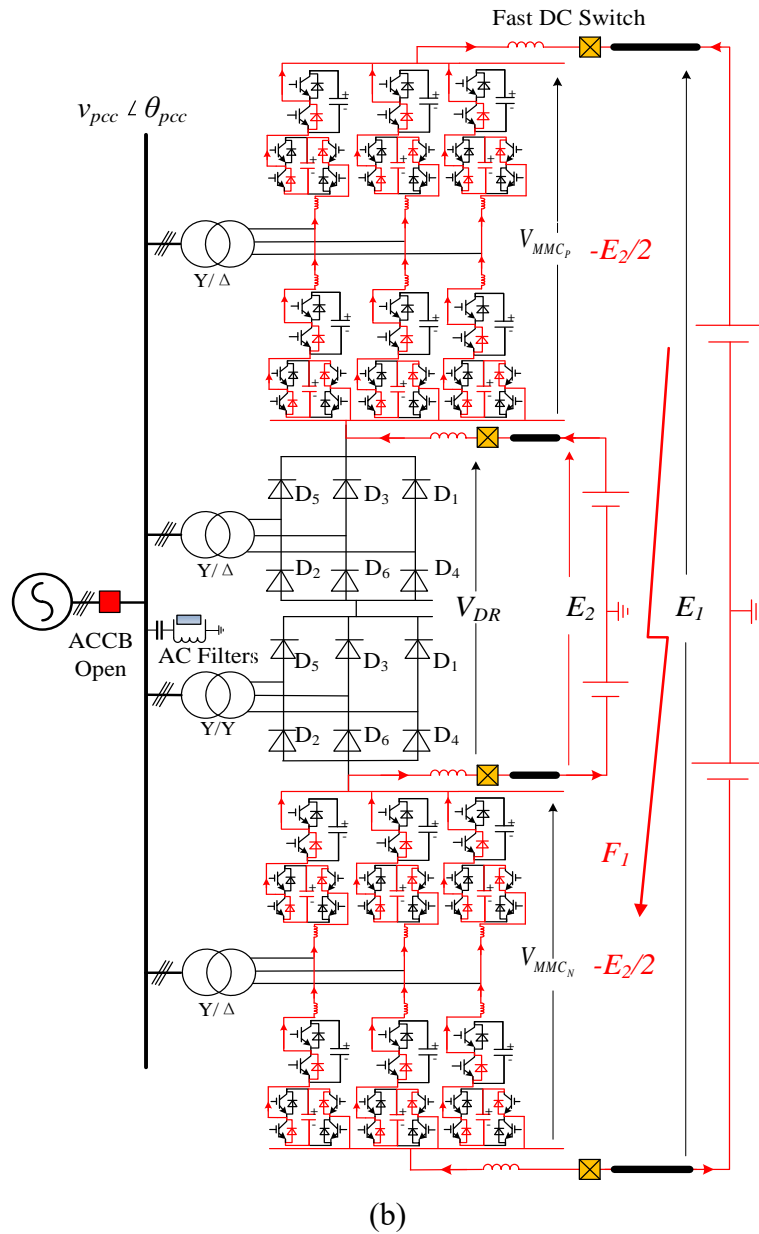


Fig. 4.6 Fault current path of blocked MMCs during different DC faults:

(a) current flow during F_2 fault, (b) current flow during F_1 fault (FBSMs are required).

In the event of a p2p fault that happened at S_2 (called F_2) as shown in Fig. 4.6 (a), the MMCs have to provide the full DC voltage E_1 to block any fault current feeding from S_1 to F_2 . The fault current path of the blocked MMCs in the DR-MMC Hub (shown in red) during F_2 fault is shown in Fig. 4.6 (a). As shown, the fault current charges all SM capacitors of the MMCs from the DC voltage E_1 . Therefore, the fault

current during F_2 fault can be blocked and diminished if the total SM capacitor voltage in each of MMC_P and MMC_N is higher than $E_1/2$.

Therefore, the required SM capacitor voltage ($V_{arm_MMC}^R$) in each arm for blocking F_2 fault, and the nominal SM capacitor voltage (V_{arm_SM}) of the MMCs can be calculated as:

$$\begin{cases} V_{arm_MMC}^R = E_1 / 4 \\ V_{arm_SM} = (1 - m)E_1 / 2 \end{cases} \quad (4.11)$$

If $V_{arm_MMC}^R > V_{arm_SM}$ (i.e. $m > 1/2$), additional HBSMs are required for each arm of the MMCs to withstand the voltage of $E_1/4$ to avoid overcharging SM capacitors.

If a p2p fault happens at S_1 (F_1), the MMCs need to withstand the full DC voltage E_2 but in opposite direction in order to block the fault current from S_1 as shown in Fig. 4.6 (b). Thus, FBSMs are required in each of the arm as the HBSMs will be bypassed during F_1 fault. As shown in Fig. 4.6 (b), the fault current from S_2 during F_1 fault can be blocked if the total capacitor voltages of the FBSMs in MMC_P and MMC_N are higher than $E_2/2$. Therefore, the required capacitor voltage ($V_{arm_FBSM}^R$) of the total FBSMs in each arm to block F_1 fault is given as:

$$V_{arm_FBSM}^R = E_2 / 4 = mE_1 / 4 \quad (4.12)$$

If the SM number of each MMC arm without fault considerations is denoted as N_{SM} , according to (4.11) and (4.12), the required FBSMs (N_{FB}^R) and HBSMs (N_{HB}^R) numbers in the hybrid MMCs in the proposed hub for blocking both DC faults can be calculated as:

$$N_{FB}^* = \frac{m}{2-2m} N_{SM}, \quad N_{HB}^* = \begin{cases} \frac{2-3m}{2-2m} N_{SM}, & m \leq 1/2 \\ \frac{1}{2} N_{SM}, & 1/2 < m < 1 \end{cases} \quad (4.13)$$

Fig. 4. 7 show the required number of FBSMs and HBSMs in the hybrid MMCs to isolate DC faults. From (4.13) and Fig. 4.7, the SM cost per MVA in the hybrid MMCs will increase compared to the HB-MMCs without fault consideration.

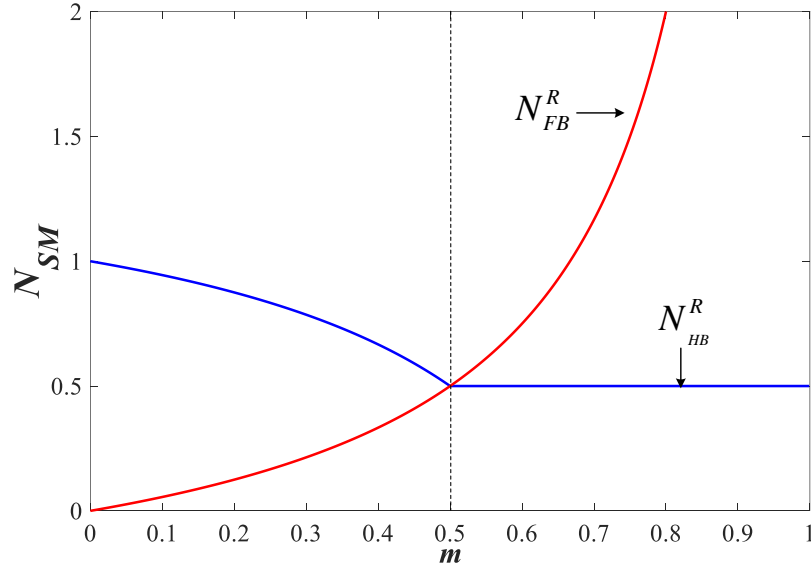


Fig. 4.7 Required number of HBSMs and FBSMs in the hybrid MMCs to isolate DC faults.

Taking a $\pm 100/\pm 320$ kV DR-MMC Hub as an example ($m = 0.3125$), to safely isolate the DC faults, the required number of FBSMs and HBSMs in the hybrid MMCs are approximately $0.23N_{SM}$ and $0.77N_{SM}$, respectively. If the cost of FBSM is approximated to be 1.5 times of HBSM [35, 67], the SM cost per MVA of the hybrid MMCs with DC fault blocking capabilities is hence 1.115 times of the HB-MMC base value. If the DR-MMC Hub has DC voltages of ± 200 and ± 320 kV ($m = 0.625$), the required number of FBSMs and HBSMs in the hybrid MMCs are approximately $0.833N_{SM}$ and $0.5N_{SM}$, respectively. Thus, the SM cost per MVA of the hybrid MMCs with DC fault blocking capabilities is about 1.75 times of the HB-MMC base value. Thus, higher m leads to increased SMs that are required in the hybrid MMCs for

isolating DC faults so the advantage of the proposed DR-MMC Hub is reduced. However, due to the increased capacity of DR, the proposed DR-MMC Hub can still have lower power loss when compared to the “conventional” design, as will be analysed later in the chapter.

Once a DC fault (F_1 or F_2) is detected, the MMCs that regulate the offshore AC voltage and frequency will be blocked immediately to prevent the fault current from the AC flowing to the DC side. Consequently, power transmission from the offshore AC network to the DC side is interrupted. If the offshore wind turbines are controlled in such a way that they continue generating active power, the surplus wind power will increase the offshore AC voltage. Consequently, overcurrent could occur in the DR. Thus, after blocking the MMCs, the ACCB that connects the offshore wind farm and DR-MMC Hub is opened to interrupt the potential overcurrent of the DR from the AC side.

When the DC current is reduced to near zero after blocking the MMCs, the fast DC switches on the faulty part can be opened. The DR-MMC Hub and offshore wind farm are then isolated from the DC fault point until fault clearance.

4.5 Power loss estimation

The power loss in the proposed DR-MMC Hub is estimated considering the losses of the DR, HBSMs and FBSMs denoted as η_{DR} , η_{HB} and η_{FB} . Thus, the estimated power loss of the “conventional” parallel system can be obtained as:

$$\eta_{con} = \frac{\eta_{HB}P_{dc1} + \eta_{DR}P_{dc2}}{P_{WF}} \quad (4.14)$$

The estimated power loss of the DR-MMC Hub is:

$$\eta_{\text{hybrid}} = \frac{\left(\eta_{FB} \frac{N_{FB}^R}{N_{SM}} + \eta_{HB} \frac{N_{HB}^R}{N_{SM}} \right) P_{\text{MMC_hybrid}} + \eta_{DR} P_{\text{DR_hybrid}}}{P_{WF}} \quad (4.15)$$

Reference [35] and [37] indicate that the valve power losses of the DR, HBSMs and FBSMs are approximately 0.11%, 0.6% and 1.1%, respectively. Table 4.1 compares the power ratings and losses of different configurations transferring 800 MW from the offshore windfarm to the two DC networks. Different system configurations with various m ($m = 0.3125$ and 0.625) and α ($\alpha = 1, 2$ and 3) are investigated. For the parallel system, the power losses increase with α from 0.355% to 0.478%. For the DR-MMC Hub with $m = 0.3125$, the power losses increase with α from 0.318% to 0.422%. For the DR-MMC Hub with $m = 0.625$, the power losses increase with α from 0.317% to 0.421%. The above data shows that the power losses increase with α in general due to the increased MMC power ratio for each system. In terms of $\alpha = 1$, although FBSM based MMCs have higher power losses than MMCs with HBSMs only, the estimated power loss of the DR-MMC Hub is only 0.318% for $m = 0.3125$, being 10.6% lower than that of the converter system in parallel connection (0.355%). For $m = 0.625$, it can be seen that the power loss the DR-MMC Hub is 0.3175%, a bit lower than that for $m = 0.3125$ due to the decreased capacity of MMC and the increased capacity of DR, although more SMs are required to ride through the DC faults. In cases with increased α ($\alpha = 2$ and 3), the losses trend follows the same trend as above. In addition, the ability of the DR-MMC Hub to block DC fault indicates the potential use of low-cost DC switch/disconnectors for DC line protection, rather than using the DCCBs.

Table 4.1 Comparison on power ratings and losses with different configurations.

| Configuration | P_{DR} | P_{MMC} | N_{FB} | N_{HB} | Power loss | DC fault blocking |
|---|----------|-----------|---------------|--------------|------------|-------------------|
| Parallel system ($\alpha = 1$) | 400 MW | 400 MW | 0 | N_{SM} | 0.355% | No |
| Parallel system ($\alpha = 2$) | 266.7 MW | 533.3 MW | 0 | N_{SM} | 0.437% | |
| Parallel system ($\alpha = 3$) | 200 MW | 600 MW | 0 | N_{SM} | 0.478% | |
| DR-MMC Hub ($m = 0.3125, \alpha = 1$) | 525 MW | 275 MW | $0.23N_{SM}$ | $0.77N_{SM}$ | 0.318% | Yes |
| DR-MMC Hub ($m = 0.3125, \alpha = 2$) | 433.3 MW | 366.7 MW | $0.23N_{SM}$ | $0.77N_{SM}$ | 0.387% | |
| DR-MMC Hub ($m = 0.3125, \alpha = 3$) | 387.5 MW | 412.5 MW | $0.23N_{SM}$ | $0.77N_{SM}$ | 0.422% | |
| DR-MMC Hub ($m = 0.625, \alpha = 1$) | 650 MW | 150 MW | $0.833N_{SM}$ | $0.5N_{SM}$ | 0.317% | |
| DR-MMC Hub ($m = 0.625, \alpha = 2$) | 600 MW | 200 MW | $0.833N_{SM}$ | $0.5N_{SM}$ | 0.386% | |
| DR-MMC Hub ($m = 0.625, \alpha = 3$) | 575 MW | 225 MW | $0.833N_{SM}$ | $0.5N_{SM}$ | 0.421% | |

4.6 Simulation studies

The system shown in Fig. 4.2 is modelled using PSCAD/EMTDC. The DC voltages are ± 100 kV/ ± 320 kV, and the DC power transmitted to S_1 and S_2 (P_{dc1} and P_{dc2}) are both 400 MW. The DC cables in S_1 (100 km) and S_2 (50 km) are modelled using the frequency-dependent model in PSCAD/EMTDC. Fast DC switches are installed between the converters and DC cables.

Table 4.2 Simulated system parameters

| Parameters | | Nominal Value |
|---|---------------------------------------|-----------------|
| MMC _P & MMC _N | Power rating | 137.5 MW |
| | Rated DC voltage | ±220 kV |
| | SM capacitor voltage | 1.83 kV |
| | SM capacitance | 7.5 mF |
| | Arm inductance | 0.0241 H |
| | SM number per arm | 125 |
| | FBSM number per arm | 35 |
| | Interfacing transformer voltage ratio | 66 kV/110 kV |
| | DC smoothing reactance | 0.1 H |
| 12-pulse DR bridge | Power rating | 525 MW |
| | Rated DC voltage | ±100 kV |
| | Reactive power compensation | 0.4 p.u. |
| | Interfacing transformer voltage ratio | 66/87.3/87.3 kV |
| | DC smoothing reactance | 0.1 H |
| Wind farm aggregated model | Power rating | 800 MW |
| | Interfacing transformer voltage ratio | 0.69 /66 kV |
| | AC cable length | 10 km |

The simulated system parameters are shown in Table 4.2. The hybrid MMC adopts the equivalent averaged model to improve simulation efficiency [84, 93]. The simulation results of MMC_P and MMC_N are the same due to the symmetrical monopole topology of the proposed system, and therefore, only the results of MMC_P are provided here. The DC voltages of S_1 and S_2 are given at the rated value as they are controlled by the other sides of the DC networks when the MMCs operate in P - V_{ac} control mode. If the MMCs operate in V_{dc} - V_{ac} control mode, the DC voltage source in S_2 is replaced by a passive load.

4.6.1 Operation in V_{dc} - V_{ac} control mode

Fig. 4.8 shows the normal operation of the DR-MMC Hub during power variation between the offshore production plant (P_{dc2}) and offshore wind farm (P_{WF}). Initially, P_{WF} is zero and ramped up to the rated value of 800 MW from 2.0 s to 2.5 s. The initial power demand of the offshore production platform (P_{dc2}) is set at zero, and is stepped to the rated value of 400 MW at 1.5 s by connecting a passive load to E_2 .

Fig. 4.8 (a) shows that the DC voltage of S_2 is well controlled by the MMCs throughout the power and load variations. According to Figs. 4.8 (b) and (c), no power is transmitted from the offshore wind farm to S_1 or S_2 initially. When the passive load at S_2 is connected at 1.5 s, the DC power P_{dc2} is stepped to 400 MW, which is provided by the power reversed from S_1 through the MMCs. When the active power of the offshore wind farm is gradually increased at 2.0 s, the infeed power from S_1 to S_2 is reduced accordingly. After the wind power becomes higher than the DC power P_{dc2} , the surplus power is transmitted to S_2 , as can be seen in Fig. 4.8 (b).

The active and reactive power of the DR and MMC_P shown in Figs. 4.8 (c) and (d) (MMC_N is identical, thus not shown here) follow the system power change smoothly, and the offshore wind farm reactive power is well regulated at zero. To maintain the DC voltage of S_2 , the MMCs regulates the common bus AC voltage (shown in the RMS value in Fig. 4.8 (e), and is varied with the change of P_{DR}).

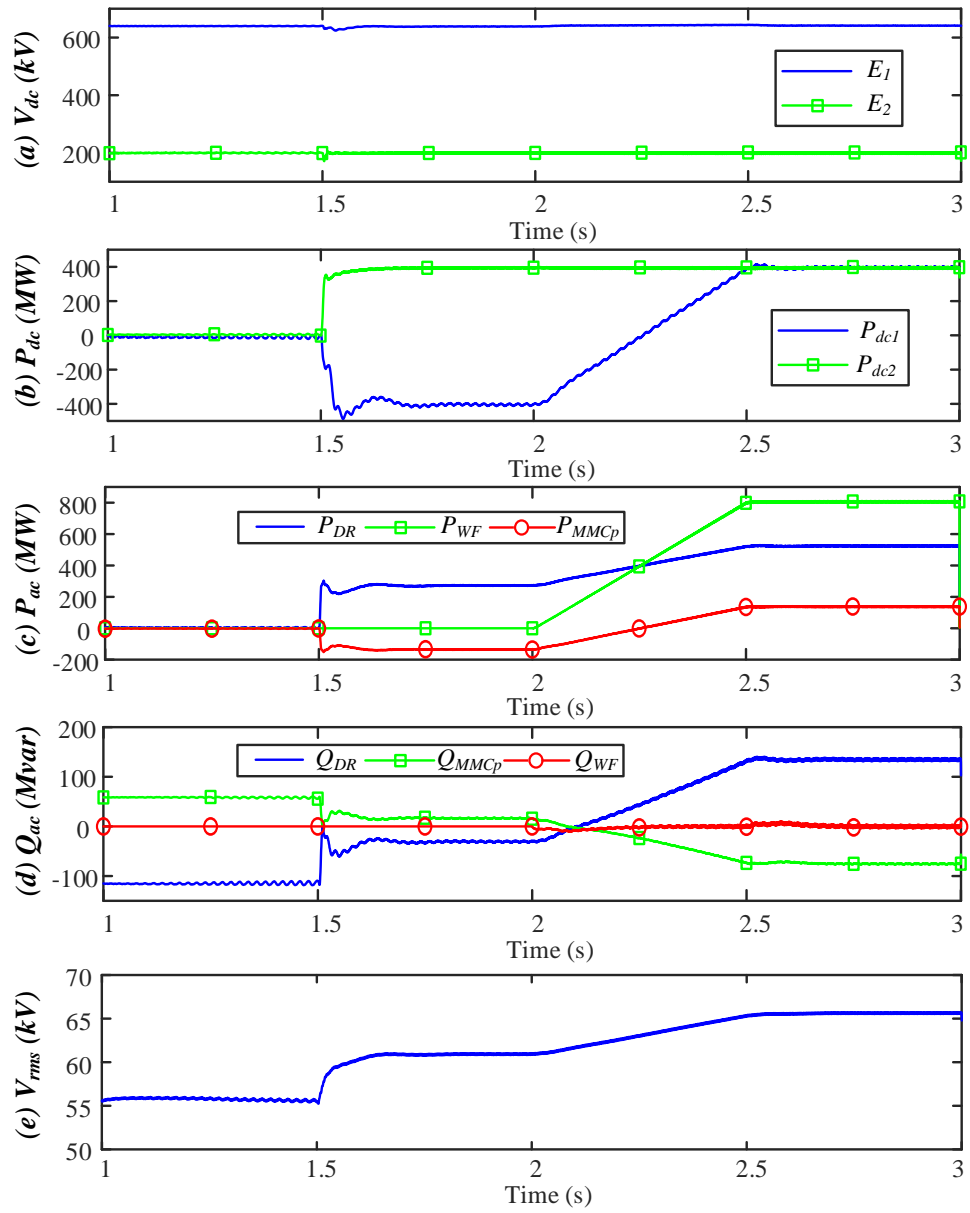


Fig. 4.8 System operation in V_{dc} - V_{ac} control mode: (a) DC voltage, (b) DC power, (c) Active power, (d) Reactive power, (e) RMS AC voltage.

4.6.2 Operation in P - V_{ac} control mode

Fig. 4.9 illustrates the normal operation of the DR-MMC Hub with the MMCs operating in P - V_{ac} control. P_{dc2} is ramped up from 0 MW at 1 s to the rated value of 400 MW at 1.5 s, while P_{WF} is ramped up from 0 MW at 2.0 s to the rated value of 800 MW at 2.5 s, and then ramped down by 0.15 p.u. (120 MW) from 3 s to 3.1 s. As seen, Figs. 4.9 (a) and (b) show that P_{dc2} is well controlled throughout the power variations. While P_{WF} remains at 0.85 p.u. (680 MW), the power reference P_{dc2}^* shown in Fig. 4.9 (d) is dropped by 0.25 p.u. (100MW) from 3.5 s to 3.6 s. As seen, P_{DR} is decreased accordingly whereas P_{MMCp} and P_{dc1} are increased so that the overall power is balanced.

Similar to Fig. 4.8 (d), the smooth reactive power exchange of the DR and MMC_P is shown in Fig. 4.9 (c) and the zero reactive power from the offshore wind farm as set by the control objective in the simulation study.

Fig. 4.9 (d) shows the power references P_{DR}^* and P_{dc2}^* from the outer controller of the MMC_P, where P_{DR}^* is varied due to the variation of P_{dc2}^* and P_{WF} . As shown in Fig. 4.9 (e), the common bus AC voltage is controlled by the MMCs in accordance with the required P_{DR} transmission.

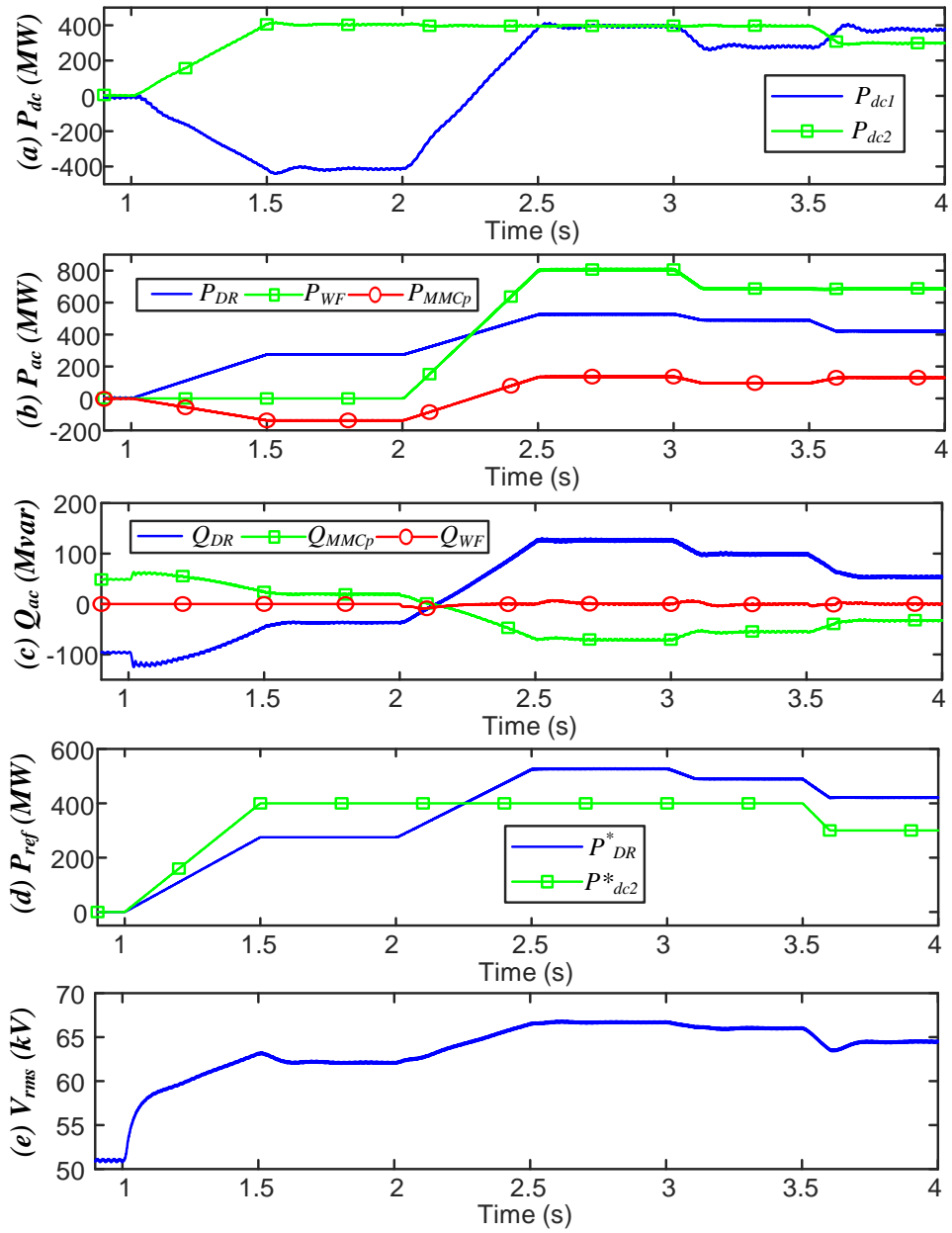


Fig. 4.9 System operation in P - V_{ac} control mode: (a) DC power, (b) Active power, (c) Reactive power, (d) Power reference, (e) RMS AC voltage.

4.6.3 AC fault ride-through

Fig. 4.10 shows the system performance during offshore AC faults in V_{dc} - V_{ac} operation while Fig. 4.11 shows the corresponding response in P - V_{ac} Control. During the studies, a 200 ms three-phase to ground fault occurs at 3.0 s.

As shown in Figs. 4.10 (a) and (b), when the DR-MMC Hub operates in V_{dc} - V_{ac} control, the DC voltage of the DR is quickly decreased to zero after the occurrence of the AC fault. MMC_P and MMC_N are blocked immediately and their SM capacitor voltages support the DC voltage E_l . Consequently, each of the MMC DC terminal voltage increases from 220 kV to 320 kV, as can be seen in Fig. 4.10 (b). Fig. 4.10 (c) shows that the DC currents of MMC_P (I_1) and the DR (I_2) are rapidly reduced to zero during the AC fault. Once the fault is cleared, MMC_P and MMC_N are re-enabled to restore the DC voltages of the MMCs and the DR, and the DC currents return to the pre-fault values. Fig. 4.10 (d) shows the arm current of MMC_P and no overcurrent is observed during the AC fault.

When the DR-MMC Hub operates in P - V_{ac} control, during the AC fault, the converters of the offshore wind farm and the MMCs all enter in current-limiting operation. As can be seen from Figs. 4.11 (a) and (b), the collapse of the offshore AC voltage during the fault quickly reduces the DC currents and power transmission to zero. There is no overcurrent in the arm currents of MMC_P due to the current control, as shown in Fig. 4.11 (c). The DC voltages of MMC_P and the DR shown in Fig. 4.11 (d) recover to their nominal values after the initial transients when the fault occurs. After fault clearance and the recovery of the offshore AC voltage, the DC currents and voltages return to pre-fault condition and no overcurrent occurs. The DR-MMC Hub in P - V_{ac} control mode is preferred if possible as it can avoid MMC blocking and DC link overvoltage during the AC fault.

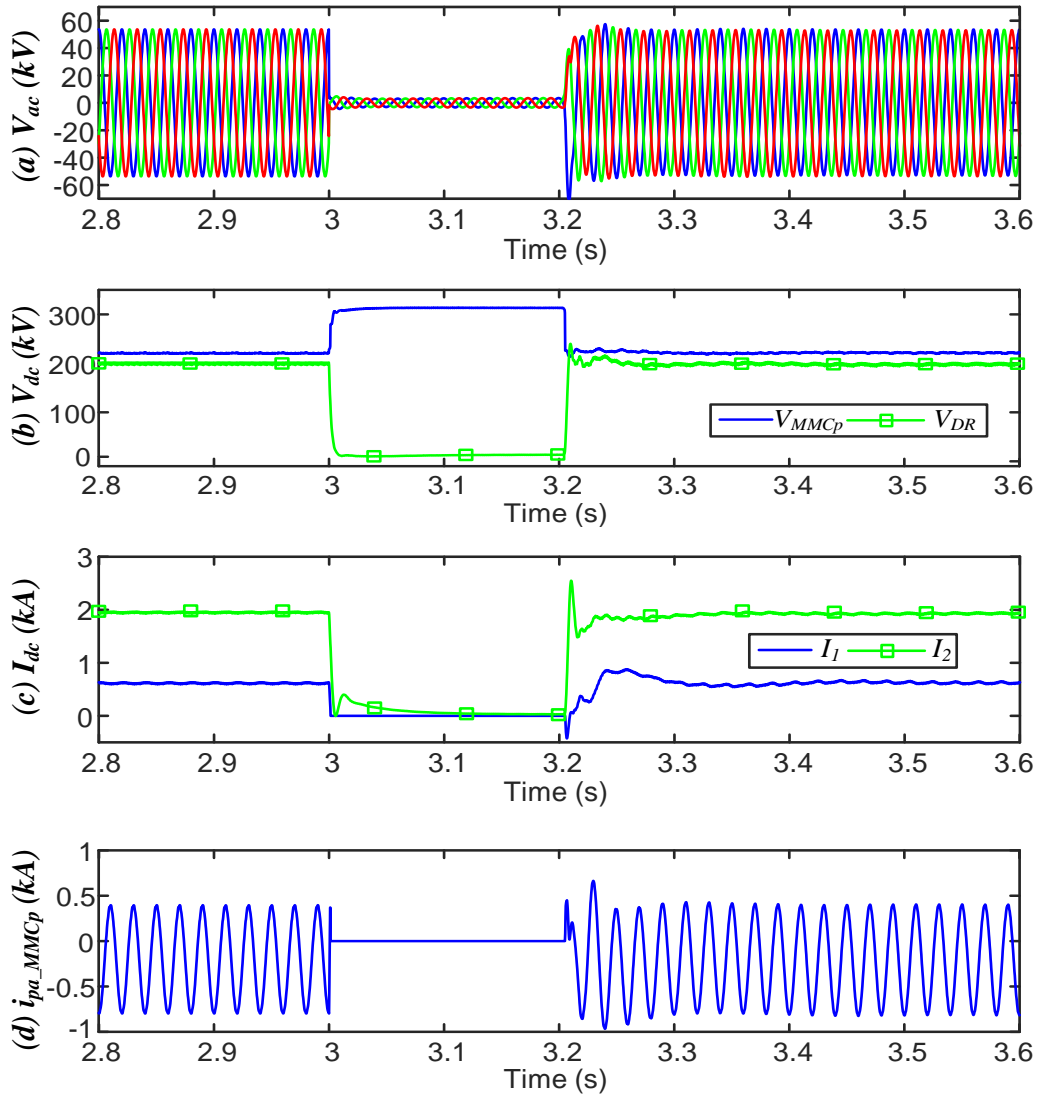


Fig. 4.10 System performance to AC fault in V_{dc} - V_{ac} control mode: (a) AC voltage, (b) DC voltage, (c) DC current, (d) Phase A MMC_p upper arm current.

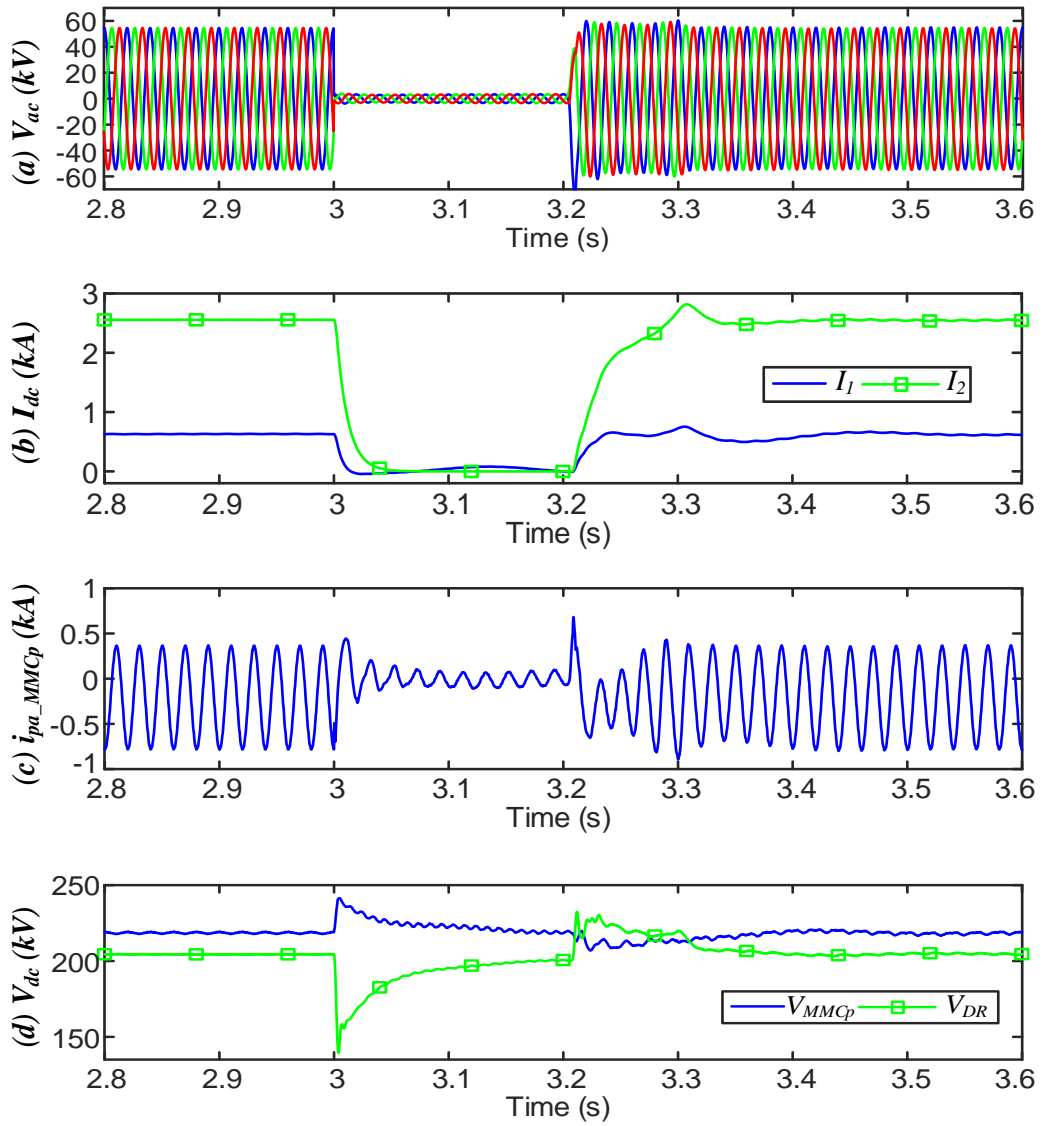


Fig. 4.11 System performance to AC fault in P - V_{ac} control mode: (a) AC voltage, (b) DC current, (c) Phase A MMC_p upper arm current, (d) DC voltage.

4.6.4 DC fault ride-through

Fig. 4.12 illustrates the system performances when permanent p2p solid faults (F_1 or F_2) are applied at 3.0 s. The waveforms in the first column show the system performance under F_2 fault and the system performance under F_1 fault is shown in the second column.

The DC link voltage at the faulty part drops immediately at 3.0 s, as shown in Fig. 4.12 (a). The blocking time of the MMCs is set at 2 ms after the fault occurrence. Then, the offshore ACCB is opened after 60 ms delay.

The MMC_P DC voltage shown in Fig. 4.12 (b) is increased to half of E_1 (320 kV) during F_2 fault to block the fault current contributed by S_2 . For F_1 fault, the MMC_P DC voltage appears negative to half of E_2 (-100 kV) due to the use of FBSMs to handle the voltage applied by S_1 . The DC currents of MMC_P (I_1) and the DR (I_2), and the current at the DC terminals of S_2 (I_3) are shown in Fig. 4.12 (c). As can be seen, I_1 drops to zero during the DC fault due to the hybrid MMCs' fault blocking capability. No power exchange can be seen in this case. Both I_2 and I_3 will experience overcurrent from the DR, and are reduced to zero after the ACCB is opened at 3.062 s. The fast DC disconnectors/switches can then open to disconnect the faulty branch so no DCCB is required.

Fig. 4.12 (d) shows the arm current of MMC_P during the DC faults. The collapse of E_2 during F_2 fault is quickly detected, MMC_P is blocked immediately and there is no arm overcurrent. In the case of F_1 fault, the drop of E_1 leads to the voltage collapse and blocking of MMC_P. The initial arm overcurrent flows through the freewheeling diodes in the MMC and is quickly reduced to zero, as shown in Fig. 4.12 (d).

Fig. 4.12 (e) shows the averaged capacitor voltages of the FBSM and HBSM in the upper and lower arms of MMC_P during the DC faults. All SMs are charged and

controlled at around the nominal value during F_2 fault. For F_1 fault, the averaged voltages of the bypassed HBSM capacitors are around the rated value while those of the FBSMs are increased up to 2.08 kV (1.14 p.u.) due to the charging by the fault current, which is within the safe margin (typically around 1.3~1.4 p.u.).

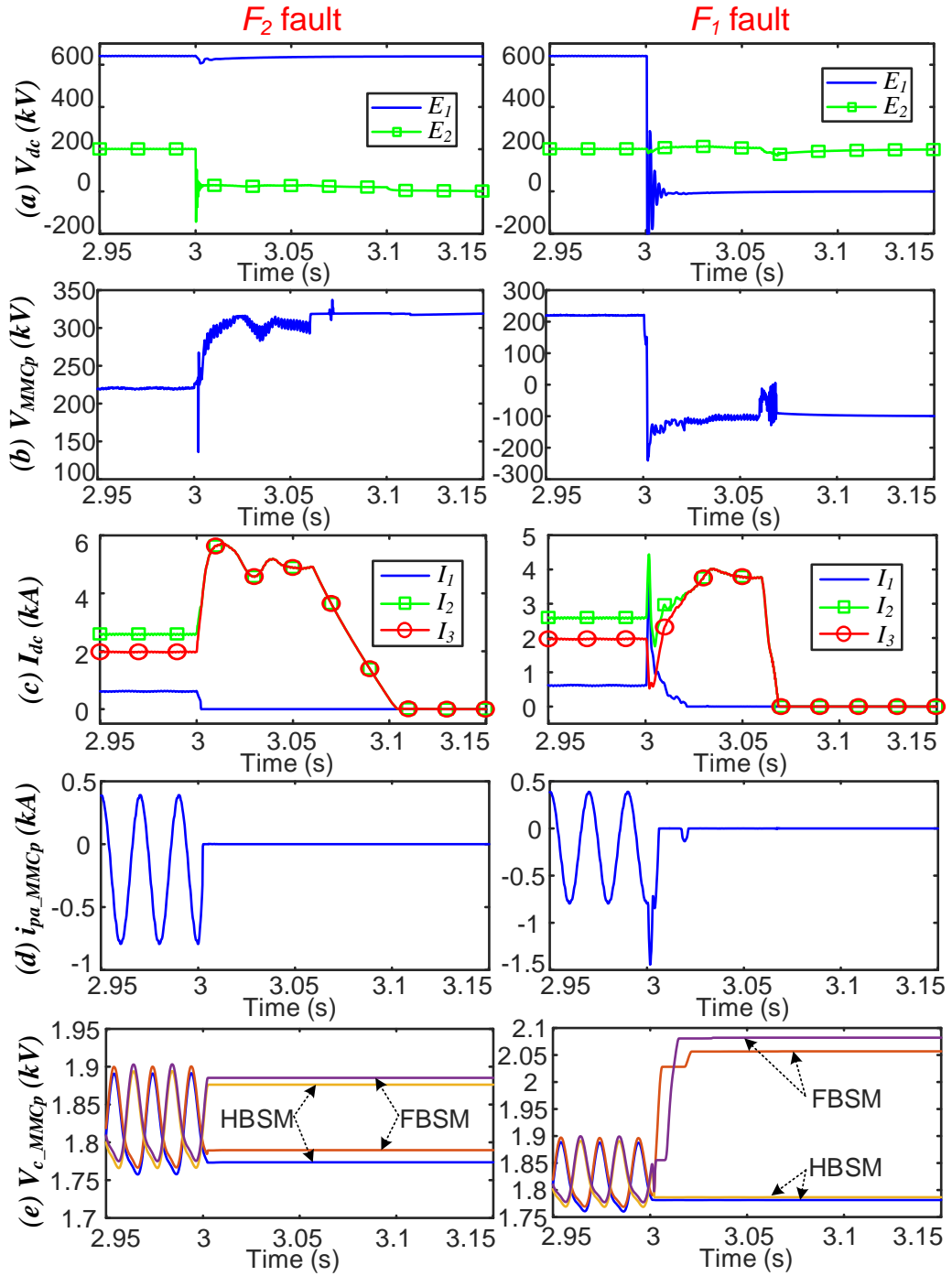


Fig. 4.12 System performance to DC faults: (a) System DC voltage, (b) Converter DC voltage, (c) System DC current, (d) Upper arm current of MMC_p phase A, (e) Average upper / lower arms FBSM and HBSM capacitor voltage of MMC_p phase A.

4.7 Summary

A DR-MMC AC/DC hub which comprises of series-connected DR and MMC for connecting offshore wind farms with onshore DC network and offshore production (e.g. hydrogen) platform has been proposed in this chapter. System configuration, efficiency, and control and operation during normal and fault conditions of the proposed DR-MMC hub have been studied. Considering a ± 100 kV/400 MW DC system for offshore production platform, and a ± 320 kV/400 MW for onshore DC network, the proposed DR-MMC Hub reduces the MMC rating from 400 MW for the “conventional” method using parallel-connected MMC and DR to 275 MW, while the DR rating is increased from 400 MW to 525 MW. Thus, the proposed hub can also reduce the power loss by 10.5% due to the lower power loss of the DR compared to MMC, while lower capacity of MMC potentially leads to reduced investment cost. Considering different operation requirements, two control modes have been developed to regulate the voltage or power of the DC system for the offshore production platform. Due to the current-limiting control and the MMC blocking capabilities, the DR-MMC Hub can securely ride through offshore AC faults under different operation scenarios. The DR-MMC Hub can also isolate DC faults of either DC network due to the adopted hybrid MMC configuration with additional FBSMs and/or HBSMs. PSCAD/EMTDC simulation have verified the performance of the proposed hub during normal operations including V_{dc} - V_{ac} and P - V_{ac} control modes, and AC/DC fault conditions.

Chapter 5 Unidirectional Hybrid F2F DC/DC Converter

5.1 Introduction

The AC/DC hub concepts using hybrid topologies of LCC-MMC and DR-MMC have been investigated in Chapters 3 and 4, respectively. In this chapter, a DC/DC converter using combinations of different converter technologies is proposed and studied.

As described in Chapter 2, even though the non-isolated DC/DC converters is more economical and efficient compared to the F2F configuration, electrical isolation would still be desirable in many applications and thus isolated DC/DC converters will be required. In addition to the benefit of galvanic isolation, the isolated topologies can be easier adopted for different DC voltage conversion ratios using the AC transformer turn ratio. For high voltage and high power applications, F2F-MMCs offer flexible bidirectional power transmission and DC fault blocking capability though converter cost and power loss are high. For unidirectional HVDC transmission applications such as wind power collection, the use of a F2F DC/DC with a MMC and an uncontrolled DR may be advantages with lower converter cost and power loss than the F2F-MMC configuration. However, a fully rated MMC is still required so alternative DC/DC converters may be further optimised to be more economical and efficient for such applications.

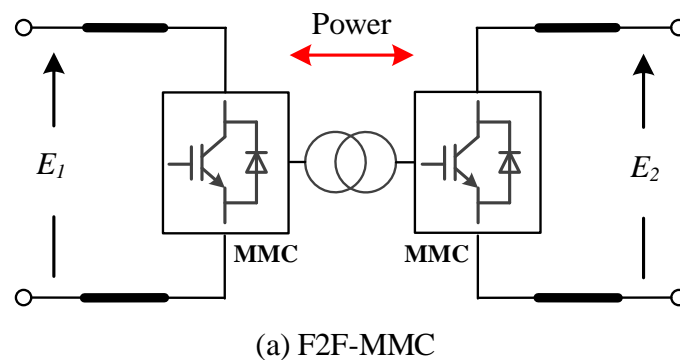
In this chapter, an alternative hybrid F2F DC/DC converter is proposed for unidirectional HVDC applications. The proposed configuration uses combinations of LCC, DR and MMC in order to reduce investment cost and power loss. The topology and efficiency of the proposed DC/DC converter are analysed and compared with conventional F2F DC/DC converters. The system control principle and start-up

procedure are developed, and detailed DC fault protection of the proposed DC/DC converter are discussed. Simulation of the proposed DC/DC converter during system start-up, normal power variation and DC fault conditions are conducted to verify the operation of the proposed DC/DC converter.

5.2 Converter topology and efficiency comparison

5.2.1 Topologies of conventional F2F DC/DC converters

Fig. 5.1 shows the circuit diagrams of two conventional F2F DC/DC converters. As shown in Fig. 5.1 (a), a F2F-MMC consists of two full-sized MMCs connected on their AC side through an isolation transformer which provide the required voltage steps. DC power can flow bidirectionally between the DC networks E_1 and E_2 . For unidirectional HVDC transmission applications, a MMC can be replaced by a DR as displayed in Fig. 5.1 (b). The transmitted power from E_2 will be inverted by the MMC to AC, and then rectified by the DR to E_1 . Compared to the MMC with the same power rating, the total investment cost of the DR can be reduced by 30% [94]. Thus, the overall cost of F2F DR-MMC topology can potentially be cheaper than F2F-MMC.



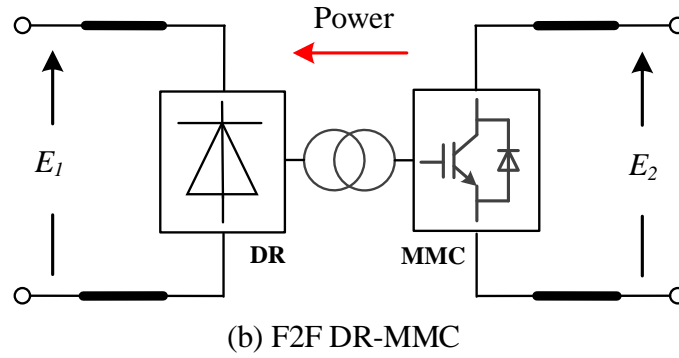


Fig. 5.1 Conventional F2F DC/DC converters.

5.2.2 Topology of unidirectional hybrid F2F DC/DC converter

Fig. 5.2 illustrated the circuit configuration of the hybrid F2F DC/DC converter for unidirectional HVDC power transmission. As seen, a LCC inverter is used to invert the power from E_2 , which is then rectified by the DR to E_1 . The DR and LCC are usually arranged as 12-pulse configurations, thus that two star-star-delta transformers are used. According to [95], the total cost of the MMC with the same power rating is 20% higher than the LCC. Moreover, the current capability of LCC thyristors is higher than that of MMC IGBTs, potentially resulting in increased power capability.

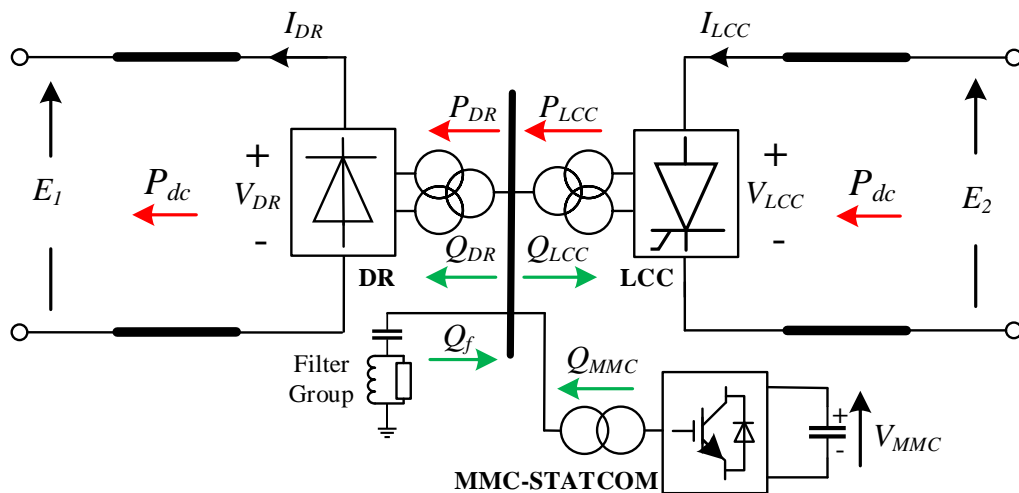


Fig. 5.2 Proposed unidirectional hybrid F2F DC/DC converter.

A small MMC operating as a static synchronous compensator (MMC-STATCOM) is used to establish the internal AC grid with fixed frequency and controlled voltage magnitude. It also provides instantaneous reactive power balance for the system during power flow change. A group of filters is connected to the AC bus for filtering and reactive power compensation for the DR and LCC. Assuming the power losses of the transmission lines and converters are neglectable, the power flow relationships can be expressed as:

$$\begin{cases} P_{dc} = P_{DR} = P_{LCC} \\ Q_{MMC} + Q_f = Q_{LCC} + Q_{DR} \end{cases} \quad (5.1)$$

Since the cost of AC filters is much lower than that of the MMC-STATCOM, those filters are used to provide most of the reactive power consumption in the system during power transfer. Therefore, in addition to some fixed filters, switched capacitor banks are used to provide extra reactive power compensation which will be switched in gradually with the increase of the transmitted active power. Therefore, a MMC-STATCOM with relatively low power rating can be used in that manner to reduce the converter cost and power loss.

Typical converter power loss of DR, LCC and MMC are in the range of 0.11%, 0.26% and 0.6%, respectively [35, 37, 79]. Due to the F2F configuration, the power loss ratio of F2F-MMC is thus roughly given as $0.6\% \times 2 = 1.2\%$, while that of F2F DR-MMC is around $0.6\% + 0.11\% = 0.71\%$ at full power transmission.

In the unidirectional hybrid F2F DC/DC converter, the power loss of the MMC-STATCOM should be counted. As described in the above section, a relatively small MMC-STATCOM is used. Considering the power rating of the MMC-STATCOM is 0.2 p.u., the total power loss of the proposed converter can be roughly calculated as $0.11\% + 0.26\% + 0.6\% \times 20\% = 0.49\%$, which is substantially lower than the other F2F topologies.

5.3 Control principles

For the unidirectional hybrid F2F DC/DC converter, the DC voltages of the two DC networks are set to be the nominal values (E_1 and E_2), so the main objectives are to control the transmitted active power and to the DC voltage of the MMC-STATCOM. A simplified control block diagram for the proposed DC/DC converter is shown in Fig. 5.3. However, as previously discussed in Chapter 4, voltage control for the DC network E_1 can also be achieved by the proposed DC/DC converter. As the operation with E_1 DC voltage control is similar to active power control, no further study is provided here.

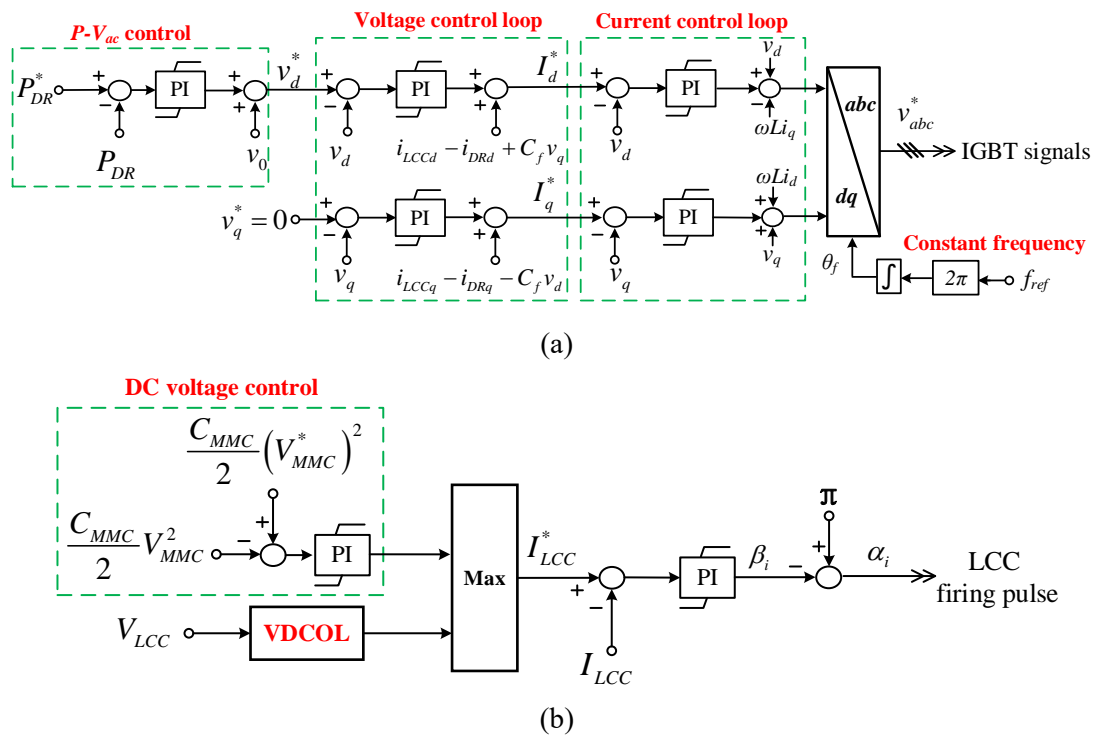


Fig. 5.3 Schematic control diagrams of the unidirectional hybrid F2F DC/DC converter:

(a) Control of the MMC-STATCOM, (b) Control of the LCC inverter.

5.3.1 Control of MMC-STATCOM

As there is a significant number of capacitors at the internal AC bus for filtering and reactive power compensation for the DR and LCC, equations of the AC capacitor

voltages will be used to construct the AC voltage control loop of the MMC-STATCOM. According to KCL, the relationship between current and voltage at the internal AC bus can be expressed as:

$$\begin{bmatrix} i_{MMCa} \\ i_{MMCb} \\ i_{MMCc} \end{bmatrix} = \begin{bmatrix} i_{LCCa} \\ i_{LCCb} \\ i_{LCCc} \end{bmatrix} - \begin{bmatrix} i_{DRa} \\ i_{DRb} \\ i_{DRc} \end{bmatrix} - C_f \frac{d}{dt} \begin{bmatrix} v_a \\ v_b \\ v_c \end{bmatrix} \quad (5.2)$$

where i_{MMC} , i_{LCC} and i_{DR} are the AC currents of the MMC, LCC and DR, respectively. C_f is the total capacitance at the internal AC bus. The subscript a , b and c denote variables in the abc frame.

Transforming (5.2) into dq frame yields:

$$\begin{bmatrix} i_{MMCd} \\ i_{MMCq} \end{bmatrix} = \begin{bmatrix} i_{LCCd} \\ i_{LCCq} \end{bmatrix} - \begin{bmatrix} i_{DRd} \\ i_{DRq} \end{bmatrix} + \begin{bmatrix} 0 & \omega C_f \\ -\omega C_f & 0 \end{bmatrix} \begin{bmatrix} v_q \\ v_d \end{bmatrix} - \begin{bmatrix} C_f & 0 \\ 0 & C_f \end{bmatrix} \frac{d}{dt} \begin{bmatrix} v_d \\ v_q \end{bmatrix} \quad (5.3)$$

where ω is the grid frequency in rad/s and the subscript d and q denote variables in the dq frame. It can be seen from (5.3) that the internal AC voltage can be regulated by adjusting the current references of the inner current controller of the MMC-STATCOM. Thus, the outer voltage control loop can be constructed accordingly using PI controllers [48].

Fig. 5.3 (a) shows the schematic control of the MMC-STATCOM. It is composed of an outer voltage control loop and an inner current control loop. The MMC-STATCOM also uses a constant internal AC frequency (e.g. 50 Hz) to derive the phase angle. Detailed controller tuning approach is not the focus of this study, whereas the PI compensator parameter tuning for outer voltage and inner current controllers is referred to [76].

Given that the DC voltages of the two DC networks are controlled at the rated value, the transmitted active power of the proposed DC/DC converter is primarily decided by the DC voltage provided by the DR (V_{DR}) while V_{DR} is given in [20] as:

$$V_{DR} = \frac{6}{\pi} (\sqrt{3} T_{DR} V_{ac} - \frac{P_{DR} X_{DR}}{V_{DR}}) \quad (5.4)$$

where the internal AC bus voltage is denoted as V_{ac} . T_{DR} and X_{DR} are the turn ratio and reactance of the DR transformer, respectively.

Equation (5.4) shows that the DC voltage at the DR terminal and the active power exported to DC grid E_I can be controlled by adjusting the internal AC voltage magnitude. Therefore, as shown in Fig. 5.3 (a), an outer P - V_{ac} control loop is used to control the transmitted active power of the proposed DC/DC converter by acting on the internal AC voltage of the DC-DC converter. A set-point v_0 is added to keep the offshore AC voltage in a small range, e.g. from 0.9 to 1.1 p.u..

5.3.2 Control of LCC

Fig. 5.3 (b) shows the schematic control diagram of the LCC. The MMC-STATCOM only generate reactive power in steady state where only a small amount of active power is required to compensate for its power loss. However, any active power change of the DC/DC converter during transient conditions will change the energy stored in the DC capacitors of the MMC-STATCOM. Hence, the MMC-STATCOM DC voltage is an immediate indicator of any active power unbalance in the DC/DC converter, which can thus be used to rapidly change the current order for the LCC inverter. The power balancing equation of the proposed DC/DC converter can be obtained as:

$$P_{DR} = V_{MMC} C_{MMC} \frac{dV_{MMC}}{dt} + V_{LCC} I_{LCC} \quad (5.5)$$

where V_{MMC} and C_{MMC} are the total voltage and capacitance of the MMC-STATCOM DC capacitors. The DC voltage and current of the LCC are denoted as V_{LCC} and I_{LCC} .

The above equation can be rewritten as:

$$\frac{d\left(\frac{C_{MMC} V_{MMC}^2}{2}\right)}{dt} = (P_{DR} - V_{LCC} I_{LCC}) \quad (5.6)$$

Thus, it can be seen from (5.6) that the total stored capacitor energy $\frac{C_{MMC} V_{MMC}^2}{2}$ can be considered as a state variable, which can be controlled by the LCC current I_{LCC} . As seen from Fig. 5.3 (b), the current order I_{LCC}^* is generated by the MMC-STATCOM DC voltage controller, where the inputs are the reference $\frac{C_{MMC} (V_{MMC}^*)^2}{2}$ and that of the measured total energy storage in the MMC DC capacitors. A Voltage-Dependent Current Order Limiter (VDCOL) controller helps to reduce the current order if the LCC DC voltage drops.

Considering the internal AC voltage magnitude varies according to the transmitted active power by the DR, this potentially leads to high reactive power absorption by the LCC when the AC voltage and transmitted active power are higher. In order to optimise and limit LCC reactive power absorption, the transformer tap changer in the LCC converter station can be used [96]. In this paper, the transformer tap changer is controlled in open loop mode to reduce LCC reactive power consumption and the use of additional AC filters, as will be demonstrated later.

5.4 System start-up procedure

Fig. 5.4 illustrates the procedure of start-up operation of the unidirectional hybrid F2F DC/DC converter.

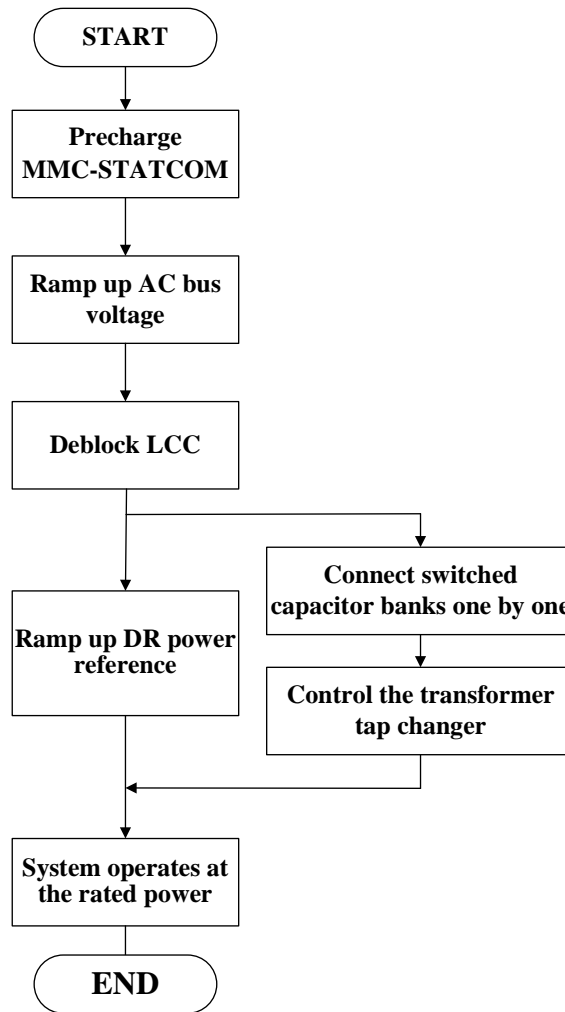


Fig. 5.4 Flow chart of system start-up.

To startup the system, the MMC-STATCOM DC capacitors will need be precharged using a small auxiliary power supply, such as an emergency diesel generator [96] or battery energy storage [97]. Considering the system power losses compensated by the MMC-STATCOM, the auxiliary power supply should feed the DC capacitors until the whole DC/DC converter starts to transmit active power. Once the DC capacitors are fully charged, the MMC-STATCOM can ramp up the internal AC voltage, and then the LCC inverter can be deblocked in preparation for power transmission.

The transmitted active power is regulated by the active power reference P_{DR}^* that can be ramped up to the required value. In order to prevent the MMC-STATCOM from exceeding its power rating limit, switched capacitor banks for reactive power compensation of the DR and LCC are switched in/out one by one during power changes. In addition, the transformer tap changer can be used to reduce the reactive power absorption, as previously described which will be further demonstrated in the simulation section.

5.5 DC fault protection

Fig. 5.5 shows two most severe DC fault scenarios considered in the unidirectional hybrid F2F DC/DC converter. The p2p fault that happened at the DC cable between the DR and E_1 is denoted as F_1 , and F_2 is the p2p fault at the DC cable between the LCC and E_2 .

There are various DC fault detection methods that can be used [34], e.g., the change rates of the DC reactance voltages are monitored to detect and locate the DC faults without communication, which can activate the fault protection within 1 ms [98]. As seen in Fig. 5.5, DCCBs are installed at the DC network E_2 to protect its network and the proposed DC/DC converter, which will be explained in the following subsection.

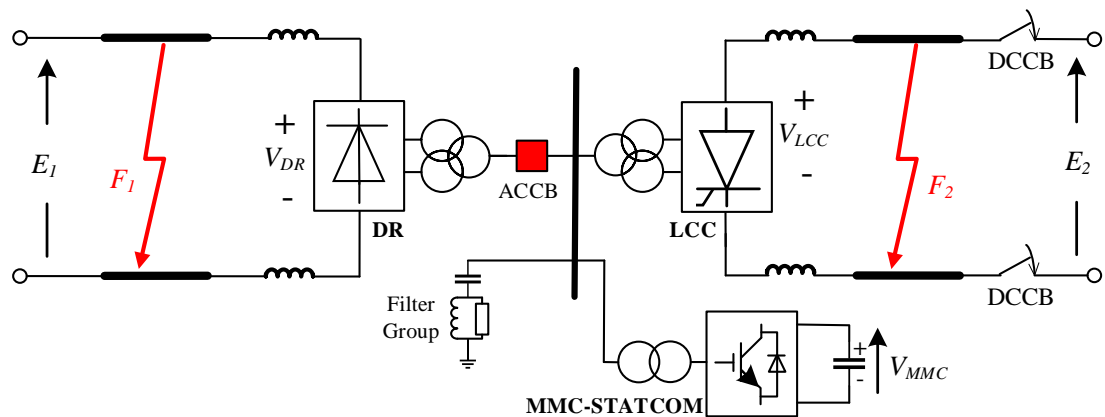


Fig. 5.5 System during DC faults.

5.5.1 DC protection under F_I fault

After F_I fault, the DC voltage of DR collapses to around zero. The DC fault also propagates to the internal AC grid due to the use of diode rectifier, behaving similar as an AC fault. Consequently, the internal AC voltage drops significantly during F_I fault [99]. If the MMC-STATCOM remains operational during F_I fault, the outer P - V_{ac} and the voltage control loops saturate so that its current will be limited to the maximum allowed value due to the inner current control loop.

The collapse of the internal AC voltage also leads to the LCC commutation failure, which means that the DC network E_2 will experience a DC short circuit. Considering the AC circuit breaker (ACCB) installed at the AC terminals of the DR as indicated in Fig. 5.5, its opening could isolate the DR and F_I fault from other parts of the DC-DC converters, thereby allowing the internal AC voltage to restore. However, the operation of MMC-STATCOM with limited current capacity leads to slow diminishing of the DC offshore in the DR AC grid current during F_I fault. Consequently, the AC current zero-crossing which is required for opening ACCB may not happen and thus, the ACCB may not be opened.

To solve the problem, a set of DCCBs can be used to protect the system and rapidly isolate DC faults. Fig. 5.6 shows four possible DCCB deployment positions (points A, B, C and D) that can be considered, which will be analysed as follows.

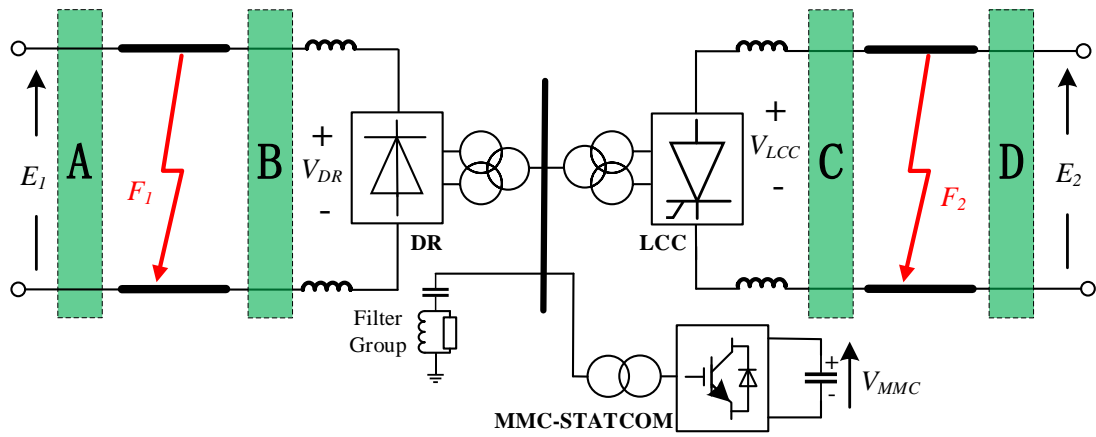


Fig. 5.6 Potential locations of the DCCB.

- Point A: The DCCBs installed at point A cannot protect the DC network during F_1 fault, and thus is not suitable.
- Point B: The installation of DCCBs at point B can help the DR isolate F_1 fault. However, any disturbance on the internal AC grid before opening DCCBs may happen, which could cause the LCC commutation failure leading to DC short circuit at E_2 . Thus, Point B is not adequate either.
- Point C: The DCCBs installed at point C can isolate the LCC from E_2 after LCC commutation failure caused by F_1 fault propagated through the DR. After F_1 fault is cleared, the DC voltage of the DR recovers and the MMC-STATCOM rebuilds the internal AC voltage. The DCCBs can then be reclosed and the LCC can be deblocked to start transmitting active power from E_2 .
- Point D: The DCCBs at point D can not only isolate F_1 fault in a similar way as Point C, but also provide effective protection against F_2 fault.

In conclusion, both Point C and D can isolate F_1 fault while Point D provides the additional benefit in isolating F_2 fault. The exact location to install the DCCBs has to consider the system configuration, e.g., which part is offshore or onshore and how the general networks E_1 and E_2 are protected. In this study, the DCCBs are installed at Point D. When F_2 fault is detected, the blocking signal will be sent to MMC-

STATCOM. The AC voltage drops due to the blocking of MMC and the DR power transfer is stopped. The DCCBs detect the overcurrent due to the LCC commutation failure, and the DCCBs are tripped to isolate the fault. The LCC can then be blocked after opening the DCCBs. When the fault is cleared, the proposed DC/DC converter can be restarted as presented in Section 5.4 (considering the fault is on other part of the DC network).

5.5.2 DC protection under F_2 fault

In the occurrence of a F_2 fault, the proposed DC/DC converter is tolerant to F_2 fault due to the unidirectional current flow of the thyristors in the LCC, and the DCCBs at Point D can isolate the fault from system E_2 as previously described.

Thus, once F_2 fault is detected, the blocking signals are sent to LCC and MMC-STATCOM. Hence, the DR will stop power transfer as the internal AC voltage decreases due to the blocking of MMC-STATCOM. Meanwhile, the potential discharging of MMC-STATCOM during F_2 fault can be avoided. The DC voltage and current of LCC decrease to zero due to F_2 fault so that the LCC can be blocked. After fault clearance, the proposed DC/DC converter can follow the start-up procedure to restore the power transmission.

5.6 Simulation results

A simulation model of Fig. 5.2 is built in PSCAD/EMTDC to test the technical feasibility of the unidirectional hybrid F2F DC/DC converter. The DC voltages of the two DC networks are rated at 640 kV (at the DR side) and 500 kV (at the LCC side), and power is rated at 1000 MW. The relevant parameters of the proposed DC/DC converter are shown in Table 5.1.

Table 5.1 Parameters of the unidirectional hybrid F2F DC/DC converter

| | Parameters | Nominal Value |
|--|---------------------------------------|--------------------------|
| MMC-STATCOM | Power rating | 200 MVA |
| | Rated DC voltage | 300 kV |
| | SM capacitor voltage | 1.83 kV |
| | SM capacitance | 11.5 mF |
| | Arm inductance | 0.0159 H |
| | SM number per arm | 164 |
| | Interfacing transformer voltage ratio | 200kV/132 kV |
| 12-pulse DR | Power rating | 1000 MW |
| | Rated DC voltage | 640 kV |
| | Interfacing transformer voltage ratio | 200 kV/261.8 kV/261.8 kV |
| | Transformer leakage reactance | 0.18 p.u. |
| | DC smoothing reactance | 0.2 H |
| 12-pulse LCC | Power rating | 1000 MW |
| | Rated DC voltage | 500 kV |
| | Interfacing transformer voltage ratio | 200 kV/220 kV/220 kV |
| | Transformer leakage reactance | 0.18 p.u. |
| | DC smoothing reactance | 0.2 H |
| AC filters for reactive power compensation | Stage 1 | 180 MVAr |
| | Stage 2 | 250 MVAr |
| | Stage 3 | 250 MVAr |
| | Stage 4 | 190 MVAr |
| DC cables | Length of cables to E_1 | 200 km |
| | Length of cables to E_2 | 200 km |

Same to previous converter system models, the equivalent averaged model is used for the MMC-STATCOM for faster simulation [84]. The 500 kV LCC inverter is

modified from the CIGRE benchmark model [83]. As discussed in Section 5.5.1 and shown in Fig. 5.6, hybrid DCCBs are installed at point D to interrupt the fault current rapidly [80, 100]. The 200 km DC cables are built using the frequency-dependent model provided by PSCAD/EMTDC.

5.6.1 System start-up and normal active power variation

Fig. 5.7 shows simulation results of the unidirectional hybrid F2F DC/DC converter during start-up operation.

As previously described, it considers that the MMC-STATCOM has been precharged. The internal AC voltage is shown in the RMS value in Fig. 5.7 (a). From 0.5 s to 1.0 s, the MMC-STATCOM smoothly ramps up the AC voltage to the preset value, which is lower than the minimum DR conduction voltage (i.e. $\pi E_f/6\sqrt{2}T_{DR}$).

Fig. 5.7 (d) shows the sum of the reactive power of the DR and LCC (Q_{total}), and that of the filters (Q_f) and MMC-STATCOM (Q_{MMC}). Due to the existence of the stage 1 AC filters for harmonic suppression, Q_{MMC} increases its inductive Q to 180 MVar (negative shown in Fig. 5.7 (d)) to balance the capacitive Q provided by the filters. At 1.5 s, the LCC inverter is deblocked to prepare for power transmission.

Afterwards, the active power reference of the DR is ramped up from 0 MW at 2.0 s to the rated value (1000 MW) at 8.0 s. As shown in Fig. 5.7 (d) and (e), the AC voltage and total reactive power absorption by the DR and LCC (i.e. Q_{total}) increase accordingly. To avoid the overload of MMC-STATCOM when the transmitted active power increases, three filter stages (i.e. the stages 2, 3 and 4) are switched in and the transformer tap changer is adjusted, at different times. Therefore, a sawtooth waveform of Q_{MMC} is shown in Fig. 5.7 (d). The detailed corresponding sequence and the system performance are described as follows:

1. The active power ramps up from 0 MW at 2.0 s. Q_{MMC} and Q_{total} increase.
2. Q_{MMC} reaches 150 MVar at 4.5 s, and then the stage 2 AC filter is switched in. Thus, Q_{MMC} is reduced and Q_f is stepped up to 430 MVar.
3. Q_{MMC} reaches 150 MVar at 6.0 s, and the stage 3 AC filter is switched in. Thus, Q_{MMC} is reduced and Q_f is stepped up to 680 MVar.
4. To further reduce the reactive power consumption, the transformer tap changer is controlled to be decreased by 5% from 6.9 s to 7.1 s. As a result, both Q_{total} and Q_{MMC} are reduced.
5. At 7.5 s, the stage 4 AC filter is switched in, resulting in the decrease of Q_{MMC} and the step-up of Q_f to 870 MVar. When the active power reaches the rated value (1000 MW) at 8.0 s, Q_{MMC} offers 20 MVar capacitive Q (positive shown in Fig. 5.7 (d)).

The active power of the DR (P_{DR}), LCC (P_{LCC}) and MMC-STATCOM (P_{MMC}) are shown in Fig. 5.7 (c), and the DC power (P_{DC}) are measured at the DC terminals of the DR as shown in Fig. 5.7 (b). P_{DR} , P_{LCC} and P_{DC} are ramped up to the rated value. P_{MMC} oscillates during power flow change, but it is maintained at 0 MW in steady state by the power balance controller in the LCC.

Fig. 5.7 (a) shows the DC voltages of the DR (V_{DR}), LCC (V_{LCC}) and MMC-STATCOM (V_{MMC}). V_{DR} and V_{LCC} are sustained at their rated values. V_{MMC} will slightly change during power variation, and it is also kept at the rated value with the help of the power balance controller.

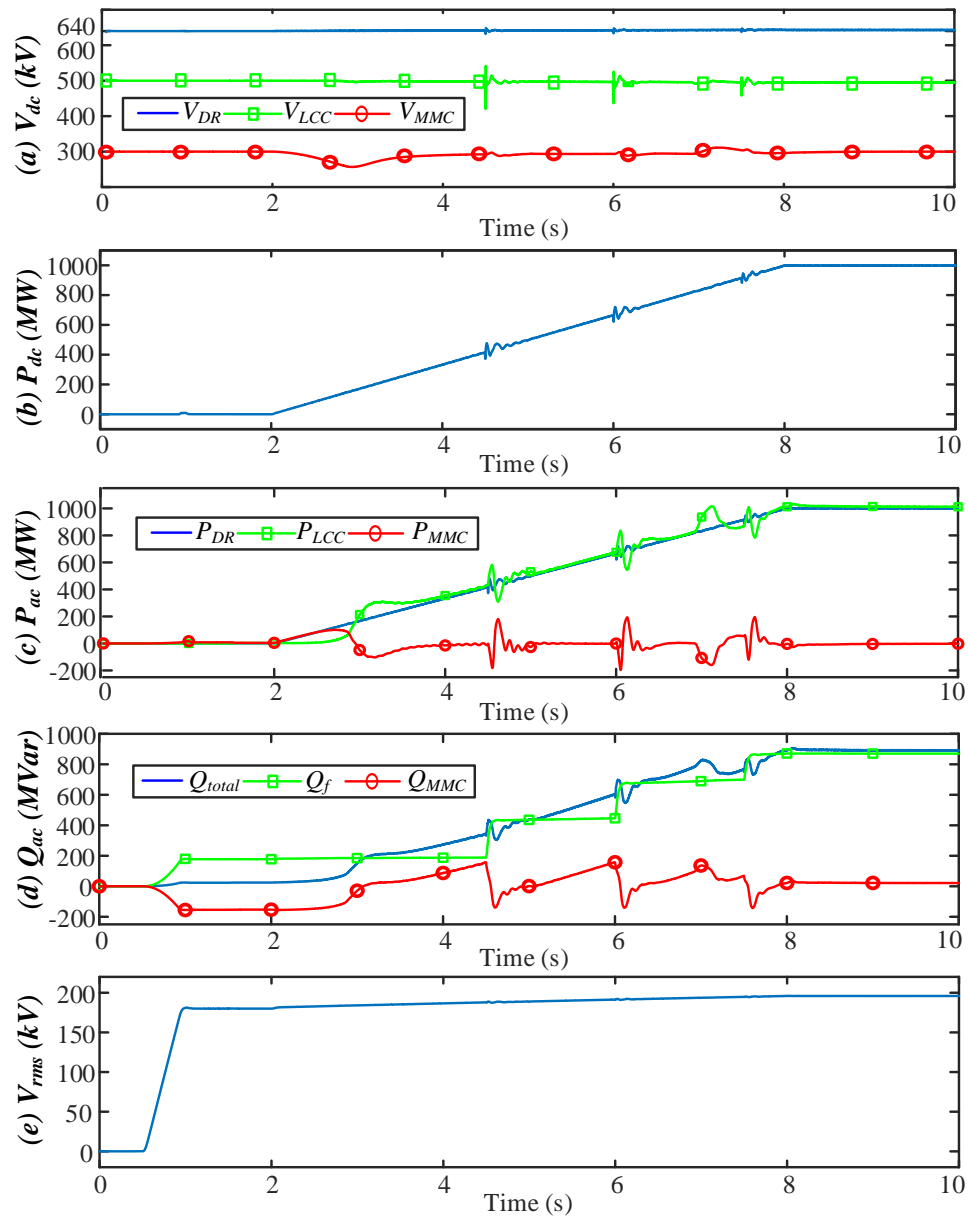


Fig. 5.7 System start-up operation: (a) DC voltage, (b) DC power, (c) Active power, (d) Reactive power, (e) RMS AC voltage.

Further studies of the unidirectional hybrid F2F DC/DC converter during active power step changes are carried out and the simulated waveforms are shown in Fig. 5.8. In the simulation, the active power reference of the DR is stepped up from 500 MW to 650 MW at 6.0 s, and then stepped back to 500 MW at 8.0 s.

Fig. 5.8 (a) shows the DC voltages of DR, LCC and MMC-STATCOM. There are small oscillations of converter DC voltages during power step changes, but are largely maintained at their nominal values.

The DC power (P_{DC}) and the active power of the DR (P_{DR}), LCC (P_{LCC}) and MMC-STATCOM (P_{MMC}) are shown in Figs. 5.8 (b) and (c). As can be seen, P_{DR} and P_{DC} follow the active power reference smoothly during both step up and step down operations. P_{MMC} is regulated by the power balance controller of the LCC, thus the active power of MMC is stabilised at 0 MW after a transient period and the active power of LCC follows the active power reference in steady state. Therefore, the proposed converter achieves smooth control and operation during the power step.

Fig. 5.8 (d) shows the reactive power provided by AC filters and converters. The reactive power of AC filters (Q_f) is unchanged as no additional capacitor bank is switched in during this period. The total reactive power absorption of the DR and LCC (Q_{total}), and that of MMC-STATCOM (Q_{MMC}), have step changes and follow the active power variation. It is noticed that the value of Q_{MMC} is closed to the rated capacity value (200MVar). Thus, if the power step change is further increased (e.g. more than 150 MW), the power rating of MMC-STATCOM in the system have to increase to provide additional reactive power compensation for the LCC and DR. Otherwise, the power balance of the proposed DC/DC converter may be out of control, which can potentially cause operation issues for the converter system. A power step of 200MW has been tested in the simulation and the results (not provided here) show that the system becomes oscillative. The internal RMS AC voltage generated by the MMC-STATCOM shown in Fig. 5.8 (e) varies smoothly with the change of the system active power reference.

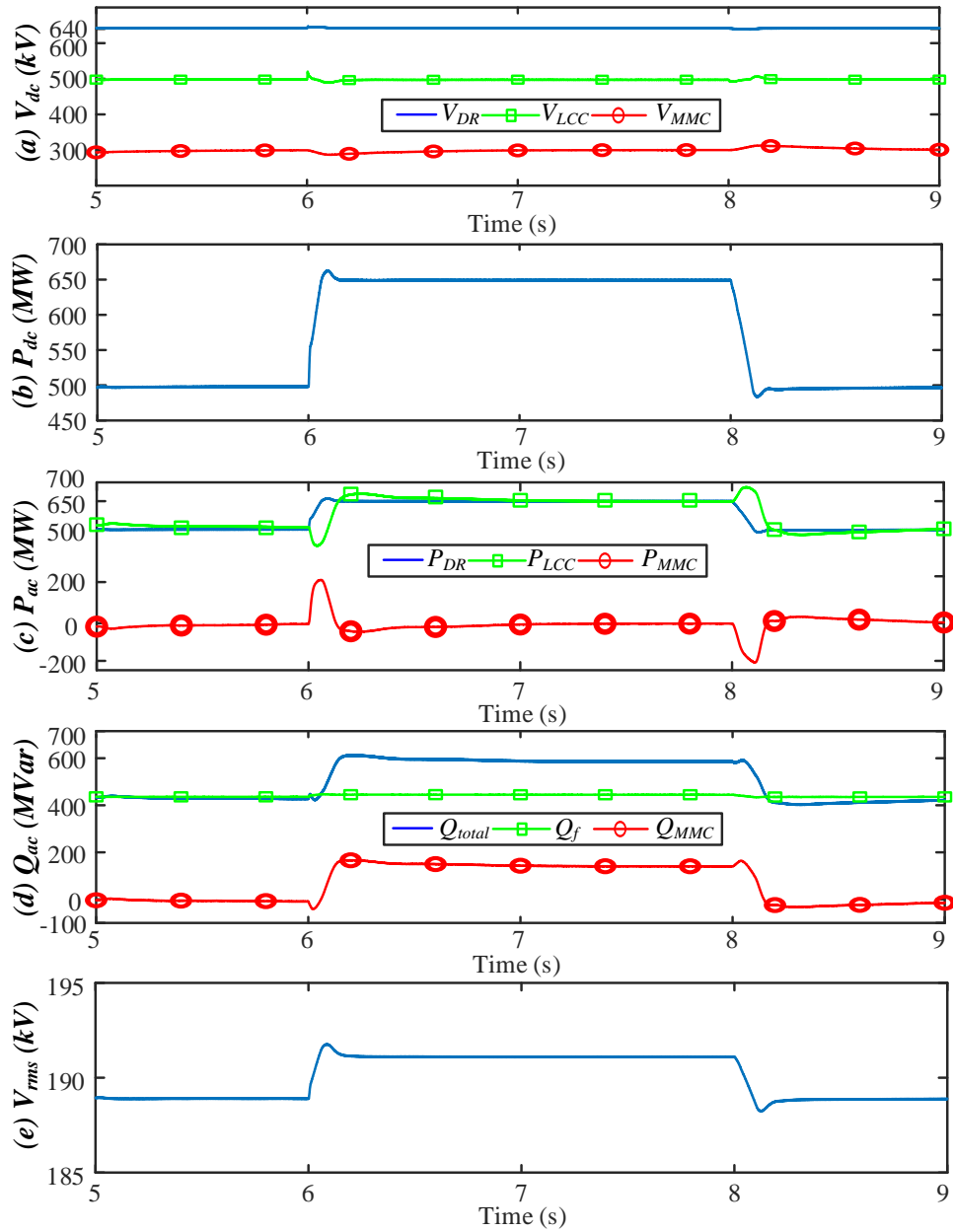


Fig. 5.8 System performance during active power step changes: (a) DC voltage, (b) DC power, (c) Active power, (d) Reactive power, (e) RMS AC voltage.

5.6.2 System response during F_1 fault

Fig. 5.9 illustrates the system response of the unidirectional hybrid F2F DC/DC converter when a permanent solid p2p fault F_1 is applied at the DR side of the DC network with the distance of 100 km at 6.0 s. Using the change rates of the DC

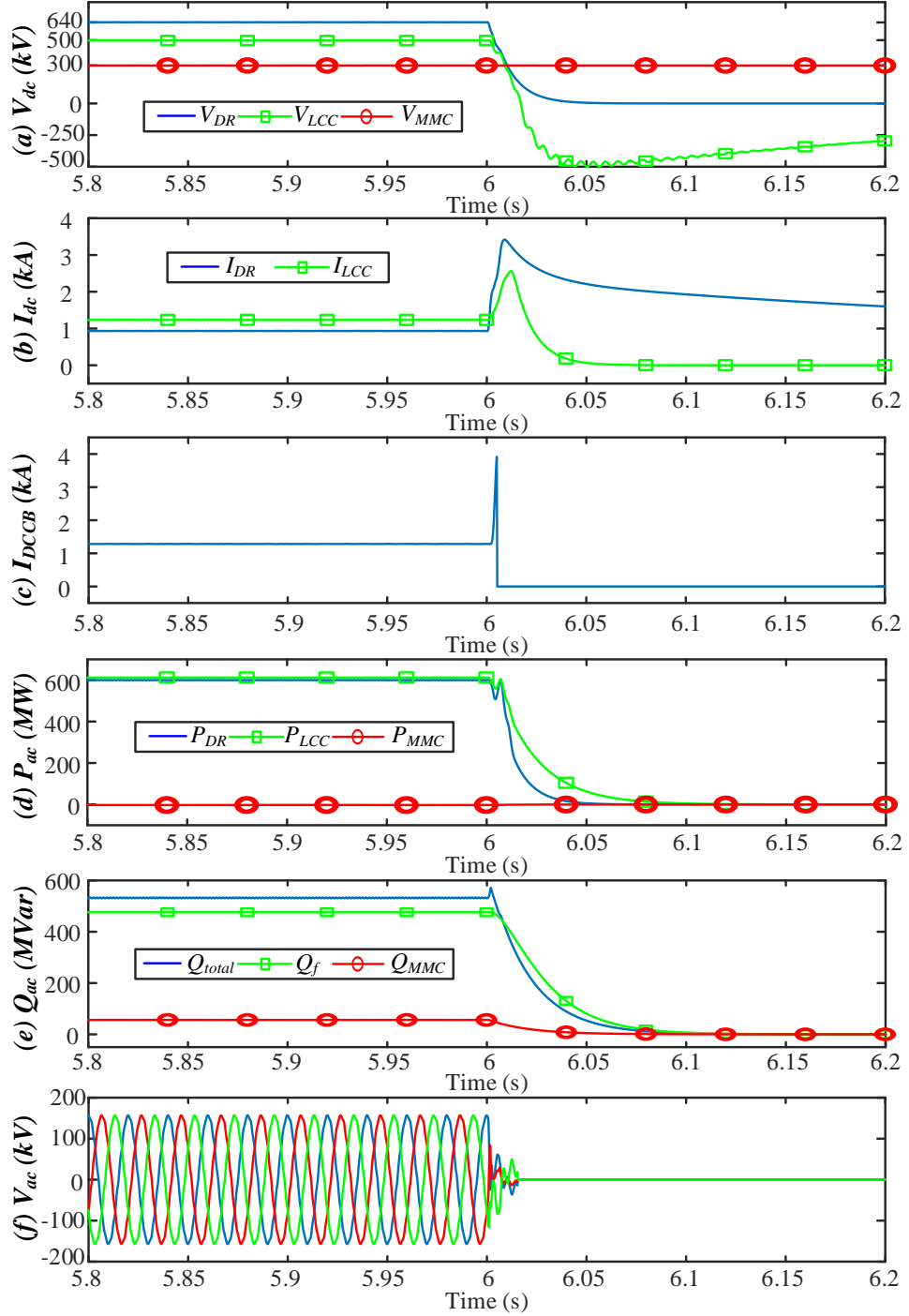
reactance voltage, as presented in Section 5.5, the DC fault is quickly detected within 1 ms after fault initiation [98], and the blocking time of the LCC and MMC-STATCOM is set at 6.001 s. The trippings of DCCBs are based on the locally measured overcurrent threshold (i.e. 2 p.u.).

Fig. 5.9 (a) shows the DC voltages of the DR, LCC and MMC-STATCOM. As can be seen, the DC voltage of DR (V_{DR}) immediately drops to zero during F_1 fault. Due to the decrease of the internal AC voltage (V_{ac}) as shown in Fig. 5.9 (f), the LCC has commutation failure, resulting in the collapse of the other side of the DC voltage of LCC (V_{LCC}). As the MMC-STATCOM is blocked, the DC voltage of MMC-STATCOM (V_{MMC}) is maintained at its rated value.

Figs. 5.9 (b) and (c) shows the DC currents of the DR (I_{DR}), LCC (I_{LCC}) and DCCB (I_{DCCB}), respectively. As seen, I_{DR} increases during F_1 fault, and I_{LCC} also increases due to commutation failure. The overcurrent is detected at the DCCBs, which are opened to isolate the DC network E_2 and LCC. Thus, I_{DCCB} reduces to zero at 6.0053 ms, and I_{LCC} also decreases to zero at 6.07 s, while the LCC is blocked until system restart. Since V_{DR} is zero during F_1 fault, and the DR stops power transfer due to the blocked MMC-STATCOM, I_{DR} will decay to zero in a relatively long duration for the studied case.

Fig. 5.9 (d) shows the active power of the DR, LCC and MMC-STATCOM. The active power of DR and LCC decrease to zero during F_1 fault, and the active power of MMC-STATCOM remains at zero. The reactive power of AC filters and converters are shown in Fig. 5.9 (e). Since the MMC-STATCOM is blocked, V_{ac} shown in Fig. 5.9 (f) decreases to zero, and the reactive power of AC filters and converters also drops to zero during F_1 fault. The phase A upper arm current of the MMC-STATCOM shown in Fig. 5.9 (g) also reduces to zero after blocking the MMC-STATCOM.

To conclude, the converter safety of the unidirectional hybrid F2F DC/DC converter is ensured during F_I fault. When the fault is cleared, the system can restart as presented earlier.



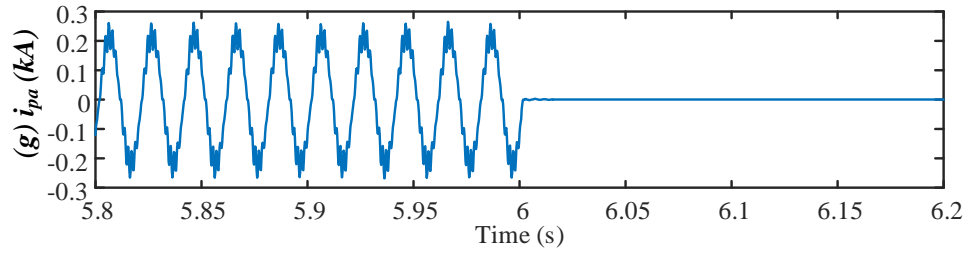


Fig. 5.9 System response during F_1 fault: (a) DC voltage, (b) Converter DC current, (c) DCCB DC current, (d) Active power, (e) Reactive power, (f) AC voltage, (g) Phase A upper arm current of MMC-STATCOM.

5.6.3 System response during F_2 fault

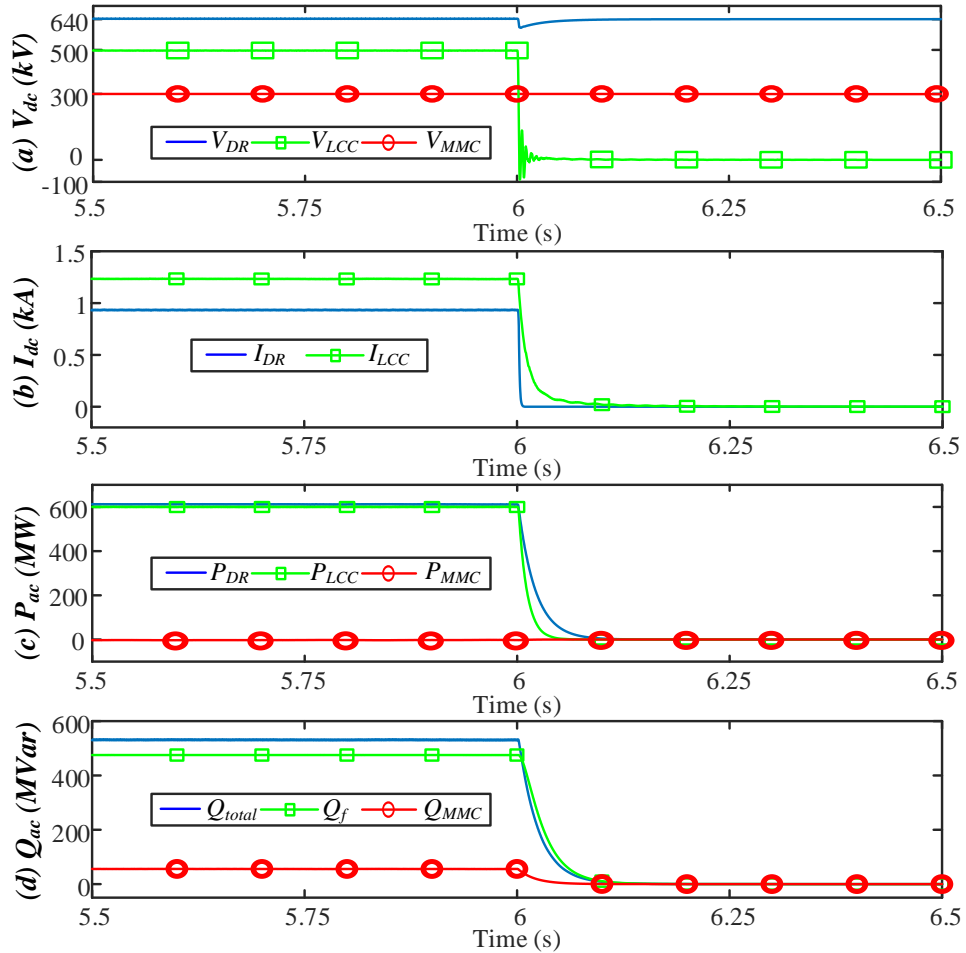
Fig. 5.10 demonstrates the system response of the unidirectional hybrid F2F DC/DC converter when a permanent solid p2p fault F_2 occurs the LCC side of the DC network with the distance of 100 km at 6.0 s. The blocking signals are sent to the LCC and MMC-STATCOM at 6.001 s, as similar to F_1 fault.

Fig. 5.10 (a) shows the DC voltages of the DR, LCC and MMC-STATCOM. The DC voltage of LCC drops to zero during F_2 fault. The MMC-STATCOM is blocked during F_2 fault so that the internal AC voltage (V_{ac}) shown in Fig. 5.10 (e) decreases to zero, and the DC voltage of DR slightly reduces to the rated value DC network E_l of 640 kV due to the collapse of V_{ac} . The MMC-STATCOM does not experience discharging during F_2 fault, and thus its DC voltage remains at the rated value.

The DC currents of DR and LCC are shown in Fig. 5.10 (b). As analysed in Section 5.5.2, the F_2 fault will not propagate to the proposed DC/DC converter due to the unidirectional current flow of the LCC. Therefore, The DC current of LCC decays to zero at 6.15 s during F_2 fault. The DC current of DR also reduces to zero at 6.01 s during F_2 fault as the internal AC voltage is lower than the minimum DR conduction voltage.

The active power of the DR, LCC and MMC-STATCOM are shown in Fig. 5.10 (c). Similar to F_1 fault, the active power of DR and LCC reduce to zero during F_2 fault, and the active power of MMC-STATCOM maintains at zero. The reactive power of AC filters and converters shown in Fig. 5.10 (d) drops to zero during F_2 fault, as the internal AC voltage in Fig. 5.10 (e) reduces to zero due to the blocked MMC-STATCOM. Fig. 5.9 (g) shows the phase A upper arm current of the MMC-STATCOM, which also decreases to zero after blocking the MMC-STATCOM.

To sum up, the unidirectional hybrid F2F DC/DC converter can operate securely during F_2 fault. The system can use the previously discussed approach to restart normal operation after fault clearance.



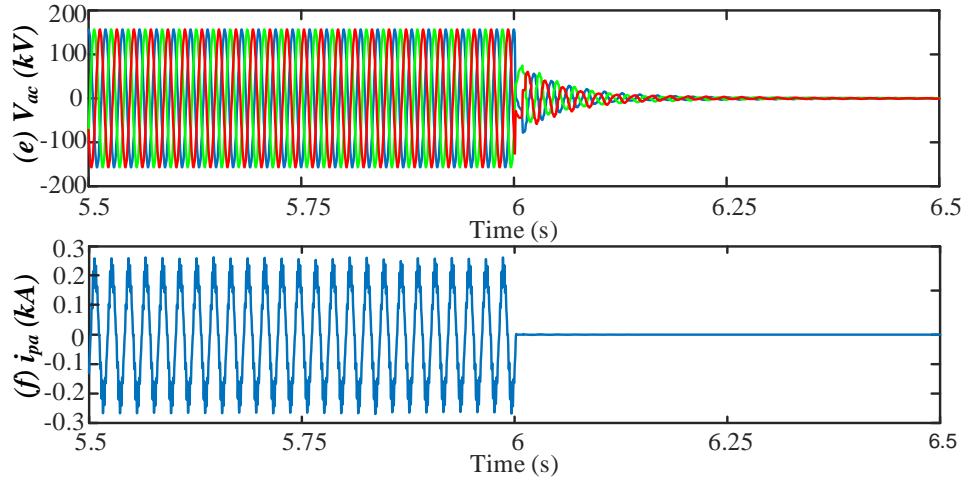


Fig. 5.10 System response during F_2 fault: (a) DC voltage, (b) Converter DC current, (c) Active power, (d) Reactive power, (e) AC voltage, (f) Phase A upper arm current of MMC-STATCOM.

5.7 Summary

A hybrid F2F DC/DC converter has been studied in this chapter for unidirectional HVDC transmission applications. The converter topology, control principle and DC fault protection have been investigated and analysed. The proposed DC/DC converter combines the advantages of the DR and LCC, with an internal AC grid formed by a MMC-STATCOM. The proposed DC/DC converter has higher power capability, higher converter efficiency, and lower investment cost potentially compared with conventional MMC based F2F topologies. The operation control principle of LCC and MMC-STATCOM has been developed, and the system start-up procedure has been described. Detailed analysis of the behaviours and protection methods during DC faults has been presented. Simulation results based on PSCAD/EMTDC have shown satisfactory performance during system start-up and DC faults, which validates the viability of the proposed DC/DC converter for unidirectional HVDC transmission applications.

It needs to acknowledge that the converter requires large amount of passive AC filters which may lead to large footprint and limit the use of the topology, e.g., offshore. In addition, the proposed DC/DC converter can only provide unidirectional power flow. Nevertheless, the principle of hybrid configuration which combines different converter technologies can potentially lead to improved system design.

Chapter 6 Conclusion and Future Work

6.1 General conclusion

This thesis focuses on investigating potential cost-effective converter system designs for interconnecting HVDC networks with different voltage levels, where different topologies of hybrid converters are proposed and analysed.

The development of large offshore wind farms requires reliable and economic grid integration while HVDC systems will play a major role in facilitating grid integration and connection of renewables. Due to the different voltage ratings among the different onshore and offshore DC networks, there rises the challenges of interconnecting different DC networks for increased operation flexibility and reliability. In addition, the increased interest in offshore production platform which is supplied by offshore wind energy also requires offshore converter stations that can connect different DC systems supplying power to a variety of loads. Traditionally, DC network interconnection is achieved by using DC/DC converters, which can be classified into two primary categories, i.e., galvanic isolated and non-isolated topologies. Isolated DC/DC converters can benefit from electrical isolation and friendly adoption for different DC voltage conversion ratios due to the use of isolation transformer. However, the use of two AC/DC conversion stages (F2F configurations) in isolated topologies leads to high converter power rating and operating power loss. Alternatively, the DC AUTO is an attractive non-isolated topology reduced DC/AC/DC conversion. However, practical converter cost and efficiency of the DC AUTO could still be very high as full-bridge submodules may have to be adopted to achieve DC fault isolation.

To reduce the cost of DC/DC converters, several hybrid converter systems with series-connected MMC and LCC or DR may be used to reduce the required power

rating of MMC. In addition, there is a need to design converter system to connect both AC and multiple DC networks. Therefore, hybrid topologies which combines DR, LCC and MMC could provide feasible solutions to achieve lower cost and higher efficiency, e.g. the F2F configurations based on other converter technologies rather than only MMCs.

In consideration of the above challenges, different topologies of hybrid converters are investigated in an effort to increase system capability and/or reduce overall cost for HVDC applications in the future. The general starting point throughout this study is to seek ways to substitute MMC-based systems with DR and/or LCC based ones, which feature higher power capability, higher operational efficiency and lower capital cost. Therefore, the concepts of hybrid AC/DC Hubs for connecting AC network and different DC grids are proposed in this thesis, where the MMC and DR or LCC are connected in parallel at the AC side and in series at the DC side. In that manner, the required power rating of MMC can be reduced, potentially contributing to lower cost and higher efficiency of the whole converter system, compared to the “conventional” approaches using DC/DC converters or parallel point-to-point HVDC links. On the other hand, an internal AC grid can be constructed with passive AC filters and MMC based STATCOM, and hence LCC and DR can be connected to form a F2F DC/DC converter for unidirectional applications.

The main contributions of this thesis are summarised as follows:

- A hybrid AC/DC hub consisting of LCC and MMC converters has been proposed to integrate onshore wind farm and interconnect onshore and offshore DC networks. Compared to the “conventional” DC network interconnection based on a DC/DC converter, the hybrid LCC-MMC Hub requires a smaller MMC with large part of the power handled by a LCC, which contributes to higher overall efficiency and lower cost. In addition, even with the use of unidirectional LCC converter, flexible power reversal of

the proposed hybrid LCC-MMC Hub can be achieved. The coordinated controls of the LCC and MMC developed ensures stable system operation, including during AC faults due to the MMC with the closed-loop current control and the inherent characteristic of the LCC rectifier. A comprehensive DC fault protection scheme using one DCCB has also been proposed and demonstrated by simulation for the LCC-MMC Hub for effective protection during DC faults.

- A DR-MMC AC/DC hub has been proposed for connecting offshore wind farms with onshore DC network and offshore DC production platform with different DC voltages. Compared to the parallel operation of the DR-HVDC link for supplying the offshore production platform, and the MMC-HVDC for connecting the onshore DC network, the required converter power rating of MMCs in the DR-MMC Hub is reduced due to the series connection. Depending on different operation scenarios of the offshore production platform, specific control modes of the MMCs in the proposed hybrid system have been investigated. the DR-MMC Hub can securely ride through offshore AC faults due to the MMCs' current-limiting control and the self-blocking capabilities. For isolating faults at any of the DC networks, hybrid MMCs with DC fault blocking capability, are adopted. Compared to the “conventional” parallel system, the proposed DR-MMC Hub requires fewer switching devices (i.e. IGBTs) under fault consideration, resulting in lower investment cost and power loss.
- A unidirectional hybrid F2F DC/DC converter consisting of a DR, LCC and MMC-STATCOM has been studied. In the proposed hybrid topology, the internal AC grid is established by the small power rating MMC-STATCOM, and the active power is transferred through the DR and LCC. The proposed DC/DC converter potentially offers higher power capability, higher converter efficiency and lower investment cost than those of the MMC based F2F DC/DC converters. The operation control principle of LCC and MMC-STATCOM has been developed together with the switching of AC filters and

transform tap changers, where the MMC-STATCOM controls the internal AC grid and the LCC regulates the system power balance through the control of the MMC DC energy. The behaviours and protection methods of the proposed F2F DC/DC converter during DC faults have also been discussed and demonstrated using simulation.

6.2 Future work

The proposed converter systems have unique features and potentially can provide improved designs compared to many existing topologies. However, it is recognised that they have many constraints for practical applications. Potential areas for future research include:

- To interconnect multiple DC networks with different voltage levels, the use of DC-DC converters to interconnect each of the two DC networks requires a large number of DC/DC converters. Therefore, the topologies of the multiport hybrid AC/DC hubs for multiport DC networks can be further developed.
- This study generally assumes other connected DC networks as ideal DC voltage sources or passive loads. In order to apply the proposed converter systems in practical HVDC systems, detailed operation features of each DC network and even the overall power system should be considered. Moreover, flexible system-level power flow control in the proposed hybrid AC/DC hubs should be explored.
- The proposed hybrid converter systems discuss the different combinations of DR, LCC and MMC, while DC faults are mainly addressed by conventional DCCBs. To further extend the work, other HVDC converter topologies (e.g. alternative arm converters) and novel DCCBs, can be included in future research.

References

- [1] REN21 Community, "Renewables 2020 Global Status Report," June 2020. Accessed in March 2021. [Online]. Available at <https://www.ren21.net/gsr-2020/>.
- [2] UK Department for Business, Energy & Industrial Strategy, "BEIS electricity generation cost report (2020)," August 2020. Accessed in June 2021. [Online]. Available at <https://www.gov.uk/government/publications/beis-electricity-generation-costs-2020>.
- [3] Global Wind Energy Council, "GWEC Global Wind Report 2019," March 2020. Accessed in March 2021. [Online]. Available at <http://www.gwec.net/>.
- [4] Power Technology, "Top 10 biggest wind farms," June 2019. Accessed in March 2021. [Online]. Available at <https://www.power-technology.com/features/feature-biggest-wind-farms-in-the-world-texas/>.
- [5] Global Wind Energy Council, "GWEC Global Offshore Wind Report 2020," August 2020. Accessed in March 2021. [Online]. Available at <http://www.gwec.net/>.
- [6] WindEurope, "Wind energy in Europe in 2019 - Trends and statistics," February 2020. Accessed in March 2021. [Online]. Available at <https://windeurope.org/wp-content/uploads/files/about-wind/statistics/WindEurope-Annual-Offshore-Statistics-2019.pdf>.
- [7] W. He et al., "Case Study of Integrating an Offshore Wind Farm with Offshore Oil and Gas Platforms and with an Onshore Electrical Grid", *Journal of Renewable Energy*, vol. 2013, 10 pages, 2013.
- [8] "Hydrogen production takes system to new levels" Tractebel Engie, October 2019. Accessed in June 2020. [Online]. Available at <https://tractebel->

engie.com/en/news/2019/400-mw-offshore-hydrogen-production-takes-system-to-new-levels.

- [9] "Bring North Sea Energy Ashore Efficiently" World Energy Council (WEC), Netherlands, 2017. Accessed in June 2020. [Online]. Available at <https://www.worldenergycouncil.nl/>.
- [10] "Delivery of an offshore hydrogen supply programme via industrial trials at the Flotta Terminal - Phase 1 project report", The Oil&Gas Technology Centre. Accessed in September 2020. [Online]. Available at <https://bit.ly/347wvDq>.
- [11] L. Xu and B. R. Andersen, "Grid connection of large offshore wind farms using HVDC," *Wind Energy*, vol. 9, no. 4, pp. 371–382, Jul. 2006.
- [12] X. Xiang, M. M. C. Merlin, and T. C. Green, "Cost analysis and comparison of HVAC, LFAC and HVDC for offshore wind power connection," in *12th IET International Conference on AC and DC Power Transmission (ACDC 2016)*, 2016, pp. 1-6.
- [13] N. B. Negra, J. Todorovic, and T. Ackermann, "Loss evaluation of HVAC and HVDC transmission solutions for large offshore wind farms," in *Electric Power Systems Research*, vol. 76, pp. 916-927.
- [14] Alassi, A., Bañales, S., Ellabban, O., Adam, G., & MacIver, C. (2019). "HVDC Transmission: Technology Review, Market Trends and Future Outlook," in *Renewable and Sustainable Energy Reviews*, 112(October 2018), pp. 530–554.
- [15] O. E. Oni, I. E. Davidson, and K. N. I. Mbangula, "A review of LCC-HVDC and VSC-HVDC technologies and applications," in *2016 IEEE 16th International Conference on Environment and Electrical Engineering (EEEIC)*, 2016, pp. 1-7.
- [16] Offshore Wind Industry Council, "Grid-access Technologies for GB Offshore Wind Industry," January 2020. Accessed in March 2021. [Online]. Available at

https://www.hvdccentre.com/wp-content/uploads/2020/01/Grid-Access-Technologies_V3.pdf.

- [17] Q. Chen, J. L. Rueda Torres, B. W. Tuinema and M. van der Meijden, "Comparative Assessment of Topologies for an Offshore Transnational Grid in the North Sea," in *2018 IEEE PES Innovative Smart Grid Technologies Conference Europe (ISGT-Europe)*, 2018, pp. 1-6.
- [18] TenneT, "NordLink Technical Design," April 2021. Accessed in August 2021. [Online]. Available at <https://www.tennet.eu/our-grid/international-connections/nordlink/>.
- [19] Z. Li, Q. Song, F. An, Biao. Zhao, Z. Yu and R. Zeng, "Review on DC transmission systems for integrating large-scale offshore wind farms," *Energy Conversion and Economics*, vol. 2, no. 1, pp. 1–14, March 2021.
- [20] R. Li, L. Yu, L. Xu, and G. P. Adam, "Coordinated Control of Parallel DR-HVDC and MMC-HVDC Systems for Offshore Wind Energy Transmission," *IEEE Journal of Emerging and Selected Topics in Power Electronics*, vol. 8, pp. 2572-2582, 2020.
- [21] D. Van Hertem and M. Ghandhari, "Multi-terminal VSC HVDC for the European supergrid: Obstacles," *Renewable and Sustainable Energy Reviews*, vol. 14, pp. 3156-3163, 2010/12/01/ 2010.
- [22] C. W. Gellings, "A globe spanning super grid," *IEEE Spectrum*, vol. 52, no. 8, pp. 48-54, August 2015.
- [23] S. Sanchez, A. Garcés, G. Bergna-Diaz, and E. Tedeschi, "Dynamics and Stability of Meshed Multiterminal HVDC Networks," *IEEE Transactions on Power Systems*, vol. 34, pp. 1824-1833, 2019.

- [24] F. Yan, G. Tang, Z. He, and M. Kong, "An improved droop control strategy for MMC-based VSC-MTDC systems," *Proceedings of the Chinese Society of Electrical Engineering*, vol. 34, pp. 397-404, 01/25 2014.
- [25] E. Prieto-Araujo, A. Egea-Alvarez, S. Fekriasl, and O. Gomis-Bellmunt, "DC Voltage Droop Control Design for Multiterminal HVDC Systems Considering AC and DC Grid Dynamics," *IEEE Transactions on Power Delivery*, vol. 31, pp. 575-585, 2016.
- [26] F. Thams, R. Eriksson, and M. Molinas, "Interaction of Droop Control Structures and Its Inherent Effect on the Power Transfer Limits in Multiterminal VSC-HVDC," *IEEE Transactions on Power Delivery*, vol. 32, pp. 182-192, 2017.
- [27] Cigré B4.76 Working Group, "DC-DC converters in HVDC grids and for connections to HVDC systems," *Cigré Technical Brochure*, March 2021.
- [28] PROMOTioN, "About PROMOTioN: The Project," 2016. Accessed in March 2021. [Online]. Available at https://www.promotion-offshore.net/about_promotion/the_project/.
- [29] Jacobson, B., P. Karlsson, G. Asplund, L. Harnefors and T. Jonsson. "VSC-HVDC Transmission with Cascaded Two-Level Converters," in *CIGRE B4-110*, Sweden, 2010.
- [30] J.-H. Ying, H. Duchon, M. Karlsson, L. Ronstrom, and B. Abrahamsson, "HVDC with voltage source converters - a powerful standby black start facility," in *2008 IEEE/PES Transmission and Distribution Conference and Exposition*, 2008, pp. 1-9.
- [31] A. Lesnicar and R. Marquardt, "An innovative modular multilevel converter topology suitable for a wide power range," in *2003 IEEE Bologna Power Tech Conference Proceedings*, 2003, p. 6 pp. Vol.3.

- [32] R. Marquardt, "Modular Multilevel Converter topologies with DC-Short circuit current limitation," in *8th International Conference on Power Electronics - ECCE Asia*, Jeju, Korea (South), 2011, pp. 1425-1431.
- [33] S. Debnath, J. Qin, B. Bahrani, M. Saeedifard and P. Barbosa, "Operation, Control, and Applications of the Modular Multilevel Converter: A Review," *IEEE Transactions on Power Electronics*, vol. 30, no. 1, pp. 37-53, Jan. 2015.
- [34] R. Li and L. Xu, "Review of DC fault protection for HVDC grids," *Wiley Interdisciplinary Reviews: Water*, vol. 7, no. 2, p. e278, Mar. 2018.
- [35] R. Zeng, L. Xu, L. Yao and B. W. Williams, "Design and Operation of a Hybrid Modular Multilevel Converter," *IEEE Transactions on Power Electronics*, vol. 30, no. 3, pp. 1137-1146, March 2015.
- [36] R. Blasco-Gimenez, S. Ano-Villalba, J. Rodriguez, F. Morant, and S. Bernal, "Uncontrolled rectifiers for HVDC connection of large off-shore wind farms," in *2009 13th European Conference on Power Electronics and Applications*, 2009, pp. 1-8.
- [37] S. Bernal-Perez, S. Ano-Villalba, R. Blasco-Gimenez and J. Rodriguez-D'Erlee, "Efficiency and Fault Ride-Through Performance of a Diode-Rectifier- and VSC-Inverter-Based HVDC Link for Offshore Wind Farms," *IEEE Transactions on Industrial Electronics*, vol. 60, no. 6, pp. 2401-2409, June 2013.
- [38] S. Seman, R. Zurowski, Christos Taratoris, "Interconnection of advanced Type 4 WTGs with Diode Rectifier based HVDC solution and weak AC grids," in *Proceedings of 14th Wind Integration Workshop*, Bruxelles, October 2015.
- [39] L. Yu, R. Li and L. Xu, "Distributed PLL-Based Control of Offshore Wind Turbines Connected with Diode-Rectifier-Based HVDC Systems," *IEEE Transactions on Power Delivery*, vol. 33, no. 3, pp. 1328-1336, June 2018.

- [40] H. Xiao, K. Sun, J. Pan, Y. Li and Y. Liu, "Review of hybrid HVDC systems combining line communicated converter and voltage source converter," *International Journal of Electrical Power & Energy Systems*, vol. 129, 2021.
- [41] L. Yu, C. Guo, C. Zhao, J. Xu, N. An and X. Hu, "Power Reversal of Hybrid HVDC System," in *11th IET International Conference on AC and DC Power Transmission*, Birmingham.
- [42] G. Tang and Z. Xu, "A LCC and MMC hybrid HVDC topology with DC line fault clearance capability", *International Journal of Electrical Power & Energy Systems*, vol. 62, pp. 419-428, 2014.
- [43] H. Zhou, G. Yang and J. Wang, "Modeling, Analysis, and Control for the Rectifier of Hybrid HVdc Systems for DFIG-Based Wind Farms," *IEEE Transactions on Energy Conversion*, vol. 26, no. 1, pp. 340-353, March 2011.
- [44] Huang Y, Huang W, Li M, Liu T. "Steady-state control strategy of multi-terminal hybrid UHVDC," in *2017 19th European Conference on Power Electronics and Applications (EPE'17 ECCE Europe)*, Warsaw, Poland; 2017. p. 1–10.
- [45] H, Xiao, K. Sun, J Pan and Y. Liu, "Operation and control of hybrid HVDC system with LCC and full-bridge MMC connected in parallel," *IET Generation Transmission & Distribution*, vol. 14, no. 7, pp. 1344-1352, Apr. 2020.
- [46] K. Sun, H. Xiao, J. Pan and Y. Liu, "A Station-Hybrid HVDC System Structure and Control Strategies for Cross-Seam Power Transmission," *IEEE Transactions on Power Systems*, vol. 36, no. 1, pp. 379-388, Jan. 2021.
- [47] G. Andersson, N. Hyttinen. "Skagerrak the next generation," in *Proceedings of CIGRE*, Paris, French, 2015, pp. 1-9.
- [48] W. Lin, J. Wen, M. Yao, S. Wang, S. Cheng and N. Li, "Series VSC-LCC converter with self-commutating and dc fault blocking capabilities," in *2014 IEEE PES General Meeting | Conference & Exposition*, USA, 2014, pp. 1-5.

- [49] T. H. Nguyen, D. Lee, and C. Kim, "A Series-Connected Topology of a Diode Rectifier and a Voltage-Source Converter for an HVDC Transmission System," *IEEE Transactions on Power Electronics*, vol. 29, pp. 1579-1584, 2014.
- [50] J. Cao and J. Y. Cai, "HVDC in China," presented at *EPRI 2013 HVDC & FACTS Conference*, USA, 2013.
- [51] G. Chen, M. Hao, Z. Xu, A. Vaughan, J. Cao and H. Wang, "Review of high voltage direct current cables," *CSEE Journal of Power and Energy Systems*, vol. 1, no. 2, pp. 9-21, June 2015.
- [52] V. Hussenether, J. Rittiger, A. Barth, D. Worthington, G. Dell'Anna, M. Rapetti, et al., "Projects BorWin2 and HelWin1—large scale multilevel voltage-sourced converter technology for bundling of offshore windpower," *CIGRE Technical Program Session B4-306*. Paris, France: CIGRE, pp. 1-11, 2012.
- [53] J. D. Páez, D. Frey, J. Maneiro, S. Bacha and P. Dworakowski, "Overview of DC-DC Converters Dedicated to HVdc Grids," *IEEE Transactions on Power Delivery*, vol. 34, no. 1, pp. 119-128, Feb. 2019.
- [54] G. P. Adam, I. A. Gowaid, S. J. Finney, D. Holliday, and B. W. Williams, "Review of dc-dc converters for multi-terminal HVDC transmission networks," *IET Power Electronics*, vol. 9, no. 2, pp. 281–296, 2016.
- [55] A. M. Omran, K. H. Ahmed, M. S. Hamad and I. F. Al-Arabawy, "Interconnection between different DC technologies at multi-terminal HVDC network," in *2014 International Conference on Renewable Energy Research and Application (ICRERA)*, Milwaukee, WI, USA, 2014, pp. 295-300.
- [56] W. Chen, X. Ruan, H. Yan and C. K. Tse, "DC/DC Conversion Systems Consisting of Multiple Converter Modules: Stability, Control, and Experimental Verifications," *IEEE Transactions on Power Electronics*, vol. 24, no. 6, pp. 1463-1474, June 2009.

- [57] R. Giri, R. Ayyanar, and E. Ledezma, "Input-series and output-series connected modular DC-DC converters with active input voltage and output voltage sharing," in *Applied Power Electronics Conference and Exposition*, 2004. APEC'04. Nineteenth Annual IEEE, 2004, vol. 3, pp. 1751–1756.
- [58] T. Lagier and P. Ladoux, "A comparison of insulated DC-DC converters for HVDC off-shore wind farms," in *Clean Electrical Power (ICCEP)*, 2015 International Conference on, 2015, pp. 33–39.
- [59] S. Kenzelmann, A. Rufer, D. Dujic, F. Canales, and Y. R. De Novaes, "Isolated DC/DC structure based on modular multilevel converter," *IEEE Transactions on Power Electronics*, vol. 30, no. 1, pp. 89–98, 2015.
- [60] T. Lüth, M. M. C. Merlin, T. C. Green, F. Hassan and C. D. Barker, "High-Frequency Operation of a DC/AC/DC System for HVDC Applications," *IEEE Transactions on Power Electronics*, vol. 29, no. 8, pp. 4107-4115, Aug. 2014.
- [61] I. Gowaid, G. Adam, A. M. Massoud, S. Ahmed, D. Holliday, and B. Williams, "Quasi two-level operation of modular multilevel converter for use in a high-power DC transformer with DC fault isolation capability," *IEEE Transactions on Power Electronics*, vol. 30, no. 1, pp. 108–123, 2015.
- [62] Y. Zhang, G. Adam, S. Finney and B. Williams, "Improved pulse-width modulation and capacitor voltage-balancing strategy for a scalable hybrid cascaded multilevel converter", *IET Power Electronics*, vol. 6, no. 4, pp. 783-797, Apr. 2013.
- [63] I. Gowaid, G. Adam, A. M. Massoud, S. Ahmed, and B. Williams, "Hybrid and Modular Multilevel Converter Designs for Isolated HVDC–DC Converters," *IEEE Journal of Emerging and Selected Topics in Power Electronics*, vol. 6, no. 1, pp. 188–202, 2018.
- [64] M. M. Merlin, T. C. Green, P. D. Mitcheson, D. R. Trainer, R. Critchley, W. Crookes, and F. Hassan, "The alternate arm converter: A new hybrid multilevel

converter with dc-fault blocking capability," *IEEE transactions on power delivery*, vol. 29, no. 1, pp. 310–317, 2014.

- [65] A. Schön and M.-M. Bakran, "Comparison of modular multilevel converter based HV DC-DC-converters," in *Power Electronics and Applications (EPE'16 ECCE Europe)*, 2016 18th European Conference on, 2016, pp. 1–10.
- [66] A. Schön and M. Bakran, "A new HVDC-DC converter with inherent fault clearing capability," in *2013 15th European Conference on Power Electronics and Applications (EPE)*, Lille, France, 2013, pp. 1-10.
- [67] W. Lin, "DC-DC Autotransformer with Bidirectional DC Fault Isolating Capability," *IEEE Transactions on Power Electronics*, vol. 31, no. 8, pp. 5400–5410, 2016.
- [68] Yang, Z., Li, M., Lu, X., et al.: "Interconnection of VSC-HVDC and LCC-HVDC using DC-DC autotransformer", *The Journal of Engineering*, 2019, 2019, (18), pp. 5033–5037.
- [69] Suo, Z., Li, G., Li, R., et al.: "Submodule configuration of HVDC-DC autotransformer considering DC fault", *IET Power Electronics*, 2016, 9, (15), pp. 2776–2785.
- [70] M. Zhou, W. Xiang, W. Zuo, W. Lin, and J. Wen, "A Unidirectional DC-DC Autotransformer for DC Grid Application," *Energies*, vol. 11, no. 3, p. 530, Mar. 2018.
- [71] W. Xiang, W. Lin, T. An, J. Wen and Y. Wu, "Equivalent Electromagnetic Transient Simulation Model and Fast Recovery Control of Overhead VSC-HVDC Based on SB-MMC," *IEEE Transactions on Power Delivery*, vol. 32, no. 2, pp. 778-788, April 2017.
- [72] N. Ahmed, A. Haider, D. Van Hertem, L. Zhang and H. Nee, "Prospects and challenges of future HVDC SuperGrids with modular multilevel converters," in

Proceedings of the 2011 14th European Conference on Power Electronics and Applications, 2011, pp. 1-10.

- [73] P. S. Jones and C. C. Davidson, "Calculation of power losses for MMC-based VSC HVDC stations," in *2013 15th European Conference on Power Electronics and Applications (EPE)*, 2013, pp. 1-10.
- [74] R. Zeng, L. Xu, L. Yao and S. J. Finney, "Analysis and Control of Modular Multilevel Converters under Asymmetric Arm Impedance Conditions," *IEEE Transactions on Industrial Electronics*, vol. 63, no. 1, pp. 71-81, Jan. 2016.
- [75] M. Perez, J. Rodriguez, J. Pontt and S. Kouro, "Power Distribution in Hybrid Multi-cell Converter with Nearest Level Modulation," in *2007 IEEE International Symposium on Industrial Electronics*, 2007, pp. 736-741.
- [76] N. R. Chaudhuri, R. Oliveira and A. Yazdani, "Stability Analysis of Vector-Controlled Modular Multilevel Converters in Linear Time-Periodic Framework," *IEEE Transactions on Power Electronics*, vol. 31, no. 7, pp. 5255-5269, July 2016.
- [77] L. Shi, G. P. Adam, R. Li and L. Xu, "Control of Offshore MMC During Asymmetric Offshore AC Faults for Wind Power Transmission," *IEEE Journal of Emerging and Selected Topics in Power Electronics*, vol. 8, no. 2, pp. 1074-1083, June 2020.
- [78] X. Yu, J. Yi, N. Wang, Y. Teng and Q. Huang, "Analysis on Dynamic Response of LCC-VSC Hybrid HVDC System with AC/DC Faults," in *2018 IEEE Innovative Smart Grid Technologies - Asia (ISGT Asia)*, 2018, pp. 323-327.
- [79] C. H. Lee, J. S. Kwak and S. W. Kim, "Verification on Valve Losses of LCC HVDC Converter Station in Korea," in *2020 3rd International Conference on Power and Energy Applications (ICPEA)*, 2020, pp. 46-51.

- [80] J. Häfner and B. Jacobson, "Proactive Hybrid HVDC Breakers - A key innovation for reliable HVDC grids," in *Integrating Supergrids and Microgrids International Symposium*, Italy, pp. 1-8, 2011.
- [81] X. Li, Q. Song, W. Liu, H. Rao, S. Xu and L. Li, "Protection of Nonpermanent Faults on DC Overhead Lines in MMC-Based HVDC Systems," *IEEE Transactions on Power Delivery*, vol. 28, no. 1, pp. 483-490, Jan. 2013.
- [82] W. Xiang, R. Yang, C. Lin, J. Zhou, J. Wen and W. Lin, "A Cascaded Converter Interfacing Long-Distance HVdc and Back-to-Back HVdc Systems," *IEEE Journal of Emerging and Selected Topics in Power Electronics*, vol. 8, no. 4, pp. 4109-4121, Dec. 2020.
- [83] M. Szechtman, T. Wess and C. V. Thio, "A benchmark model for HVDC system studies," in *International Conference on AC and DC Power Transmission*, 1991, pp. 374-378.
- [84] J. Peralta, H. Saad, S. Denetiere, J. Mahseredjian and S. Nguefeu, "Detailed and Averaged Models for a 401-Level MMC–HVDC System," *IEEE Transactions on Power Delivery*, vol. 27, no. 3, pp. 1501-1508, July 2012.
- [85] Y. Zhou, D. Jiang, J. Guo, P. Hu and Y. Liang, "Analysis and Control of Modular Multilevel Converters Under Unbalanced Conditions," *IEEE Transactions on Power Delivery*, vol. 28, no. 4, pp. 1986-1995, Oct. 2013.
- [86] J. Moon, J. Park, D. Kang and J. Kim, "A Control Method of HVDC-Modular Multilevel Converter Based on Arm Current Under the Unbalanced Voltage Condition[79]," *IEEE Transactions on Power Delivery*, vol. 30, no. 2, pp. 529-536, April 2015.
- [87] R. Blasco-Gimenez, S. Anó-Villalba, J. Rodriguez-D'Derlée, S. Bernal-Perez and F. Morant, "Diode-Based HVdc Link for the Connection of Large Offshore Wind Farms," *IEEE Transactions on Energy Conversion*, vol. 26, no. 2, pp. 615-626, June 2011.

- [88] L. Yu, R. Li and L. Xu, "Hierarchical control of offshore wind farm connected by parallel diode-rectifier-based HVDC and HVAC links," *IET Renewable Power Generation*, vol. 13, no. 9, pp. 1493-1502, 2019.
- [89] M. J. Hossain, H. R. Pota, V. A. Ugrinovskii and R. A. Ramos, "Simultaneous STATCOM and Pitch Angle Control for Improved LVRT Capability of Fixed-Speed Wind Turbines," *IEEE Transactions on Sustainable Energy*, vol. 1, no. 3, pp. 142-151, Oct. 2010.
- [90] K. Huang, W. Xiang, L. Xu and Y. Wang, "Hybrid AC/DC hub for integrating onshore wind power and interconnecting onshore and offshore DC networks," *IET Renewable Power Generation*, vol. 14, no. 10, pp. 1738-1745, 27 7 2020.
- [91] K. R. W. Bell, L. Xu, and T. Houghton, "Considerations in design of an offshore network," presented at *the Cigré Paris Session*, paper C1-206, Paris, 2014.
- [92] B. Ni et al., "An Adaptive Fault Current Limiting Control for MMC and Its Application in DC Grid," *IEEE Transactions on Power Delivery*, vol. 36, no. 2, pp. 920-931, April 2021.
- [93] Li, R., Xu, L. and Guo, D., 2017. Accelerated switching function model of hybrid MMCs for HVDC system simulation. *IET Power Electronics*, vol. 10, no. 15, pp. 2199-2207, 2017.
- [94] Siemens, "New DC grid access solution," Accessed in December 2020. [Online]. Available at <http://m.energy.siemens.com/hq/pool/hq/power-transmission/grid-access-solutions/dc-solutions/DC-Flyer.pdf>, pp. 1-7, 2015.
- [95] S. Wang, G. Tang and Z. He, "Comprehensive evaluation of VSC-HVDC transmission based on improved analytic hierarchy process," in *2008 Third International Conference on Electric Utility Deregulation and Restructuring and Power Technologies*, 2008, pp. 2207-2211.

- [96] B. R. Andersen and Lie Xu, "Hybrid HVDC system for power transmission to island networks," *IEEE Transactions on Power Delivery*, vol. 19, no. 4, pp. 1884-1890, Oct. 2004.
- [97] J. H. D. G. Pinto, W. C. S. Amorim, A. F. Cupertino, H. A. Pereira, S. I. S. Junior and R. Teodorescu, "Optimum Design of MMC-Based ES-STATCOM Systems: The Role of the Submodule Reference Voltage," *IEEE Transactions on Industry Applications*, vol. 57, no. 3, pp. 3064-3076, May-June 2021.
- [98] R. Li, L. Xu and L. Yao, "DC Fault Detection and Location in Meshed Multiterminal HVDC Systems Based on DC Reactor Voltage Change Rate," *IEEE Transactions on Power Delivery*, vol. 32, no. 3, pp. 1516-1526, June 2017.
- [99] R. Li, L. Yu, and L. Xu, "Operation of offshore wind farms connected with DRU-HVDC transmission systems with special consideration of faults," *Global Energy Interconnection*, vol. 1, pp. 608-617, 2018.
- [100] Y. Zhou, Y. Huang, H. Liu, Y. Tai, H. Yang and B. Men, "Research and development of 500kV hybrid HVDC circuit breaker with current commutation drive circuit," in 2019 4th IEEE Workshop on the Electronic Grid (eGRID), 2019, pp. 1-6.

Author's Publications

- [1] K. Huang, W. Xiang, L. Xu and Y. Wang, "Hybrid AC/DC hub for integrating onshore wind power and interconnecting onshore and offshore DC networks," *IET Renewable Power Generation*, vol. 14, no. 10, pp. 1738-1745, July 2020, doi: 10.1109/JESTPE.2019.2930399.

Abstract: A hybrid AC/DC hub is proposed in this study, where a modular multilevel converter and a line-commutated converter are paralleled at the AC side to integrate onshore wind power, and connected in series at the DC sides to interconnect two DC networks with different voltages. The hybrid AC/DC hub facilitates wind power integration and DC network interconnection with reduced converter ratings and power losses when compared with the “conventional” approach using DC/DC converters. To investigate the design requirement and performance of the hybrid AC/DC hub, power flow analysis is assessed to evaluate the converter power rating requirement. To ride through DC faults at either side of the interconnected DC networks, a coordinated DC fault protection for the hybrid AC/DC hub is proposed and studied. Simulation results in PSCAD/EMTDC verify the feasibility and effectiveness of the proposed control and protection of the hybrid AC/DC hub under power flow change, AC and DC fault conditions.

- [2] K. Huang, L. Xu and G. Liu, "A Hybrid DR-MMC AC/DC Hub for Integrating Offshore Wind Farm and Offshore Production Platform," *Energies*, vol. 14, no. 13, 3759, June 2021, doi: <https://doi.org/10.3390/en14133759>.

Abstract: A diode rectifier-modular multilevel converter AC/DC hub (DR-MMC Hub) is proposed to integrate offshore wind power to the onshore DC network and offshore production platforms (e.g., oil/gas and hydrogen production plants) with different DC voltage levels. The DR and MMCs are connected in parallel at the offshore AC collection network to integrate offshore wind power, and in series at the DC terminals

of the offshore production platform and the onshore DC network. Compared with conventional parallel-connected DR-MMC HVDC systems, the proposed DR-MMC hub reduces the required MMC converter rating, leading to lower investment cost and power loss. System control of the DR-MMC AC/DC hub is designed based on the operation requirements of the offshore production platform, considering different control modes (power control or DC voltage control). System behaviors and requirements during AC and DC faults are investigated, and hybrid MMCs with half-bridge and full-bridge sub-modules (HBSMs and FBSMs) are used for safe operation during DC faults. Simulation results based on PSCAD/EMTDC validate the operation of the DR-MMC hub.